Biocommunication between plants and honeybees through pollen fluorescence

Shinnosuke Mori

2019

Contents

Abbreviations

4CL3	4-coumarate-coenzyme A ligase 3
ABCG	ATP-binding cassette subfamily G member
ACP	acyl carrier protein
ACOS5	acyl-coenzyme A synthetase 5
ARC1	armadillo repeat containing protein 1
ATA7	ARABIDOPSIS THALIANA ANTHER 7
ATP	adenosine 5'-triphosphate
AUC	area under spectral curve
C4H	cinnamate 4-hydroxylase
ca.	circa
CoA	coenzyme A
CYP	cytochrome P450
EFD	EXINE FORMATION DEFECT
Em	emission
ER	endoplasmic reticulum
Ex	excitation
FAS	fatty acid synthetase
FATB	fatty acyl thioesterase B
FT	Fourier transform
GC	gas chromatography
GFP	green fluorescent protein
HPLC	high-performance liquid chromatography
INP1	INAPERTURATE POLLEN1
IR	infrared
LAP3	LESS ADHERENT/ADHESIVE POLLEN 3

LTP	lipid transfer protein
LWS	long wavelength sensitive
MALDI	matrix-associated laser desorption ionization
MAT	methionine adenosyltransferase
Me	methyl
MLPK	*M*-locus protein kinase
MS	mass spectrometry
MS2	MALE STERILITY2
MWS	middle wavelength sensitive
NADPH	nicotinamide adenine dinucleotide phosphate
NMR	nuclear magnetic resonance
PAL	phenylalanine ammonia-lyase
PKSA	POLYKETIDE SYNTHASE A (LESS ADHESIVE POLLEN 6, LAP6)
PKSB	POLYKETIDE SYNTHASE B (LESS ADHESIVE POLLEN 5, LAP5)
PMC	pollen mother cell
RNAi	ribonucleic acid interface
ROS	reactive oxygen species
SAMDC	*S*-adenosyl-L-methionine decarboxylase
SAP	sporopollenin acceptor particle
SCR	*S*-locus cysteine-rich protein
SEM	scanning electron microscopy
SHT	spermidine hydroxycinnamoyltransferase
SI	self-incompatibility
SLF	*S*-locus F-box
SP11	*S*-locus protein 11
SPDP	spermidine synthase
SRK	*S*-locus receptor kinase
SWS	short wavelength sensitive
TEM	transmission electron microscopy
TKPR1	tetraketide α-pyrone reductase 1
TLC	thin-layer chromatography
TT4	TRANSPARENT TESTA 4 (CHALCONE SYNTHASE, CHS)
UV	ultraviolet
UVS	ultraviolet sensitive
VOC	volatile organic compound
VS	violet sensitive
vs.	versus
VSWS	very short wavelength sensitive

Note. Palynological terminology in this thesis follows Punt et al. (2007) and Hesse et al. (2009).

Chapter I
General introduction

1. Pollen: an overview

Pollen grains are the male microgametophytes of seed plants that produce gametes required for sexual reproduction, which in seed plants involves three distinct phases: pollination, fertilization, and seed dispersal. Pollination is the transfer of pollen from an anther to a stigma in angiosperms or from a microsporophyll to the micropyle of an ovule in gymnosperms (Singh 2006). Once delivered to the female reproductive structure, the pollen grain germinates and forms a pollen tube that transports the male gametes to ovules (McCormick 1993). Fertilization is achieved when a male gamete nucleus combines with an egg nucleus of the ovule to form a zygote, which gives rise to fruits and seeds (Fahn 1967; Kandasamy et al. 1994). Unless stated otherwise, the following sections refer to angiosperms.

1.1. Morphology

In the 1640s, the English botanist Nehemiah Grew made the first microscopic observations of pollen, and discovered that pollen grains in different plant species are of different sizes and forms (Manten 1967). Advances in microscopy, especially scanning electron microscopy (SEM) and transmission electron microscopy (TEM), enabled the detailed characterization of pollen morphology, which is nowadays applied to many fields including aeropalynology, biostratigraphy, cryopalynology, paleopalynology, and pharmacopalynology.

Pollen grains vary in diameter from approximately 5 μm in *Myosotis* to >200 μm in *Cucurbita*, with an average of around 35 μm (Stanley and Linskens 1974; Willmer 2011); and in volume by up to five orders of magnitude (Muller 1979). Pollen grains of wind-pollinated (anemophilous) species are usually smaller in diameter relative to those of animal-pollinated (zoophilous) ones (20–60 μm vs >200 μm), small size being advantageous for dispersal (Harder et al. 1988; Ackerman 2000). However, a recent aerodynamic study demonstrated that the settling velocities of anemophilous pollen exceed those of zoophilous pollen (Hall and Walter 2011). While pollen grains of bat-pollinated plant species seem to be larger than those transferred by other pollinators (Stroo 2000),

there is no difference in pollen size between bird-pollinated plants and bee-pollinated plants (Harder 1988; Ackerman 2000), and so the relationship between pollen size and pollinating agents is currently unclear. Although cellular size usually correlates positively with genome size (Beaulieu et al. 2008), there is no significant global correlation between the pollen grain size and genome size (C-value) (Knight et al. 2010).

The 3D shape of pollen grains is usually described in terms of their equatorial and polar views. In the equatorial view, the shape is categorized by ratio of the lengths of their polar and equatorial axes (P/E) as follows: peroblate (less than 0.5); oblate (0.5–0.75); subspheroidal (0.75–1.33); prolate (1.33–2.0); and perprolate (greater than 2.0) (Erdtman 1952). The most common subspheroidal class is further divided into four categories: suboblate, P/E 0.75 to 0.88; oblate-spheroidal, 0.88 to 1.0; prolate-spheroidal, 1.0 to 1.14; and subprolate, 1.14 to 1.33 (Erdtman 1952). In the polar view, the shape is categorized as circular, elliptical, polygonal, concave-polygonal (angular with concave sides), or lobate (curved with convex sides separated by indentations) (Wortley et al. 2015).

Pollen cells are encased in intricately ornamented wall (Edlund et al. 2004; Kesseler and Harley 2006; Zavada 1983). Pollen ornamentation is diverse and includes spines, spinules, warts, granules, reticulations, etc., depending on the species; the corresponding pollen grains are described as echinate, reticulate, granulate, etc.; although a combination of multiple ornamentations is common (Hesse et al. 2009). Highly diversified morphology of pollen grains has been proposed to be associated with pollinator type; however, the reasons accounting for such variation in the ornamentation of pollen grains still remain unclear (Sannier et al. 2009).

Despite the diversity of ornamentation, pollen walls exhibit a common structural stratification that serves critical functions as a barrier against unfavorable environment conditions (Fig. 1; Hesse et al. 2009; Wallace et al. 2011). Pollen wall can be divided into three principal strata: inner intine (approximately 0.2 μm thickness), directly external to the plasma membrane; outer exine (approximately 1.0 μm thickness) composed of a durable biopolymer sporopollenin; and pollen coat (approximately 1.0 μm thickness) typically composed of lipids, proteins, and pigments, which fills

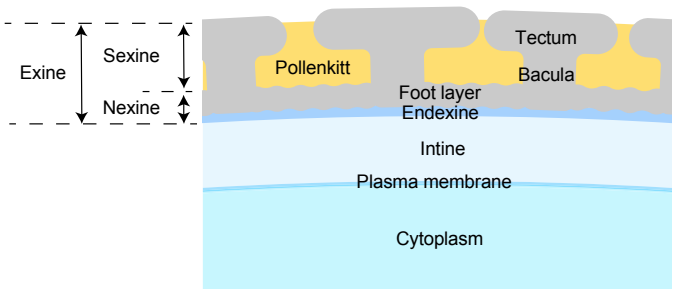

Fig. 1 Cross-section view of pollen wall stratification (revised from Fig. 2 in Ariizumi and Toriyama 2011).

the sculptured cavities of exine (Brooks and Shaw 1968; Heslop-Harrison 1968a; Section 1.4). The intine usually comprises two layers: an outer granular exintine, and inner microfibrillar and/or lamellar endintine (van der Ham 1991; Heslop-Harrison and Heslop-Harrison 1982; Simpson 1989). The intine is composed primarily of pectin, cellulose, and hemicellulose, and maintains the structural integrity of pollen grains (Persson et al. 2007). The exine typically comprises two layers: inner nexine and outer sexine (Ariizumi and Toriyama 2011). The nexine is bilayered, consisting of foot layer (nexine I) and endexine (nexine II) (Ariizumi and Toriyama 2011). The sexine contains an outermost edge, tectum, and radially directed rods, bacula (columellae) (Ariizumi and Toriyama 2011).

Pollen can be further characterized by the number and location of apertures on the surface of the outer wall; an aperture is a thin or missing part of the exine, which is independent of the patterning of the exine, and serves as the emerging site of pollen tube. In basal angiosperm including monocots, pollen is predominantly monoaperturate (Furness and Rudall 2004). Pollen grains lacking clearly defined apertures on the surface (inaperturate) are also common (Furness 2007); multi-aperturate and inaperturate pollen are sometimes found in closely related species, i.e., Trimeniaceae, Chloranthaceae, and Alismatales (Furness and Rudall 1999; Furness et al. 2002). Inaperturate pollen is usually thin-walled, so that the pollen tube can potentially emerge at any point (Furness and Rudall 2004). In contrast, most eudicot pollen grains bear three elongated, slit-like apertures arranged equidistantly around the equator (i.e., Arabidopsis) (Furness and Rudall 2004; Halbritter 2015). Pollen with four, five, six, or more apertures scattered over the grain surface are found in some species (e.g. Caryophyllales) (Furness and Rudall 2004; Wortley et al. 2015). In the evolution process of angiosperms, the number of pollen apertures has been found to tend to increase, with an apparently fundamental shift of their position from polar to equatorial (Furness and Rudall 2004). The increased aperture number may facilitate the contact between aperture(s) and stigmatic surface, offering a potential selective advantage.

1.2. Anther and pollen development

Anther development

The floral meristem typically consists of three germ layers: L1, L2, and L3 (Satina et al. 1940), which give rise to different anther tissues following stamen primordia initiation (Goldberg et al. 1993). The L1 layer differentiates into the stomium and epidermis, the L2 layer into the primary

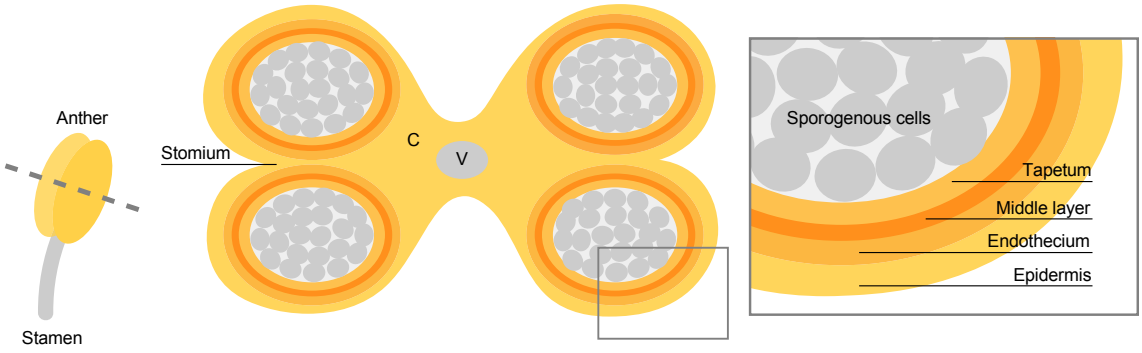

Fig. 2 Cross-section view of anther wall. C, connective; V, vascular bundle.

parietal and sporogenous layers, and the L3 layer into the connective and vasculature tissues (Wilson et al. 2011). The primary parietal cells further divide into three layers of anther: endothecium, middle layer, tapetum (Wilson et al. 2011). These differentiations result in a final anther structure comprised of four maternal cell layers: outermost epidermis, endothecium, middle layer, and tapetum, surrounding the inner sporogenous cells (Fig. 2; Scott et al. 2004).

Sporophytic anther tissues, particularly the tapetum, support the nutrition and development of pollen grains (Gómez et al. 2015; Section 1.3 & 1.4). At least two types of tapeta are recognized in seed plants: amoeboid (invasive) and secretory (glandular) types, although their functions are essentially the same (Pacini 1997, 2010). In anthers bearing amoeboid tapetum, the tapetal protoplasts invade the locule and completely envelop the developing microspores to provide materials (Pacini 2000). The microspore developmental stage at which the invasion occurs varies; in monocotyledons, it is usually during meiosis or the tetrad period, whereas in eudicots, it is usually during the early microspore period (Pacini et al. 1985). Secretory tapeta which release materials to the developing microspores via the locular fluid (Clément et al. 1998; Furness 2008), are the predominant type among land plants (Furness and Rudall 2001). The secretory tapetal cells remain intact at the periphery of the anther locule and undergo post-meiotic degeneration via programmed cell death (Gómez et al. 2015) to form the pollen coat (Pacini 2010; Section 1.4).

Pollen development

At maturity, an angiosperm pollen grain comprises either two (bicellular) or three (tricellular) haploid cells (Borg and Twell 2011). Bicellular pollen comprises a vegetative cell containing a generative cell, and tricellular pollen a vegetative cell containing two sperm cells (Borg and Twell 2011). About 70% of angiosperm species are estimated to have bicellular pollen at anthesis (Williams et al. 2014). In species that shed bicellular pollen at anthesis, the final mitotic division to produce two sperm cells occur during pollen tube growth (Gómez et al. 2015).

Pollen development in Arabidopsis, rice (*Oryza sativa*), and many other angiosperms involves similar key stages; the conservation of the regulatory pathways underlying these stages was demonstrated by the characterization of male sterile mutants from orthologs in both plants (Gómez et al. 2015; Wilson and Zhang 2009). A schematic model of bicellular pollen development in angiosperms is depicted in Fig. 3. The developmental process consists of two successive phases: microsporogenesis, the formation of four haploid microspores by meiosis; and microgametogenesis, the transformation of unicellular microspores into mature microgametophytes (Borg and Twell 2011). During microsporogenesis, L2-derived diploid sporogenous cells differentiate into pollen mother cells (PMCs) that are surrounded by a primary cell wall, predominantly composed of cellulose, hemicellulose, pectin, and glycoprotein (Albersheim et al. 2010). Subsequently, a callose wall forms between the plasma membrane and primary cell wall (Borg and Twell 2011). At this stage, an anther locule, the space between PMCs, is formed and filled by a locular fluid (Pacini 1997). Within the callose wall, PMCs undergo two successive nuclear divisions (meiosis I and II) to produce a tetrad, four haploid microspores in a tetrahedral arrangement. The microspores are released from the tetrad by callase secreted by the tapetum (Lu et al. 2014). Microgametogenesis begins with the expansion of the microspore, which is usually associated with the fusion of multiple vacuoles (Borg and Twell 2011). Vacuole formation is accompanied by repositioning of the microspore nucleus to an eccentric site against the microspore wall (Pacini et al. 2011). The polarized microspore then divides by mitosis I into a large vegetative cell and a generative cell (Pacini et al. 2011). The generative cell is subsequently engulfed by the cytoplasm of the vegetative cell by digestion of the hemispherical callose wall separating the two cells, to give a unique cell-within-a-cell structure (Borg and Twell 2011). After mitosis I, the vegetative cell differentiates to establish a dehydration resistant cell capable of extending a pollen tube (Borg and Twell 2011). The generative cell undergoes a further round of mitotic division (mitosis II) to produce a pair of sperm cells (Eady et al. 1995). During pollen maturation, the vegetative cell accumulates carbohydrates to support the active metabolism required for germination and pollen tube growth

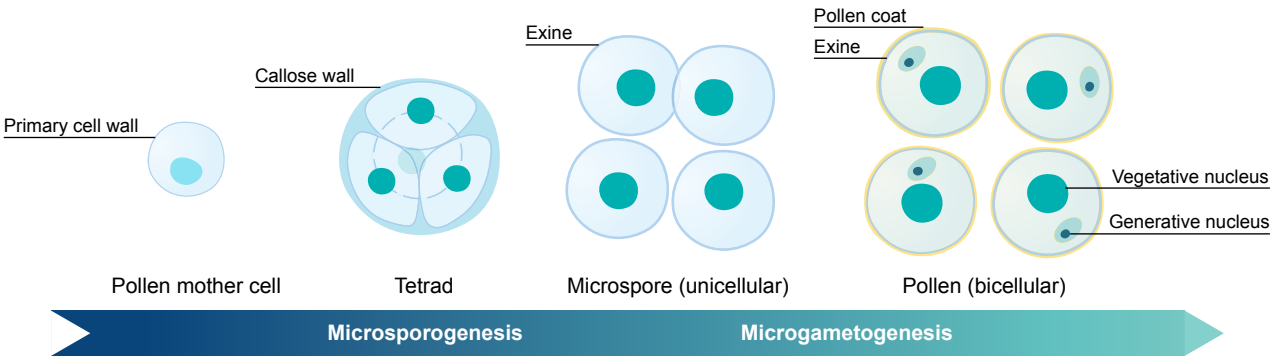

Fig. 3 Microsporogenesis and microgametogenesis in angiosperms (revised from Fig. 3 in Borg and Twell 2011).

(Pacini 1996). Osmoprotectants, such as disaccharides, proline, and glycine-betaine, also accumulate to protect vital membranes and proteins from dehydration damage (Borg and Twell 2011).

The bi and tricellular categorizations of pollen do not apply to gymnosperm pollen grains, which can contain several cells (Pacini et al. 1999). In gymnosperms, microgametogenesis begins within microsporangia where diploid microsporocytes or PMCs undergo meiosis to form tetrads of haploid microspores (Singh 2006). After the meiosis, a variable number of asymmetric mitosis arise differentiated cells, including antheridial, prothallial, tube, and sperm cells (Singh 2006; Vázquez-Lobo 2009). The number of cells in shed pollen varies between lineages from one to five, and gametes are absent since its differentiation occurs after pollination (Pacini et al. 1999).

1.3. Pollen wall assembly

Assembly mechanism of exine: A model based on colloid chemistry

Pollen wall development is initiated at the tetrad stage through the deposition of a primexine, a glycocalyx-like material, which functions as a scaffold for exine (Fig. 4; Ariizumi and Toriyama 2007, 2011; Blackmore et al. 2007). Proexine, incipient exine, has been proposed to self-assemble in the colloidal system of primexine (Gabarayeva 2000; Gabarayeva and Hemsley 2006; Hemsley et al. 2003; Hemsley and Gabarayeva 2007), consistent with the observations that exine remains fluid until late in pollen development (Rowley and Skvarla 2007; Gabarayeva et al. 2009b). Primexine is predominantly composed of amphilic glycoproteins (Heslop-Harrison 1968b; Li et al. 2017b); capable of self-assembly into micelle mesophases.

Amphiphiles form spherical micelles in aqueous solvents, as their concentration reaches the critical micelle concentration (Israelachvili et al. 1976). These micelles vary in shape, depending on

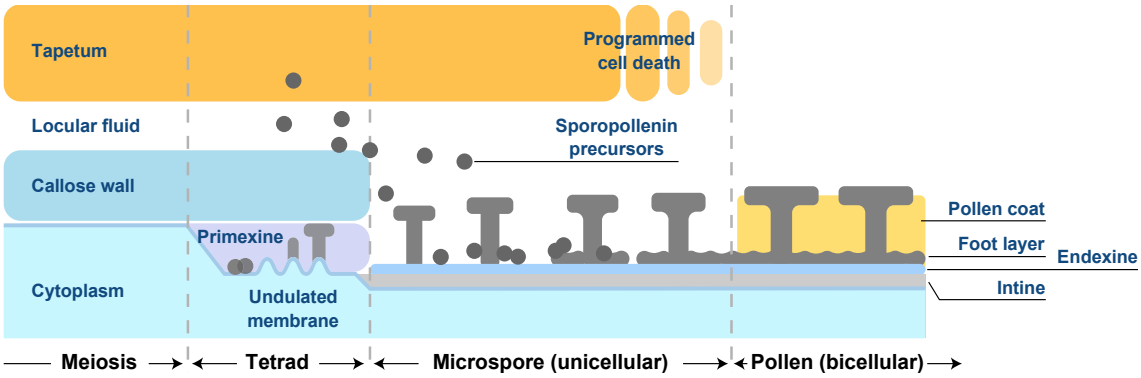

Fig. 1 Angiosperm pollen wall developmental process (redrawn from Fig. 3 in Ariizumi and Toriyama 2011).

the concentration; increasingly higher concentrations cause the spherical micelles to aggregate into the cylindrical micelles (Zana 2005), which can self-assemble into hexagonally arranged cylindrical micelles (hexagonal phase) (Zana 2005). Further increases of the concentration lead to their reconfiguration into lamellar micelles (neat phase) (Zana 2005). These self-assembly processes are implicated in pollen wall development; and the various micelle shapes may reflect considerable variation in exine ultrastructure (Hemsley and Gabarayeva 2007). Recently, the involvement of self-assembly processes in exine development has been supported by *in vitro* simulations of endexine-, bacula-, and tectum-like microarchitectures within the colloidal mixture of mimicking substances (Gabarayeva and Grigorjeva 2013, 2016).

Assembly of proexine: Tetrad period

Primexine develops in the periplasmic space between callose wall and plasma membrane at tetrad stage (Fig. 4; Heslop-Harrison 1968a; Polevova 2014; Punt et al. 2007). After meiosis and simultaneous cytokinesis, callose deposition forms a callose wall around each of the four microspores (Heslop-Harrison 1968a; Sanders et al. 1999). The microspore Golgi vesicles deliver primexine (i.e., glycoproteins and lipopolysaccharides) into the periplasmic space (radial extent, approximately 500 nm) by exocytosis, increasing their concentrations in the peripheral cytoplasm (Gabarayeva and Grigorjeva 2002; Gabarayeva et al. 2003, 2009a; Rowley 1973; Rowley et al. 1981; Suárez-Cervera et al. 1995). At the early tetrad stage, a primexine (radial extent, approximately 100 nm) covers the plasma membrane of the microspore (Gabarayeva et al. 2003, 2009a) and functions as an elaborate matrix in which the patterned accumulation of sporopollenin precursors and their subsequent polymerization take place. Slightly later, the plasma membrane surface ceases to be flat (Heslop-Harrison 1968a; Paxson-Sowders et al. 1997); the raised areas provide the anchoring site for the basis of bacula (probacula) (Li et al. 2017b; Paxson-Sowders et al. 1997). Spherical globules appear in the primexine at this stage (Gabarayeva and Grigorjeva 2004, 2017; Gabarayeva et al. 2011, 2014, 2018; Hemsley and Gabarayeva 2007; Suárez-Cervera et al. 1995). As primexine consists mainly of glycoproteins, the globules have been presumed to be spherical micelles (Gabarayeva and Hemsley 2006).

At the beginning of middle tetrad stage, the globules gradually transform into cylindrical units that predestined to be probaculae (Gabarayeva et al. 2003, 2011, 2014). The transformation has been interpreted as a mesophase transition from spherical to cylindrical micelles (Gabarayeva and Hemsley 2006; Hemsley and Gabarayeva 2007; Polevova 2011). As the cylindrical units increase in height and width, the principal structural feature of probacula is established within the primexine

(Gabarayeva et al. 2003, 2009a, 2013a). The probaculae appears as a tuft of cylindrical units (Gabarayeva et al. 2003, 2011; Grigorjeva and Gabarayeva 2018) and displays a hexagonal pattern in its cross section, likely corresponding to the hexagonal arrangement of cylindrical micelles (Ben Nasri-Ayachi and Nabli 2009; Gabarayeva and Grigorjeva 2004; Gabarayeva et al. 2009a, 2010, 2016a).

During the middle tetrad stage or microspore stage, secretory tapetum accumulates orbicles, called Ubisch bodies, and releases them into the anther locule (Gabarayeva and Grigorjeva 2017; Grigorjeva and Gabarayeva 2015). The Ubisch bodies are a mechanism by which sporopollenin precursors are transported between the tapetum and developing microspores (Huysmans et al. 1998). Histochemical studies showed that Ubisch bodies contain acidic and neutral polysaccharides, unsaturated lipids, and glycoproteins (El-Ghazaly and Jensen 1987; Suárez-Cervera et al. 1995). Numerous Ubisch bodies are observed in the tapetal cytoplasm and anther locule, as well as in the primexine, in this period (Gabarayeva and Grigorjeva 2011; Gabarayeva et al. 2009a, b; Suárez-Cervera et al. 1995). Correspondingly, roundish particles called sporopollenin acceptor particles (SAPs) deposit on the top of primexine and along the probacula, at around the middle tetrad stage (Gabarayeva and Grigorjeva 2004; Kirkpatrick and Owen 2013; Rowley et al. 1999; Tsou and Fu 2002). The SAPs are believed to contain enzymes that catalyze the polymerization of sporopollenin precursors (Gabarayeva and Grigorjeva 2004; Gabarayeva et al. 2018; Grigorjeva and Gabarayeva 2018), as histochemical analyses showed that SAPs contain proteins (Rowley et al. 1999). Sporopollenin precursors are accumulated in the primexine, wherein they polymerize, likely associated with SAPs. At the middle or late tetrad stage, the discontinuous protectum and profoot layer are observed (Gabarayeva et al. 2003, 2009a, 2013a, 2018; Grigorjeva and Gabarayeva 2018). The formation of protectum and profoot layer has been suggested to be due to the initial sporopollenin accumulation on the proximal ends of the probaculae (Blackmore et al. 2010; Gabarayeva and Grigorjeva 2011; Gabarayeva et al. 2003, 2009a).

At the late tetrad stage, a primordial endexine (proendexine) bears inward to the primexine (Gabarayeva and Grigorjeva 2011; Grigorjeva and Gabarayeva 2018). The proendexine develops upon distinctive tripartite lamellae (Rowley and Southworth 1967), also known as lamellae with a "white line in the center", as seen in TEM observations (Furness et al. 2002; Gabarayeva and El-Ghazaly 1997). The distinctive tripartite lamellae have been interpreted as lamellar micelles, wherein the central white line corresponds to a hydrophilic molecular tail (Gabarayeva and Grigorjeva 2011; Gabarayeva et al. 2013b; Grigorjeva and Gabarayeva 2018; Polevova 2011). Slightly later, the callose wall initiates its dissolution by tapetum-derived callase (Gabarayeva and

Grigorjeva 2018; Sanders et al. 1999). By the end of the tetrad stage, the structural elements of the proexine have been established (Blackmore et al. 2010). The primexine is usually absent at aperture sites, and proexine is correspondingly not developed (Grigorjeva and Gabarayeva 2018).

In Arabidopsis, several genes have been demonstrated to affect the primexine formation at the tetrad stage (Shi et al. 2015), such as *DEFECTIVE IN EXINE FORMATION1* (*DEX1*, described in detail below); *EXINE FORMATION DEFECT* (*EFD*), which encodes a *de novo* DNA methyltransferase; *MALE STERIITY1* (*MS1*), which encodes a plant homeodomain-type finger protein; *NO EXINE FORMATION1* (*NEF1*), which encodes a plastid integral membrane protein; *NO PRIMEXINE AND PLASMA MEMBRANE UNDULATION* (*NPU*), which encodes a plasma membrane protein; and *RUPTURED POLLEN GRAIN1* (*RPG1*), which encodes a membrane-localized sugar transporter (Ariizumi et al. 2004, 2005; Chan et al. 2012; Guan et al. 2008; Hu et al. 2014). *DEX1* is expressed in the early tetrad period and encodes a putative plasma membrane-associated protein that contains several calcium-binding domains (Paxson-Sowders et al. 2001). The pollen development of *dex1* mutants is broadly defective; primexine deposition is delayed and reduced; the undulating patterns of the plasma membrane are absent; and the sporopollenin aggregation is irregular (Paxson-Sowders et al. 2001). These authors suggested three possible roles for DEX1: as a linker protein that participates in attaching either the primexine or sporopollenin precursors to the plasma membrane; as a primexine component involved in the polymerization of sporopollenin; or as a part of the rough endoplasmic reticulum (ER) involved in processing and/or transport of primexine components to the membrane (Paxson-Sowders et al. 2001). A putative ortholog of Arabidopsis *DEX1*, *OsDEX1*, has been identified in rice (*O. sativa*) by phylogenetic analyses (Yu et al. 2016). *OsDEX1* is expressed in microspores during the early tetrad period and was hypothesized to play a fundamental role in modulating Ca^{2+} homeostasis within primexine; experiments with recombinant OsDEX1 having been shown to bind Ca^{2+} and regulate its homeostasis *in vitro* (Yu et al. 2016). The modulation of Ca^{2+} concentration within primexine by DEX1 may contribute the shape taken on by the micelle during developmental processes (Blackmore et al. 2007).

Exine maturation and intine formation: Microspore period

Upon release of the microspores from the callose wall, sporopollenin precursors progressively accumulate in the core of proexine, increasing in its thickness (Gabarayeva and Grigorjeva 2017; Gabarayeva et al. 2009b, 2018; Jiang et al. 2012). The mature exine structure is visually completed by the late microspore stage (Ariizumi and Toriyama 2011).

Once the exine has matured, the intine falls under the control of the microspore (Gabarayeva et al. 2009b, 2011). Globular, microfibrillar, and/or lamellar intine structures are thought to reflect the transitive micelle mesophases of the glycoproteins that self-assemble into those structures (Gabarayeva and Grigorjeva 2010, 2011; Gabarayeva et al. 2010, 2016b; van der Ham 1991; Simpson 1989). An immunohistochemical study confirmed that glycoproteins are also distributed in intine (Suárez-Cervera et al. 2005), where they are hypothesized to be responsible for micelle formation.

At a late stage of pollen development, tapetal proplastids begin to differentiate into one of two types of specialized plastids, elaioplasts and tapetosomes (Clément and Pacini 2001; Hsieh et al. 2003; Piffanelli et al. 1998; Quilichini et al. 2014a). Elaioplasts are filled with steryl ester-rich globules maintained by plastid lipid-associated proteins (Wu et al. 1999). Tapetosomes are ER-derived storage organelles that produce a plethora of metabolites, including alkanes and triacylglycerol-rich oil droplets, which are structurally maintained by oleosins and surrounded by vesicles associated with flavonoids (Hsieh and Huang 2004, 2005, 2007). As the tapetal cells that make up the programmed cell death, their cellular contents, including the components in these organelles, are released into the anther locule to coat the pollen (Vizcay-Barrena and Wilson 2006; Parish and Li 2010; Section 1.4). The developmental process described above seems to be conserved across vast range of taxa from aquatic to land angiosperms (Blackmore et al. 2007; Gabarayeva and El-Ghazaly 1997; Gabarayeva and Grigorjeva 2002, 2004; Gabarayeva et al. 2003, 2009a, b, 2010; Gómez et al. 2015; Kreunen and Osborn 1999; Scott 1994; Southworth and Jernstedt 1995).

Aperture formation

The aperture pattern of pollen grains is precise, with a certain number of apertures placed at distinct positions (Furness and Rudall 2004; Kuprianova 1967), indicating that developing pollen possess robust mechanisms that designate particular membrane domains as the future aperture sites. Recently, the *INAPERTURATE POLLEN1* (*INP1*) protein of Arabidopsis was characterized as an essential aperture factor, the pollen grains of *inp1* null mutants having been found to completely lack apertures (Dobritsa and Coerper 2012; Reeder et al. 2016). After meiotic cytokinesis, INP1 aggregates at the interface between the plasma membrane and the callose wall, which prevent exine formation at the sites destined to be apertures (Dobritsa and Reeder 2017; Dobritsa et al. 2018). Putative INP1 homologs have been found in most angiosperms with available genomic or transcriptomic data (Dobritsa and Coerper 2012); therefore, the involvement of INP1 in aperture formation has been suggested to be evolutionarily conserved, despite the significant divergence of

aperture patterns (Li et al. 2018).

Sporopollenin: Chemical composition and biosynthesis pathway

Sporopollenin is a biopolymer that resists physical, biological, and chemical degradation, and fortifies pollen grains (Mackenzie et al. 2015). Although its chemical structure remains unclear due to its insolubility and inertness (Domínguez et al 1999), pyrolysis-GC-MS experiments identified *p*-coumaric acid and ferulic acid as components of the sporopollenin of broad bean, silver birch, stinking hellebore, and Scots pine (Rozema et al. 2001). Phenolics and aliphatic derivatives have been identified as the chemical degradation products of sporopollenin by FT-IR, NMR, and X-ray photoelectron spectroscopies (Ahlers et al. 2000, 2003; Bubert et al. 2002). Solid state 13C NMR spectroscopy confirmed that the oxygen atoms in sporopollenin are present in ether, aliphatic and phenolic hydroxy, carboxy, and ester groups (Ahlers et al. 2000; Guilford et al. 1988). Covalent coupling of the monomeric units of sporopollenin by ether linkage may be responsible for the chemical resistance (Ahlers et al. 2000).

Recent genetic and biochemical approaches primarily in Arabidopsis have identified a number of genes encoding key enzymes required for sporopollenin biosynthesis, i.e., *MALE STERILITY2* (*MS2*), *ACYL-COENZYME A SYNTHETASE5* (*ACOS5*), *CYTOCHROME P450*s (*CYP703A2* and *CYP704B1*), *POLYKETIDE SYNTHASE*s (*PKSA* and *PKSB*), *TETRAKETIDE α-PYRONE REDUCTASE1* (*TKPR1*) (Fig. 5; Ariizumi and Toriyama 2011; Quilichini et al. 2015). *MS2* was first identified as a gene required for exine formation, based on abnormalities in exine formation and a severe reduction in male fertility in the *ms2* mutant (Aarts et al. 1997). MS2 is characterized as a fatty acyl-acyl carrier protein (ACP) reductase localized to the plastid of tapetal cells, which reduces fatty acyl-ACP substrates into the corresponding fatty alcohols (Chen et al. 2011). Fatty acyl-ACP can be also hydrolyzed by fatty acyl thioesterase to release free fatty acids in plastid stroma (Li et al. 2015). ACOS5 functions as a medium- to long-chain fatty acyl-CoA synthetase, with a preference for hydroxy fatty acids as the substrate (de Azevedo Souza et al. 2009). The *acos5* mutant microspore is devoid of exine and exhibits sterility, indicating the crucial role of ACOS5 in exine formation (de Azevedo Souza et al. 2009; Xie et al. 2017). Free fatty acids have been expected to be exported from the plastids prior to the esterification by ACOS5 (Quilichini et al. 2015). CYP703A2 and CYP704B1, which catalyze the in-chain and ω-hydroxylation of fatty acids, respectively, have also been implicated in sporopollenin biosynthesis, as *cyp703a2* and *cyp704b1* mutants exhibit the absence of exine and abnormal exine, respectively (Dobritsa et al. 2009; Morant et al. 2007a). Coexpression analysis resulted in the identification of *PKSA* and *PKSB*, which are coexpressed with

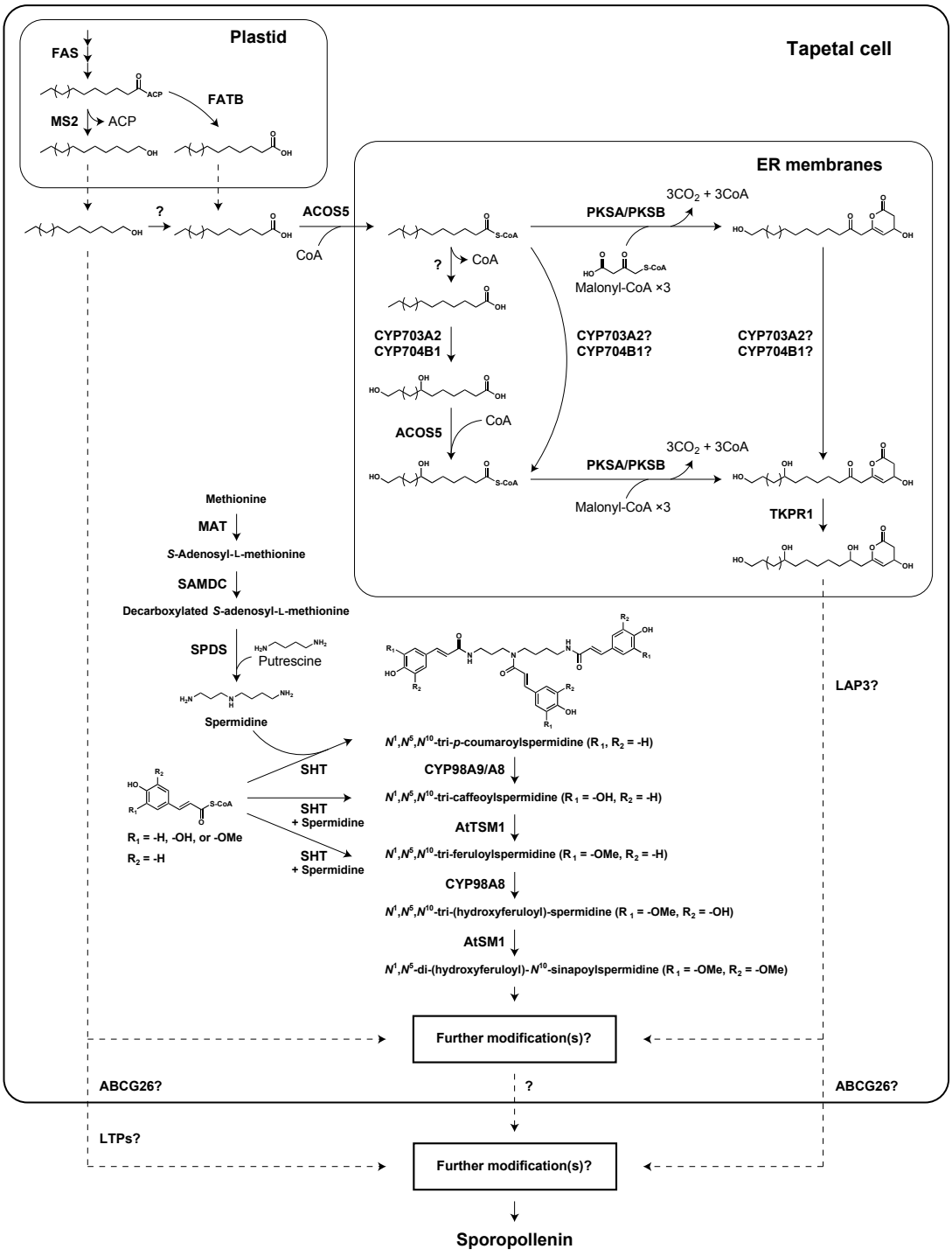

Fig. 2 Proposed biosynthesis pathway of sporopollenin. ABCG26, ATP-binding cassette subfamily G member 26; ACOS5, acyl-CoA synthetase 5; ACP, acyl carrier protein; AtTSM1, *Arabidopsis thaliana* tapetum-specific methyltransferase 1; CYP, cytochrome P450; FAS, fatty acid synthetase; FATB, fatty acyl thioesterase B; LAP3, LESS ADHERENT/ADHESIVE POLLEN 3; LTP, lipid transfer protein; MAT, methionine adenosyltransferase; Me, methyl; MS2, MALE STERILITY2; PKSA, polyketide synthase A; PKSB, polyketide synthase B; SAMDC, *S*-adenosyl-L-methionine decarboxylase; SHT, spermidine hydroxycinnamoyl transferase; SPDP, spermidine synthase; TKPR1, tetraketide α-pyrone reductase 1.

ACOS5 (Dobritsa et al. 2010; Kim et al. 2010). Recombinant PKSA and PKSB generated tri and tetraketide α-pyrones *in vitro* from a broad range of ACOS5-catalyzed products and malonyl-CoAs (Kim et al. 2010). A mutation of either *PKSA* or *PKSB* results in abnormal exine patterning, and the double *pksa pksb* mutant lacked exine deposition and subsequently collapsed, causing male sterility (Dobritsa et al. 2010; Kim et al. 2010). *PKSA* and *PKSB* work downstream of ACOS5 (Grienenberger et al. 2010; Kim et al. 2010). *TKPR1* is also coexpressed with *ACOS5* (Tang et al. 2009), and recombinant TKPR1 reduces the ketone functional group of tetraketide α-pyrones produced by PKSA and PKSB in the presence of NADPH. Male sterility and severely malformed exine are observed in *tkpr1* mutants, implying that TKPR1 plays a crucial role in sporopollenin biosynthesis, acting downstream of PKSA and PKSB (Grienenberger et al. 2010).

Lallemand et al. (2013) demonstrated the colocalization and interactions of ACOS5, CYP703A2, CYP704B1, PKSA, PKSB, and TKPR1 in the ER of tapetum. All these enzymes are encoded by genes that were found to be clustered together (Fig. 5; Pearce et al. 2015), and are thought to catalyze a series of biosynthetic reactions yielding polyhydroxylated tetraketide α-pyrones in the ER of tapetum, which serve as sporopollenin precursors (Grienenberger et al. 2010; Quilichini et al. 2014b). Polyhydroxylated tetraketide α-pyrones likely enable the formation of ester and ether linkages with other units such as phenylpropanoids (Dobritsa et al. 2009; Morant et al. 2007a). The biosynthetic pathway from fatty acids to sporopollenin units is hypothesized to have arisen early in land plant evolution, putative orthologs of *ACOS5*, *CYP703A2*, *CYP704B1*, *PKSA*, and *PKSB* having been found in spreading earthmoss, gymnosperms, and angiosperms (de Azevedo Souza et al. 2008, 2009; Grienenberger et al. 2010; Kim et al. 2010; Morant et al. 2007a; Varbanova et al. 2003).

Several genes encoding enzymes that participate in the phenylpropanoid pathway also affect the composition of exine, i.e., *CINNAMATE 4-HYDROXYLASE* (*C4H*) and *4-COUMARATE-COENZYME A LIGASE 3* (*4CL3*) (Quilichini et al. 2015). The initial three reactions in the general phenylpropanoid pathway catalyzed by phenylalanine ammonia-lyase (PAL), C4H, and 4CL are essential for the synthesis of flavonoids, monolignols, sinapate esters, and lignans (Fraser and Chapple 2011; Vogt 2010). The mutations in *C4H* and *4CL3* result in deficiencies in sporopollenin deposition, with notable reduction in the flavonoid content (Dobritsa et al. 2011; Schilmiller et al. 2009). Spermidine hydroxycinnamoyltransferase (SHT) catalyzes the conjugation of spermidine to hydroxycinnamoyl-CoA, with substrate preference for *p*-coumaroyl-, caffeoyl-, and feruloyl-CoAs (Dobritsa et al. 2011; Grienenberger et al. 2009). The *sht* knockout mutant displays the abnormally crushed phenotype of pollen grains, indicating that the hydroxycinnamoylspermidine derivatives are also components of sporopollenin (Fig. 5; Grienenberger et al. 2009).

Translocation from tapetum to microspores

In plants with secretory tapeta, the spatial separation of microspores from the tapetum requires the translocation of sporopollenin precursors during pollen wall development. Several Arabidopsis ATP-binding cassette G (ABCG) transporters are specifically expressed in tapetal plasma membrane and implicated in the transport of sporopollenin precursors (Zhao et al. 2016). For example, ABCG26 has been identified in Arabidopsis, which is responsible for the transport of tetraketide as a sporopollenin precursor from the tapetum to the surface of microspores (Kuromori et al. 2011; Quilichini et al. 2010, 2014b). The *abcg26* mutant lacks exine and exhibits severely reduced male fertility (Quilichini et al. 2010). Similarly, ABCG1 and ABCG16 are hypothesized to be the transporters of sporopollenin precursors, which are required for nexine development (Yadav et al. 2014). Rice ABCG15, an ortholog of Arabidopsis ABCG26, was shown to be required for exine formation, suggesting the role of ABCG in the transport of sporopollenin precursors to be conserved (Niu et al. 2013; Qin et al. 2013).

Arabidopsis ABCG9 and ABCG31 transporters localize to the tapetal plasma membrane (Choi et al. 2014). Neither of the single mutants *abcg9* or *abcg31* displayed any visible defects, whereas the double mutant *abcg9 abcg31* exhibited an incomplete pollen coat, indicating the collaborative function of ABCG9 and ABCG31 (Choi et al. 2014). ABCG9 and ABCG31 may participate in the specific transport of steryl glycosides from the tapetum to the pollen coat, as steryl glycosides in the double mutant pollen are reduced to about half amount of wild type level (Choi et al. 2014).

Several lipid transfer proteins (LTPs) have been noted for their anther- or tapetum-specific expression pattern in Arabidopsis and rice (Huang et al. 2009; Jiang et al. 2012; Li et al. 2017a). For example, *ARABIDOPSIS THALIANA ANTHER 7* (*ATA7*), encoding an LTP-related protein, expresses tapetum-specifically after meiosis (Rubinelli et al. 1998). The expression of three genes encoding type III LTPs (At5g62080, At5g07230, and At5g52160) are also restricted to the tapetum (Huang et al. 2013). At the early tetrad stage, the type III LTP (At5g62080) appears in the tapetum; it is subsequently secreted via the ER-trans-Golgi network machinery into the locule, and then accumulates on the microspore surface to remain as a component of exine (Huang et al. 2013). The double RNAi silencing of *At5g62080* and *At5g07230* exhibited abnormal intine and dehydration-sensitive pollen, presumably as a consequence of abnormality in exine (Huang et al. 2013). Either LTPs-alone or -bound sporopollenin precursors appear to be assembled into exine.

Altogether, polyhydroxylated tetraketide α-pyrones yielded by the sequential enzymatic reactions of ACOS5, CYP703A2, CYP704B1, PKSA, PKSB, and TKPR1 or further modified precursors by unknown reactions are transported into the anther locule, possibly by the ABCG transporters and/or

the LTPs, for in vivo polymerization into the exine (Fig. 5; Quilichini et al. 2015). However, the mechanism underlying transport of sporopollenin precursors such as hydroxycinnamoylspermidine derivatives remains elusive (Quilichini et al. 2015; Zhao et al. 2016).

1.4. Pollen coat

The pollen of many plant species is characterized by a lipidic extracellular coating, and accounts for as much as 10–15% of the total mass of a pollen grain (Piffanelli et al. 1997). There are two types of pollen coat: pollenkitt, most common in angiosperms; and tryphine, which appears to be restricted to Brassicaceae (Pacini and Hesse 2005). Both types of pollen coats originate from the tapetum, but pollenkitt differs from tryphine in the ontogenesis and also in that tryphine contains remnants of tapetal organelles (Pacini 1997; Punt et al. 2007).

In the case of pollenkitt, the whole process of degeneration occurs inside the tapetal protoplasts (Hesse 1981). The tapetal plasma membrane ruptures after all the tapetal organelles have degenerated and intermingled, at the final stage of pollen maturation (Pacini and Hesse 2005). Pollenkitt can coexist with Ubisch bodies, whereas tryphine has never been observed with those (Pacini and Hesse 2005). In the case of tryphine, the tapetal plasma membrane disappears during the microspore period to disperse their cytoplasmic contents including intact organelles in the anther locule (Pacini and Franchi 1992, 1993; Piffanelli et al. 1998). The contents merge around the pollen grains and degenerate into tryphine (Pacini and Hesse 2005); hence, tryphine is usually less homogenous compared to pollenkitt (Murphy 2006; Pacini and Hesse 2005). Pollenkitt is produced by the tapetum, irrespective of its type (secretory and amoeboid), whereas tryphine is always produced by amoeboid tapetum (Pacini 1997).

Pollenkitt is a hydrophobic mixture of saturated and unsaturated lipids, pigments, carbohydrates, and proteins (Dickinson et al. 2000; Gong et al. 2015; Gould and Lister 2006; Hesse 1993; Lunau 1995; Parkinson and Pacini 1995; Santos et al. 2003; Weber 1996; Wiermann and Gubatz 1992). Although the chemical composition seems to vary between plant species, it has been little studied (Pacini and Hesse 2005). Tryphine is a complex mixture of hydrophobic and hydrophilic (Dickinson and Lewis 1973; Parkinson and Pacini 1995) neutral lipids, volatile lipid derivatives, free fatty acids, very-long-chain wax esters, flavonoids, alkanes, and hydroxycinnamoylspermidine derivatives (Dobson 1988; Quilichini et al. 2015; Rejón et al. 2016; Wu et al. 1997, 1999; Zinkl et al. 1999), as well as a number of proteins, the majority of which are either oleosin or self-incompatibility proteins

(Kim et al. 2002; Mayfield et al. 2001; Piffanelli and Murphy 1998). Many of these components accumulate in tapetosomes and elaioplasts during pollen development (Quilichini et al. 2015; Section 1.3).

Despite the differences in ontogenesis and constitution of pollenkitt and tryphine, they share many functions (Hesse 2000, 2010; Pacini and Franchi 1993; Pacini and Hesse 2005), as described below.

Adhesion

The pollen coat is responsible for holding the pollen grain onto the anther wall, until dispersal; even in upside down anthers such as the blue passionflower, and vertical anthers such as the bear's breeches (Pacini and Hesse 2005). In the dandelion, the pollenkitt-coated pollen grains show significantly higher adhesive force in the range of 190–310 nN, compared to approximately 45 nN of the corresponding pollen without pollenkitt (Lin et al. 2013). Pollen surface morphology (size and shape of echinate or reticulate ornamentations) also contributes to the adhesive force (Lin et al. 2013), in addition to the physicochemical properties of the pollen coat. Similarly, pollen coat enables pollen to adhere to pollinator bodies and stigma (Heizmann et al. 2000). For example, honeybees (*Apis mellifera*) can collect only half as many pollen grains when the pollenkitt is removed (Amador et al. 2017). Stigma exudates, mainly composed of lipids and proteins, are also expected to facilitate the adhesion (Rejón et al. 2014).

Protection of male gametes

The pollen coat must also protect the male gametes. Pollen grains are susceptible to excessive dehydration (Franchi et al. 2011; Taylor and Hepler 1997), and the hydrophobic pollen coat protects them against desiccation to a far greater extent than exine (Edlund et al. 2004; Murphy 2006). This property is imparted mainly by the lipidic components of pollen coat; for example, three fatty acids (palmitic acid, linolenic acid, and stearic acid) of rice pollenkitt have been reported to be responsible for preventing excessive dehydration (Xue et al. 2018).

Most plant species undergo anthesis during the day, so that pollen is exposed to sunlight. Ultraviolet (UV) radiation, especially UV-B, can damage plants (Jansen et al. 1998; Section 7), and reductions in pollen viability under excessive UV-B radiation has been observed in many taxa (Feng et al. 2000; Torabinejad et al. 1998; Zhang et al. 2014). Flavonoids, with absorption maxima in the UV-B region, have been identified as major pigments in pollen coat (Linskens 1964), which has been hypothesized to protect pollen against UV radiation (Harborne and Williams 2000; Pacini and Hesse 2005). In Arabidopsis, a mutation in *TRANSPARENT TESTA 4* (*TT4*) yielded pollen grains

considerably more susceptible to UV-B irradiation than wild-type; given that the *TT4* gene encodes chalcone synthase, a key enzyme of flavonoid biosynthesis, this suggests that flavonoids in tryphine protect pollen from solar UV-induced damage (Hsieh and Huang 2007).

Attraction of pollinating animals

Flower visitors exhibit positive behavioral reaction to the visual cue of pollen (Lepage and Boch 1968; Lunau 1988, 1991, 1992, 2000; Lunau and Wacht 1994). Pollen varies in color, depending on plant species; violet, blue, green, yellow, red, as well as a variety of intermediate colors are all known (Reiter 1947), and these colors serve as a visual cue to pollinators (Lunau 2000; Nicholls and Hempel de Ibarra 2014). Yellow is by far the most common color, derived from flavonoids and carotenoids (Lunau 1995; Wiermann and Vieth 1983), and the following compounds have been identified as yellow pigments in pollen coats: kaempferol, quercetin, isorhamnetin, myricetin, taxifolin, and their derivatives (all flavonoids) (Ceska and Styles 1984; Tomás-Lorente et al. 1992; Wiermann 1981; Zerback et al. 1989); and α- and β-carotenes, flavoxanthin, antheraxanthin, lutein, and auroxanthin (all carotenoids) (Stanley and Linskens 1974). Anthocyanins, such as the glycosides of delphinidin, petunidin, pelargonidin, cyanidin, and malvidin, are responsible for the coloration of blue pollen, i.e., the tree fuchsia, the poppy anemone, and the Paterson's curse (Di Paola-Naranjo et al. 2004; Stanley and Linskens 1974; Webby and Bloor 2000).

Pollen odor, which originates from pollen coat, can be an olfactory cue to pollinators in addition to those provided by flower itself (Dobson 1988; Dobson and Bergström 2000; Nicholls and Hempel de Ibarra 2016). Bees are capable of distinguishing pollen odors from that of the whole flower (Carr et al. 2015; Dobson et al. 1999), implying that pollen and flowers exude odor bouquets that differ in composition (Dobson and Bergström 2000; Dobson et al. 1996). Chemical analyses of the pollen headspace have identified three major classes of volatile compounds: fatty acid derivatives, isoprenoids, and benzenoids; the exact composition of which is species-specific (Dobson and Bergström 2000; Knudsen et al. 1993). For example, the hexane extract of pollenkitt of the Japanese rose contains pentadecane, 2-tridecanone, tetradecanal, hexadecanal, tetradecyl acetate, hexadecyl acetate, isoprenoids (geranial, geraniol, geranyl acetone, citronellyl acetate, neryl acetate, geranyl acetate, and α-farnesene), and benzenoids (2-phenyl ethanol, methyleugenol, eugenol, and 2-phenylethyl acetate) (Dobson 1987; Dobson and Bergström 2000). Pollen-derived olfactory cues have been shown to elicit the foraging behavior of social (*A. mellifera* and *B. terrestris*) and solitary (*Colletes fulgidus*) bees, and beetles (*Bruchus pisorum*, *Zygogramma bicolorata*, and *Meligethes aeneus*) (Beekman et al. 2016; Charpentier 1985; Dobson 1987; Dötterl and Vereecken 2010;

Jayanth et al. 1993; Konzmann and Lunau 2014; Lunau 2000; Pernal and Currie 2002).

Defense against predators and microbial infection

Pollen odorants such as 2-undecanone and 2-tridecanone are known to repel predators such as insects (Farrar et al. 1992; Kennedy et al. 1991; Marr and Tang 1992; Maluf et al. 1997). Pollen odor of anemophilous species, the dropwort, the sheep's sorrel, and the queen sago, contains greater proportion of α-methyl alcohols and α-methyl ketones than that of zoophilous species (Dobson et al. 1996; Pellmyr et al. 1991), which is hypothesized to serve in defense by Dobson and Bergström (2000). Similarly, hydroxycinnamoylspermidines such as *N*',*N*''-di-coumaroyl, -caffeoyl, and -feruloylspermidines, are found in pollenkitt of various taxa and in the tryphine of Arabidopsis (Martin-Tanguy et al. 1978; Meurer et al. 1988a, b; Grienenberger et al. 2009; Walters et al. 2001), and impart anti-fungal and anti-viral activities (Martin et al. 1978; Mayama et al. 1981; von Röpenack et al. 1998; Walters 2003; Walters et al. 2001).

Pollen-stigma recognition

Pollen coat also serves as the medium through which signaling takes place between the stigma and pollen grain (Heslop-Harrison 1975). One such signaling process is the self-incompatibility (SI) response, a self- and nonself-recognition process between pollen and pistil that is followed by selective inhibition of the self-pollen tube development (Murphy 2006; Takayama and Isogai 2005; Section 2). Both the female and male determinants were first identified in the tryphine of the Brassicaceae. The main component of tryphine involved in the recognition and genetic incompatibility response is a peptide (6kDa), called *S*-locus protein 11 (SP11) or *S*-locus Cys-rich protein (SCR) (Hiscock 2000; Schopfer et al. 1999; Takayama et al. 2000; Section 2 about SI). The female determinant is the *S*-locus receptor kinase (SRK), a membrane-spanning Ser/Thr receptor kinase, that is localized to the plasma membrane of stigmatic papilla cells (Takasaki et al. 2000). A specific interaction between SP11/SCR and SRK from the same *S*-haprotype induces the incompatibility response in the stigma, leading to the rejection of self-pollen (Kachroo et al. 2001; Shimosato et al. 2007; Takayama et al. 2001). Several candidate downstream molecular components of the SP11/SCR-SRK self-recognition rejection pathway have been identified, such as *M*-locus protein kinase (MLPK; Murase et al. 2004) and Arm repeat containing 1 (ARC1; Gu et al. 1998; Stone et al. 1999); however, the molecular mechanisms associated with the self-pollen rejection remain unclear (Fujii et al. 2016). Recent studies also identified the male determinant in the pollenkitt of the Rosaceae, Solanaceae, and Plantaginaceae as *S*-locus F-box (SLF) proteins, all of

which share the same female determinant S-RNase (Takayama and Isogai 2005).

Medium at pollen-stigma interface

Within a few minutes of deposition of a pollen grain onto the stigma, the pollen coat flows out from the exine and migrates to the pollen-stigma interface (Elleman and Dickinson 1990; Kandasamy et al. 1994), a process known as coat conversion (Dickinson and Elleman 1985; Elleman and Dickinson 1986). This reorganization is followed by pollen hydration (Firon et al. 2012). The pollen coat is thought to play a role in establishing a conduit that allows water transport from the stigmatic cells, as deficiencies in tryphine lipids lead to the hydration defects in Arabidopsis mutants (Fiebig et al. 2000; Hülskamp et al. 1995; Preuss et al. 1993).

Following hydration, the pollen grain, which initially contains a relatively uniform distribution of organelles, undergoes a cytological reorganization that determines the polarity of pollen tube emergence (Kandasamy et al. 1994). Within 20 minutes of pollination, a pollen tube emerges through an aperture adjacent to the stigma surface (Johnson and Preuss 2002) and invades the expanded papillar cell wall (Kandasamy et al. 1994). Xylanase and β-glucanase are identified from pollenkitt of maize, which hydrolyze the stigma wall for pollen tube entry (Suen and Huang 2007; Suen et al. 2003; Wu et al. 2002).

2. Pollination mechanisms and pollinators

Pollination can be accomplished by self-pollination or cross-pollination. Self-pollination occurs when the pollen is deposited on the female part of genetically identical flower (Acquaah 2012). There are three mechanisms by which self-pollination can take place: autogamy, wherein pollen from one flower is transferred to the female part within the same flower (Frankel and Galun 1977); geitonogamy, wherein pollen is transferred from one flower to the female part of another flower of the same species (de Jong et al. 1993); and cleistogamy, wherein pollen is transferred to the female part before anthesis (Barrett 2010; Lord 1981). Self-pollination is generally accomplished without any biotic pollinator.

Cross-pollination (allogamy) is the pollen transfer from the stamen of one flower to the female part of another flower on a different individual that is not genetically identical (Acquaah 2012). Sexual reproduction in many plant species involves self-incompatibility (SI), which enables the pistil

to recognize and reject self-pollen or pollen from genetically related individuals (Silva and Goring 2001; Watanabe et al. 2012). SI serves to prevent inbreeding, promotes outcrossing by cross-pollination (Barrett 2002; Kumar and McClure 2010; Takayama and Isogai 2005), and has been reported in more than 100 families (i.e., Brassicaceae, Rosaceae, Scrophulariaceae, Solanaceae, and Papaveraceae) and an estimated 39% of flowering plant species (Igric et al. 2008). Cross-pollination is important even in self-compatible species to ensure the genetic diversity (Kumar and McClure 2010), and generally depends on external pollinating agents such as bees.

There are two major modes of pollen dispersal: abiotic, which relies on wind and water (Cox 1988); and biotic, wherein pollination is carried out by animals such as insects, birds, mammals, and reptiles (Abrol 2012; Fægri and van Pijl 1979).

Wind pollination (anemophily) is the dominant type of abiotic pollination (wind:water = 98:2) (Abrol 2012; Ackerman 2000). Anemophilous species are generally unisexual (either monooecious or dioecious) (Abrol 2012), and include almost all gymnosperms, such as pines, firs, and spruces (Owens et al. 1998; Lu et al. 2011). As abiotic pollination is an inefficient process, anemophilous plants have morphologically adapted to maximize pollen dispersal. The ratio of pollen to ovules (P/O) is substantially higher in anemophilous species (median = 22,150:1, quartiles = 9,238:1 and 36,000:1) than those in zoophilous species (median = 3,450:1, quartiles = 1,550:1 and 7,338:1) (Cruden 2000). At least 10% of angiosperms are anemophilous, i.e., grasses, sedges, and rushes (Ackerman 2000; Friedman and Barrett 2009; Whitehead 1968). Several plants such as the maize and the oak are pollinated by both wind and insect (ambophily) (Tchuenguem Fohouo et al. 2004; Radmacher and Strohm 2010; Saunders 2018).

Water pollination (hydrophily) is another mode of abiotic pollination, and achieved either on the water surface (ephydrophily) or in the water (hyphydrophily) (Cox 1988; Du and Wang 2014; Ernst-Schwarzenbach 1944). Ephydrophilous species are common in freshwater and in shallow coastal habitats. Hyphydrophily occurs through water currents in a limited number of aquatic plants, i.e., the horned pondweed and the Scouler's surfgrass (Cox and Tomlinson 1988; Guo et al. 1990; Cox et al. 1992). Previously, seagrasses were regarded as universally hydrophilous; however, benthos pollination (zoobenthophily) was recently discovered to take place in tropical seagrass (van Tussenbroek et al. 2016). The exine of pollen grains of hydrophilic plants is generally reduced, so the grains themselves are less rigid compared to those of terrestrial plants (Cox 1988; Pettitt and Jermy 1975).

Animal pollination (zoophily) is estimated to be required by 87.5% of all angiosperms to reproduce (Ollerton et al. 2011). More than 100,000 animal species play roles in pollinating 250,000

flowering plant species on the Earth (Abrol 2012).

Insect pollination (entomophily) is achieved by diverse groups as follows: beetles (cantharophily), flies (myophily), wasps (sphecophily), bees (melittophily), ants (myrmecophily), butterflies (psychophily), moths (phalaenophily), and thrips (Abrol 2012; Rader et al. 2015; Ollerton 2017). The pollination of approximately 75% of crop species and up to 94% of wild flowering species depends on insects (Klein et al. 2007; Vanbergen and The Insect Pollination Initiative 2013). Insect pollinators can be divided into two categories: generalist and specialist (Johnson and Steiner 2000; Kevan and Baker 1983; Ollerton et al. 2007). Most pollinators exploit floral resources from a variety of plant species; for example, about 70% of bee species are polylectic (Minckley and Roulston 2006; Bosch et al. 2009). Specialists visit only one host species, and have evolved specialized morphological and/or behavioral characteristics to effectively forage from these specific host plants (Bernays 1998). Similarly, most zoophilous plant species can be divided into generalist and specialist. Generalist plants have adapted to attract a wide variety of different pollinators. Specialist plants have often coevolved with a single type of pollinator (Herrera 1996), for example, figs and fig wasps (Wiebes 1979).

In areas with limited insect populations and activities, such as particularly hot, cold, dry, wet and isolated environments, birds serve as essential pollinators (Cruden 1972; Cronk and Ojeda 2008). Bird pollination (ornithophily) is mediated by over 1,000 avian species, such as hummingbirds (trochilophily), honeyeaters, sunbirds, white eyes, and parrots (Cronk and Ojeda 2008; Fang et al. 2012; Huang et al. 2018; Regan et al. 2015).

Mammal pollination (therophily) is accomplished by both flying and non-flying mammals (Rourke and Wiens 1977). Bats are the only mammals capable of flight. Bat pollination (chiropterophily) occurs in about 250 genera of plants; and is far less common than ornithophily (Sekercioglu 2006): at least six families of tropical and subtropical birds visit flowers for feeding nectar; compared with only two families of bats, Pteropodidae and Phyllostomidae, which inhabit the tropical and subtropical regions of Africa, Asia, America, Australia, Papua New Guinea, and certain Pacific islands (Fleming and Muchhala 2008; Fleming et al. 2009). Bats are effective pollinator especially in habitats where insect activity is limited by harsh climatic conditions, i.e., on tropical mountains, rainforest, and swampy habitats (Abrol 2012). Flower-visiting bats bear sharp snouts and long tongues, adapted for feeding nectar (Fleming et al. 2009). Non-flying mammals, such as marsupials (metatherophily), primates, and rodents (sminthophily) are involved in pollination in Australia, Africa, and South America (Carthew and Goldingay 1997). Inflorescences and flowers of certain members of Proteaceae and Myrtaceae in Australia are suggested to be

adapted to pollination by marsupials, rats, and squirrels (Rourke and Wiens 1977). In South Africa, the Northern vampire cup has shown to be sminthophilous, and the short-snouted elephant shrew and the striped field mouse are identified as its pollinators (Johnson et al. 2011). Primates have been identified or suspected as pollinators due to their feeding nectar on flowers, and the foraging behavior of pollinating primates is often nondestructive (Gautier-Hion and Maisels 1994; Pavé et al. 2009; Heymann 2011). However, the knowledge of pollination by the non-flying mammals are still rudimentary (Mayer et al. 2011; Abrol 2012).

Several species of lizards, such as the Madeiran wall lizard, Duvaucel's gecko, and Round Island skink also contribute to pollination and seed dispersion, while feeding on nectar and fruits (Whitaker 1987; Olesen and Valido 2003; Ortega-Olivencia et al. 2012). Previously, lizard pollination was considered to be rare, since most lizard species are carnivorous; it is only recently that their important contributions have come to light (Olesen and Valido 2003).

3. Pollination as an ecosystem service

Ecosystem services are the benefits to human welfare derived from organisms interacting in ecosystems; and are categorized as follows: regulating services, provisioning services, cultural services, and supporting services (Millennium Ecosystem Assessment 2003, 2005). Regulating services are benefits obtained from the regulation of ecosystem processes, i.e., climate regulation, disease regulation, water regulation, water purification, and pollination. Provisioning services are products obtained from ecosystems, i.e., food, fresh water, fuelwood, fiber, biochemicals, and genetic resource. Cultural services are nonmaterial benefits obtained from ecosystems, i.e., spiritual and religious, recreation and ecotourism, aesthetic, inspirational, educational, sense of place, and cultural heritage. Supporting services are services necessary for the production of all other ecosystem services, i.e., soil formation, nutrient cycling, pollination, and primary production.

Pollination, a regulating service, is greatly beneficial to humans both directly (fruit and seed production of crop plants such as alfalfa, apple, cherry, blueberry, raspberry, melon, cucumber, canola, cotton, longan, macadamia, squash, soy, and sunflower (Jha et al. 2013; Klein et al. 2007)); and indirectly (the reproduction of tree species valued for timber, crops in which the vegetative parts are consumed, and vegetatively propagated crops wherein pollinators are required only for breeding) (Jha et al. 2013; Klein et al. 2007; Kondo et al. 2016; White et al. 2002).

As a supporting service, pollination is essential to maintain populations of pollinator-dependent wild plants (Aguilar et al. 2006), and then contribute to the additional ecosystem services through the maintenance, such as erosion control, water filtration, carbon storage, and habitat for biodiversity (Jha et al. 2013; Kreman et al. 2007).

Recently, economic value of pollination service attracts a high degree of attention. The contribution of pollination services to global agriculture has been increasing for the last decades. Lautenbach et al. (2012) estimated the global economic value of wild and managed pollination services at 361 billion USD annually, based on 2009 market prices. In Japan, the economic value of pollination services to crop production was valued at about 4.3 billion USD annually in 2013, which corresponded to 8.3% of gross agricultural production of Japan (Konuma and Okubo 2015).

Although many of the highest volume crops such as rice and wheat are anemophilous (Ghazoul 2005), a large proportion of fruit crops are entomophilous. For example, pollination of rapeseed (Brassicaceae); melon, watermelon, and pumpkin (Cucurbitaceae); apple, pear, strawberry, peach, cherry, and apricot (Rosaceae); coffee (Rubiaceae); grapefruit (Rutaceae); eggplant and tomato (Solanaceae) are highly dependent on insects (Gallai et al. 2009; Klein et al. 2007). Zoophily directly affects the yield and/or quality of approximately 75% of globally important crop types, including most fruits and seeds (Potts et al. 2016). An estimated 5–8% of global crop production would be lost in the absence of animal pollinators (Aizen et al. 2009). In particular, a lot of the Rosaceae crops, such as almond, apple, apricot pear, and plum, are self-incompatible, and therefore cross-pollination with another cultivar by pollinating agents is crucial for the formation of fruit (Hegedűs et al. 2012).

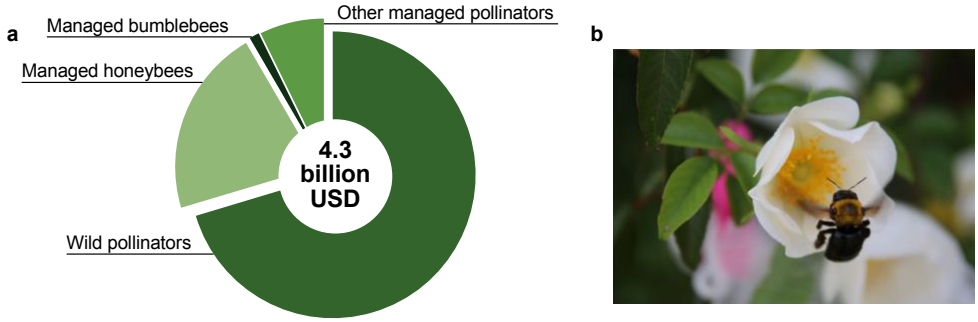

Fig. 3 Contributors to pollination services in Japan, 2013. (a) Composition of contributors to pollination services (revised from Fig. 1 in Konuma and Okubo 2015). (b) Carpenter bee visiting the Cherokee rose (*Rosa laevigata*).

Bees are among the most important pollinators, visiting more than 90% of the leading 107 global crop species (Klein et al. 2007). Over 20,000 bee species have been discovered worldwide (Potts et al. 2016), of which about 12 species are commonly managed for crop pollination, i.e., honeybees (*A. mellifera* and *A. cerana*), bumblebees (*Bombus terrestris* and *B. ruderatus*), the red mason bee (*Osmia bicornis*), and the leafcut bees (*Megachile rotundata*) (Gruber et al. 2011; Mallinger et al. 2017; Russo 2016). Non-bee wild insects are increasingly recognized for their contribution to global pollination services, i.e., flies, butterflies, moths, beetles, thrips, ants, and wasps (Garibaldi et al. 2013; Peñalver et al. 2012; Rader et al. 2015). Indeed, in Japan, 70.4% of pollination services are provided by wild pollinators, and the remaining 29.6% is by managed honeybees (15.4%) and bumblebees (1.1%), wild honeybees (5.8%), and other managed pollinators (7.3%) (Fig. 6; Konuma and Okubo 2015). Vertebrates are also important pollinators, responsible for about 63% of the fruit and seed production of zoophilous plants (Ratto et al. 2018).

A number of studies have addressed recent declines in the population of both wild and managed pollinators, with parallel declines in pollinator-dependent plants (Garibaldi et al. 2013; Potts et al. 2010). Habitat loss and fragmentation, agrochemicals, pathogens, alien species, and climate change, lack of flowers are all hypothesized to be contributory factors (Goulson et al. 2015; Potts et al. 2010; Stanley et al. 2015).

4. Color vision system of pollinators

4.1. Structure of compound eyes

Most insects possess a pair of compound eyes, composed of up to several thousand of ommatidia, each of which contains a cluster of photoreceptor cells surrounded by support cells and pigment cells, and overlaid with a transparent cornea (Land and Chittka 2013). For example, in the worker honeybee (*A. mellifera*), each compound eye consists of about 5,500 ommatidia, with an interommatidial angle of approximately 1.0–1.8° (Barlow 1952). Spatial resolution of compound eyes is defined by interommatidial angles, optical quality, and rhabdom dimensions (Land 1997). Compound eyes can be categorized into two basic types: apposition eye, where the photoreceptors reside within the ommatidium that are isolated from each other; and the superposition eye, where the optical apparatus of the facets is separated from the array of photoreceptors by a clear zone with many facets acting together as a single optical device (Borst 2009). Apposition eyes are most

common in diurnal species such as ants, bees, butterflies, dragonflies, grasshoppers, wasps, whereas superposition eyes are usually found in nocturnal insects such as beetles and moths (Borst 2009; Warrant 2017).

The cuticle covering the ommatidia is colorless and transparent, and usually forms a biconvex corneal lens (i.e., approximately 15–20 μm in diameter in honeybees; Srinivasan 2010). The corneal lenses are usually closely packed together, with an array of hexagonal facets (Kim et al. 2016). Beneath the corneal lenses, there are four cells, called Semper cells, which produce a second lens, the crystalline cone, in many species (Land and Chittka 2013). The crystalline cones are usually surrounded by primary and secondary pigment cells (Gullan and Cranston 2010). Generally, each ommatidium houses eight (in some cases, nine) photoreceptor cells (retinula cells) (Land and Chittka 2013). For example, there are eight photoreceptors (R1–R8) in *Drosophila*, and nine (R1–R9) in *Apis* and *Papilio* (Arikawa 2003; Skrzipek and Skrzipek 1973; Vorobyev and Hempel de Ibarra 2012). Each photoreceptor cell extends microvilli toward the central axis of the ommatidium, which collectively forms a rhabdomere (Land and Chittka 2013). The visual pigment, rhodopsin, is located within the microvillar membrane and involved in visual phototransduction (Gutierrez et al. 2011; Section 4.2). The photoreceptor cells within each ommatidium penetrate the basal membrane as retinal axons that project to the lamina for further processing. Visual information is then conveyed to the next ganglion, the medulla, and eventually to the lobula, where complex analysis of the image takes place, leading to the perception of color, shape, and motion (Chittka and Niven 2009; Srinivasan 2010).

4.2. Visual pigments

Rhodopsins, ligh-sensitive biological pigments, are located in microvillar membrane and composed of a chromophore, retinal, covalently bound to the ε-amino group of a Lys residue of a G-protein, opsin, via a protonated Schiff base linkage (Arikawa and Stavenga 2014; Terakita 2005). The protonated Schiff base is stabilized by a Tyr residue that functions as a counterion (Gutierrez et al. 2011). In vertebrates, the chromophore is commonly 11-*cis* retinal (vitamin A_1), but many insects use 11-*cis* 3-hydroxyretinal (vitamin A_3) (Fig. 7; Vogt and Kirschfeld 1983). Phototransduction is initiated by the absorption of a single photon by 11-*cis* chromophore. Light causes photoisomerization of the chromophore from 11-*cis* to all-*trans* configuration, which causes conversion of rhodopsin into the active metarhodopsin state via a few thermally unstable

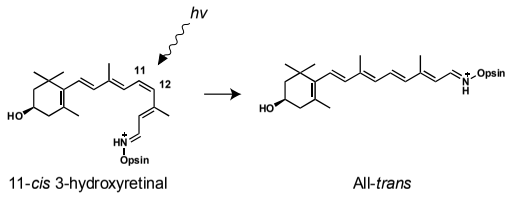

Fig. 4 Photoisomerization of the opsin-bound chromophore in insects.

intermediates (Ernst et al. 2014). In vertebrates, the Schiff base linkage between all-*trans* retinal and opsin is hydrolyzed after light stimulus, and then free all-*trans* retinal is reconverted to 11-*cis* retinal by enzymatic reactions (Ernst et al. 2014; Gutierrez et al. 2011). In insects, the all-*trans* chromophore remains bound to the opsin and is reconverted into 11-*cis* configuration by a photochemical reaction (Gutierrez et al. 2011; Hamdorf 1979; Kiselev and Subramaniam 1994). Metarhodopsin is also photosensitive, absorbing photons at a different wavelength from the rhodopsin; for example, the absorption maxima of the main rhodopsin in *Drosophila* is at 480 nm and the corresponding metarhodopsin at 560 nm (Land and Chittka 2013; Stavenga 2010). A second photon of the higher wavelength catalyzes reconversion from metarhodopsin to inactive rhodopsin (Gutierrez et al. 2011; Kiselev and Subramaniam 1994; Land and Chittka 2013). Under constant light conditions, rhodopsins are in equilibrium with metarhodopsins (Land and Chittka 2013).

Within the opsin family of insects, there are several paralogs (Briscoe 2008; Henze and Oakley 2015; Yuan et al. 2010). The difference in amino acid sequence of each opsin causes a large variation of rhodopsins in absorption wavelength covering the entire visible light spectrum (Ernst et al. 2014). Chromophore-opsin interactions such as electrostatic interactions of retinal with charged, polar, and aromatic amino acids within the binding pocket, have been implicated in the hypsochromic or bathochromic shift of rhodopsins (Ernst et al. 2014).

Pterygote insects typically have three classes of photopigments: UV sensitive (very short wavelength sensitive, VSWS) class with a peak absorbance λ_{max} at 300–400 nm; blue sensitive (short wavelength sensitive, SWS) class with a λ_{max} at 400–500 nm; and green sensitive (middle wavelength sensitive, MWS) class with a λ_{max} at 500–600 nm (Feuda et al. 2016; Land and Chittka 2013). For example, the honeybee (*A. mellifera*) has a trichromatic vision based on three opsins: AmUV, AmB, and AmG (Wakakuwa et al. 2007). The photoreceptor spectral sensitivity is primarily determined by the expressed rhodopsins. Intracellular recordings of the electrical responses of the photoreceptors confirmed their maxima of spectral sensitivities as follows: λ_{UV} at 344 nm, λ_{Blue} at 436 nm, and λ_{Green} at 544 nm (Fig. 8; Menzel and Blakers 1976). Most hymenopteran species, including bumblebees, appear to have quite similar spectral sensitivities to honeybees (Peitsch et al.

1992). Butterflies and moths often have sophisticated color vision (Arikawa et al. 1987; Briscoe 2008; Briscoe et al. 2003; Koshitaka et al. 2008; Wakakuwa et al. 2004), which appears to have evolved from an ancestral trichromacy (Chen et al. 2016; Osorio and Vorobyev 2008). For example, the eye of the Japanese yellow swallowtail butterfly contains five opsins: PxUV, PxB, and three long-wavelength PxL1–3 (Kitamoto et al. 1998, 2000), generating VSWS (λ_{max} 360 nm), SWS (λ_{max} 460 nm), and long wavelength sensitive (LWS: λ_{L1} 515 nm; λ_{L2} 530 nm; and λ_{L3} 575 nm) photopigments (Arikawa et al. 1987, 2003; Briscoe 2008; Koshitaka et al. 2008).

Bird eyes have four classes of photopigments in their cone cells: UVS/VS (λ_{max} 362–426 nm), SWS (λ_{max} 430–463 nm), MWS (λ_{max} 497–510 nm), and LWS (λ_{max} 543–571 nm), which provide them tetrachromacy (Fig. 8; Hart 2001; Ödeen and Håstad 2010). In the eye of human beings, there are three classes of photoreceptors responsible for color vision: SWS (λ_{max} 420 nm), MWS (λ_{max} 533 nm), and LWS (λ_{max} 563 nm), so that the human visible range is about from 400 nm to 700 nm (Fig. 8; Bowmaker and Dartnall 1980). The major difference in color vision between most pollinators and human beings are that pollinators can perceive UV light, which appears to be useful for their foraging behavior (Silberglied 1979), as described in Section 5.2.

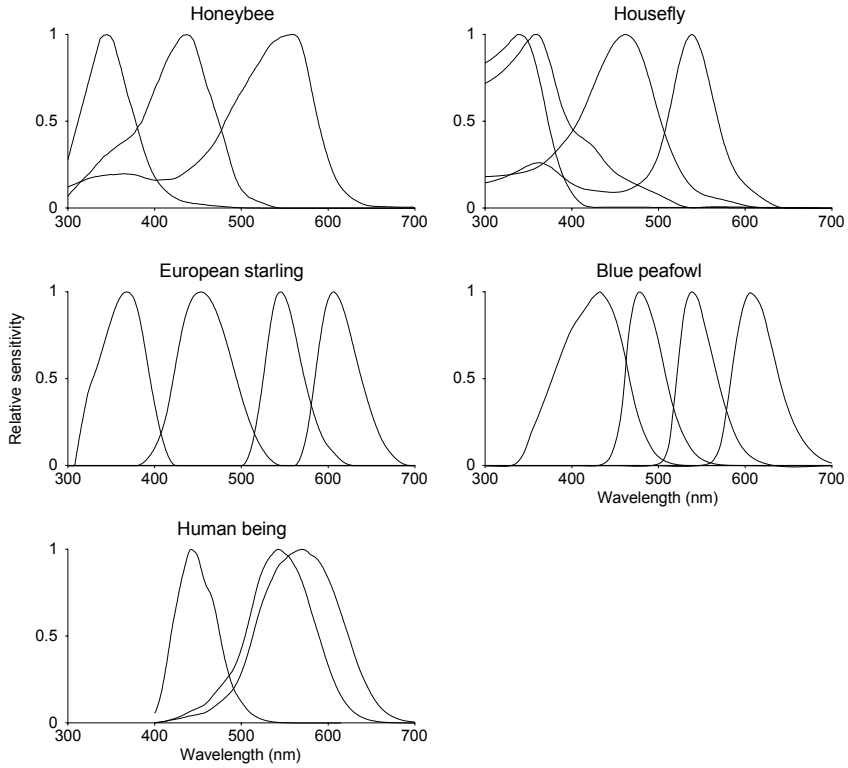

Fig. 5 Photoreceptor spectral sensitivities of the western honeybee (*Apis mellifera*), the house fly (*Musca domestica*; Osorio and Vorobyev 2005), the European starling (*Sturnus vulgaris*; Hart et al. 1998), the blue peafowl (*Pavo cristatus*; Hart 2002), and the human being (Stockman and Sharpe 2000), normalized to λ_{max}.

5. Pollen-pollinator interaction: rewards and attractants for pollinators

Zoophilous flowers offer rewards (primary attractants) and advertisements (secondary attractants) to attract pollinators (Fægri and van der Pijl 1979).

5.1. Primary attractants

Rewards are commonly nectar and pollen, which are the main attractants for pollinators (Abrol 2012). Nectar is the most common source of carbohydrates, and contains sucrose, glucose, and fructose (Haydak 1970), as well as small amounts of proteins, amino acids, lipids, vitamins, and phenolics (Haydak 1970; Nicolson and Thornburg 2007). For example, a single honeybee (*A. mellifera*) forager transports 20–40 mg of nectar at a time, and a colony of honeybees collects about 60–1,600 kg of nectar in a year, depending on colony size (Tautz 2008). Pollen is another nutritive resource consumed by pollinators, containing proteins, carbohydrates, lipids, free amino acids, minerals, vitamins (Roulston and Cane 2000; Stanley and Linskens 1974; Section 1.4). Bees can return from a flight with up to 15 mg of pollen, and a medium-sized colony of honeybees collects about 20–30 kg of pollen in a year (Tautz 2008).

Any pollen-feeding animal can ingest nutrients in extracellular pollen coat, but dismantling and/or penetration of the exine and intine is required to access cytoplasmic nutrients. Most animals are thought to extract pollen cytoplasmic nutrients through pseudo-germination, osmotic shock, and/or penetration of the pollen wall (Grant 1996; Roulston and Cane 2000). For example, adult bees possess a crop, the main part of the foregut, in which nectar and pollen may mix (Nation 2016). The crop periodically releases its contents through the proventricular valve into the midgut; thus, the ingested pollen is subjected to immersion in a sugar solution followed by a decrease in osmotic pressure in the midgut (Kroon et al. 1974; Nation 2016). Peng et al. (1985, 1986) histochemically examined the digestion process of *A. mellifera* and observed that the ingested pollen extruded cytoplasm at the aperture in the anterior midgut. As the pollen reached the posterior midgut, the exine and intine partially degraded, releasing cytoplasmic contents (Peng et al. 1986). Empty pollen and exine fragments were observed in the rectum 15 hours after feeding (Peng et al. 1986). These authors hypothesized that the digestion process comprised enzymatic partial degradation of exine in the anterior midgut, followed by extrusion of the cytoplasm due to osmotic pressure, degradation of the intine by proteases, and eventual rupture of the intine by continuous osmotic stress. *Heliconius* butterflies add their saliva, containing proteases, to collected pollen loads, which enables extraction

of amino acids and proteins from pollen (Eberhard et al. 2007). Some species of ceratopogonid flies and thrips can pierce pollen grains with their mouthpart and suck out the cytoplasmic contents (Kirk 1984; de Meillon and Wirth 1989; Roulston and Cane 2000).

5.2. Secondary attractants

Advertisements are visual, olfactory, structural, and/or tactile cues that provide information to potential pollinators about location of floral rewards (Fægri and van der Pijl 1979; Kevan and Lane 1985). Pollen-derived visual and olfactory cues are described in Section 1.4.

Olfactory cues

Floral odors play diverse roles in interaction between plants and pollinators, even from a distance (Raguso 2004), while visual cues appear to be important only in close proximity (a few centimeters to a few meters) to flowers (Dafni et al. 1997; Giurfa et al. 1996). Odorants are almost always a blend of volatile organic compounds (VOCs) that may be composed of over 100 different compounds (Levin et al. 2003). Since Dobson and Hills (1966) first characterized orchid odor with GC, over 1,700 VOCs have been identified from nearly 1,000 species and 100 families of flowering plants (Knudsen et al. 2006). Floral VOCs can be divided into seven major compound classes: aliphatics, benzenoids and phenylpropanoids, C5-branched compounds, terpenoids, nitrogen-containing compounds, sulfur-containing compounds, and miscellaneous compounds (Knudsen et al. 2006). Monoterpenes are the most common found in all orders. For example, the following monoterpenes occur in more than half of families of seed plants: limonene (71%), (*E*)-β-ocimene (71%), myrcene (70%), linalool (70%), and α- (67%) and β-pinenes (59%) (Knudsen et al. 2006). The following benzenoids, a sesquiterpene, and an irregular terpene are also common: benzaldehyde (64%), methyl 2-hydroxybenzoate (57%), benzyl alcohol (56%), 2-phenyl ethanol (54%), caryophyllene (52%), 6-methyl 5-hepten-2-one (52%) (Knudsen et al. 2006).

The primary function of floral odor in flowering plants is to attract and guide pollinators to flowers (Abrol 2012; Raguso 2001). For example, the yellow margin orchid attracts the Japanese honeybees (*A. cerana japonica*) with a mixture of 3-hydroxyoctanoic acid and 10-hydroxy-(*E*)-2-decenoic acid (Sugahara et al. 2013). The floral odor of the Northern vampire cup is dominated by 3-hexanone, which elicits innate attraction of its pollinator, the striped field mouse (Johnson et al. 2011). Some Diptera and bats prefer odors that are unpleasant and pungent to human

beings (Bänziger 1996; Goldblatt et al. 2009; Woodcock et al. 2014). Knudsen and Tollsten (1995) identified a series of methyl sulfides, such as dimethyltrisulfides, 2,3,5-trithiahexane, and 2,3,5,7-tetrathiaoctane, from several chiropterophilous plants.

As well as attracting pollinators, floral odors can also serve as landing cues, feeding cues, nectar guides, and predator repellants, etc. (Pichersky and Gershenzon 2002; Raguso 2008). The role of a specific odorant can also depend on stimulus presentation (timing, concentration, background odor, etc.) and receiver condition (age, sex, physiological state, or experience) (Raguso 2008). For example, the ubiquitous plant VOC methyl salicylate is known to attract male orchid bees (*Euglossa*) (Eltz et al. 2005), attenuate honeybee floral visits (Henning et al. 1992), block courtship attempts by the male green-veined white butterflies (Andersson et al. 2000), and elicit hunting behavior of carnivorous mites when infested with herbivorous mites (de Boer and Dicke 2004).

Visual cues

Flower colors are characterized primarily by wavelength-selective absorbance by pigments in chromoplasts or vacuoles (van der Kooi et al. 2016). The major classes of flower pigments are flavonoids, including anthocyanins, which produce human-yellow, -red, -violet, -purple, and -blue (Harborne and Williams 2000), and carotenoids, which provide principally human-yellow, -orange, and -red (Ohmiya 2011). Other classes of chlorophylls (human-green), quinones (human-red and -yellow), and betalains (human-yellow, -red, and -purple) are also common in relation to flower pigmentation (Abrol 2012).

Insect vision generally extends from about 300 nm (UV-B) to 650 nm (human-orange), with some exceptions such as *Papilio* butterflies that are also sensitive to 650–700 nm (human-red) (Briscoe and Chittka 2001; Kevan and Baker 1983). Since pollinators possess different visual systems from human beings, flower colors should not be categorized according to their color appearance to human observers. Chittka (1992) developed the color hexagon (Fig. 9), a generalized color opponent space, to categorize flower colors in terms of bee's color vision system. The color locus of given stimuli in the hexagon is calculated as follows (Chittka 1992). The sensitivity factor R for each spectral photoreceptor class is determined by the equation,

$$R = 1/\int_{300}^{700} I_{\mathrm{B}}(\lambda)\, S(\lambda)\, D(\lambda)\, \mathrm{d}\lambda \qquad (1)$$

where I_{B} (λ) is the spectral reflectance function of the background to which the receptors are assumed to be adapted; S (λ) is the spectral sensitivity function of the standard photoreceptor set of trichromatic Hymenoptera (Peitsch et al. 1992); and D (λ) is the illuminating daylight spectrum (CIE

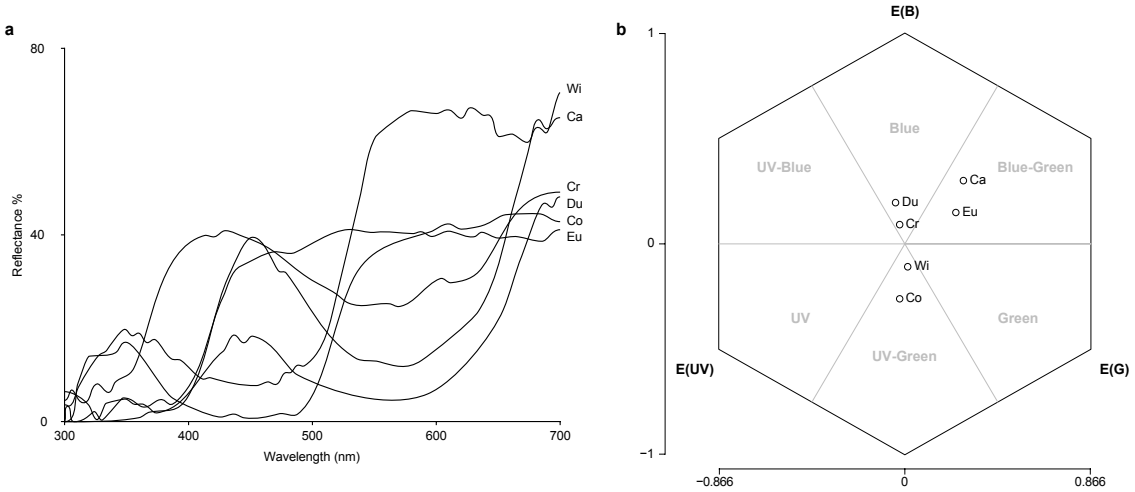

Fig. 6 Flower colorimetry. (a) Reflectance spectra of petals of six plant species obtained from The Floral Reflectance Database (Arnold et al. 2010): the common dandelion (Co, *Taraxacum officinale*; human-yellow), the creeping bellflower (Cr, *Campanula rapunculoides*; human-blue), the winter squash (Wi, *Cucurbita maxima*; human-yellow), the dusky cranesbill (Du, *Geranium phaeum*; human-pink), the Caucasian pincushion flower (Ca, *Scabiosa caucasica*; human-violet), and the European black nightshade (Eu, *Solanum nigrum*; human-white). (b) Petal color loci in bee color hexagon. The color loci were calculated with the R package 'pavo' (Maia et al. 2013), considering the honeybee visual system, a standard daylight D65 illumination, and the green vegetation background.

function, D65). The effective quantum flux for a given stimulus in the respective photoreceptor is calculated according to the equation,

$$P = R \int_{300}^{700} I_S(\lambda)\, S(\lambda)\, D(\lambda)\, d\lambda \quad (2)$$

where I_S (λ) is the spectral reflectance function of the stimulus. The calculation of physiological receptor voltage signals (relative excitations, E) from the quantum catch values is represented by the equation,

$$E = P/(P+1) \quad (3)$$

(Backhaus and Menzel 1987; Naka and Rushton 1966). The conversion of E into the x/y coordinates of the color hexagon follows:

$$x = sin\ 60° * (E(G) - E(U)) \quad (4)$$

and

$$y = E(B) - 0.5 * (E(U) + E(G)) \quad (5)$$

where E (U), E (B), and E (G) are the photoreceptor signals calculated according to equation (3) for the UV-, blue-, and green-photoreceptors. Colors in the hexagon are coded as follows (Chittka et al. 1994): spectral reflectance functions that result in a predominant stimulation of only one photoreceptor class are called bee-UV, blue, and -green, depending on which photoreceptor yields the strongest signal; and the reflectance functions that cause strong signals in two spectral receptor

classes, but not the third, are called bee-UV-blue, -blue-green, and -UV-green. Unless stated otherwise, the color names in the following sections are for human beings.

Chittka et al. (1994) analyzed petal colors of 573 plant species collected in Israel, Brazil, Norway, and Berlin by reflectance spectra, and categorized them according to the calculated loci in the color hexagon. Bee-blue-green petals are the most frequent (33%; human-white, pink, purple, or yellow), followed by bee-blue (17%; human-blue, purple, or pink), -green (17%; human-yellow), -UV-green (12%; human-yellow), -UV-blue (11%; human-violet, blue, or purple), and -UV (4%; human-red, orange, or cream) (Chittka 1997; Chittka et al. 1994). A similar flower color distribution in the color hexagon is also reported in Australian native plant species (Dyer et al. 2012). Flower-naïve and experienced honeybees (*A. mellifera*) are known to prefer bee-UV-blue (dominant wavelength λ at 410 nm) and -green (λ at 530 nm) (Giurfa et al. 1995; Menzel 1967). Australian native stingless bees (*Tetragonula carbonaria*) have an innate preference for bee-blue and -blue-green stimuli (Dyer et al. 2016). Bumblebees (*B. terrestris*) also have preferences for bee-UV-blue and -blue (Chittka et al. 2004; Raine and Chittka 2005; Raine et al. 2006). As bee-UV-blue and -blue flowers offer nectar rewards higher in concentration than species of other colors, these color preferences of bees appear to be adaptive (Chittka et al. 2004; Giurfa et al. 1995).

For successful pollen transfer, flowers are required to be distinguished from competitors by pollinators. Recently, entomophilous and ornithophilous flowers have been shown to significantly differ from each other in reflectance characteristics (Lunau et al. 2011; Shrestha et al. 2013). Flower color signals appear to be adaptive in the contexts of pollinator abilities to detect and discriminate between flowers (Lunau and Maier 1995). Color discriminability of pollinators is best where the spectral sensitivities of two photoreceptor classes overlap (Dyer et al. 2011; Kelber et al. 2003; Peitsch et al. 1992). For example, honeybees (*A. mellifera*) discriminate colors particularly well at around 400 nm and 500 nm (Chittka 1996; Helversen 1972; Peitsch et al. 1992). Maximal color discrimination in the hummingbird occurs near at 425 nm, 490 nm, 555 nm, and 585 nm (Goldsmith et al. 1981). Inflection points in reflectance spectra of entomophilous flowers are clustered at around 400 nm or 500 nm, which are consistent with discrimination optimum wavelengths of Hymenoptera (Chittka and Menzel 1992; Dyer et al. 2012; Shrestha et al. 2013). Similarly, inflection points in the reflectance spectra of ornithophilous flowers correspond to the discrimination optimum wavelengths of avian species (Shrestha et al. 2013). Pollinators obviously use visual cues of flower colors, including pollen colors, to forage and are likely to be influential drivers of flower color evolution (Dyer et al. 2012; Hopkins and Rausher 2012; Shrestha et al. 2013).

Flowers of many species show a UV pattern, called the nectar guide (or honey guide), on their

petals, derived from the reflecting apex and absorbing base (Dafni and Kevan 1996; Dyer 1996; Gronquist et al. 2001; Penny 1983; Silberglied 1979). For example, the black-eyed Susan is known to have nectar guide (Thompson et al. 1972) formed by the local accumulation of the flavonol glycosides (quercetin 7-*O*-glucoside, quercetagetin 7-*O*-glucoside, patuletin 7-*O*-glucoside, eupatolitin, eupatolitin 3-*O*-glucoside, kaempferol 3-*O*-glucoside, and patuletin) in the petal base (Schlangen et al. 2009). Similarly, in the burr marigold, chalcones and aurones cause the UV pattern on petals (Miosic et al. 2013; Scogin and Zakar 1976). Although these UV patterns are invisible to human-beings, the nectar guides serve as a visual cue in hymenopterous pollination systems, in combination with the nectaries (Goodale et al. 2014; Jones and Buchmann 1974; Waser and Price 1983, 1985).

Almost all major angiosperms possess nanostructures on the surface of petals; for example, parallel cuticular striations are found in several species of Ranunculales, Fabales, Myrtales, Malvales, Cornales, Lamiales, and Asterales, which generate angle-dependent scattering color in the UV-blue region, termed the 'blue halo' (Moyroud et al. 2017). As the blue halo of artificial striations enhanced the foraging efficiency of bumblebees (*B. terrestris*) even when associated with a yellow or blue pigmented background, the halo has been suggested to be highly salient to insect pollinators (Moyroud et al. 2017).

6. Fluorescence in biocommunication

6.1. Principles of fluorescence

Fluorescence occurs when an orbital electron of a molecule relaxes to its ground state (S_0) by emitting a photon from an excited singlet state (Lakowicz 2006). The general process of absorption and emission of light in the electronic state is illustrated in the Jablonski diagram (Fig. 10; Jablonski 1935). A fluorophore is usually excited to higher vibrational level (S_n, $n \geq 1$) and subsequently loses the excess energy by fast internal conversion (within approximately 10^{-12} sec or less) to reach the lowest vibrational level (S_1). The excess energy is transformed into heat. Return to the S_0 state from the S_1 level occurs to a higher excited vibrational ground state level, which then rapidly reaches thermal equilibrium (approximately 10^{-12} sec). Fluorescence lifetime is typically approximately 10^{-8} sec (Lakowicz 2006).

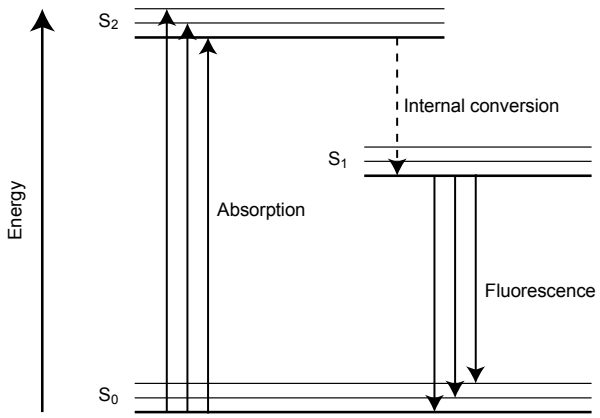

Fig. 7 Jablonski diagram including vibrational levels for absorbance, non-radiative decay, and fluorescence.

As illustrated in the Jablonski diagram (Fig. 10), the energy of emission is typically less than that of absorption due to the energy decay to S_1. Fluorescence, therefore, occurs at longer wavelength compared to excitation light. This difference in wavelength between maxima of excitation and emission was first observed by Stokes (1852), and is named the Stokes shift.

6.2. Animal-animal interactions

Fluorescence has been found both in terrestrial and marine organisms which has been implicated in the biocommunication (Marshall and Johnsen 2017). Among parrots (Psittaciformes), 68% of surveyed (35 out of 51) species have fluorescent plumage (Hausmann et al. 2003). For example, both sexes of the budgerigar possess a yellow fluorescent plumage on their crown and cheeks that is used in courtship displays (Hausmann et al. 2003; Pearn et al. 2001). The fluorescent plumage of the crown region imparts an additional 14% of photons to the reflection (Arnold et al. 2002). A mate choice experiment demonstrated that males prefer fluorescent females and vice versa, indicating that the fluorescent plumage plays a role in mate choices (Arnold et al. 2002).

A lot of spiders emit UV or blue fluorescence (λ_{max} 325–466 nm) under UV irradiation from the cuticle and setae (Andrews et al. 2007). The fluorescence is found across many spider families (i.e., Theridiidae, Araneidae, and Salticidae) and has probably evolved many times during spider diversification (Andrews et al. 2007). In the ornate jumping spider, females have palps with UV-induced green fluorescence that is absent in males (Lim et al. 2007). The green fluorescence serves as a sexual signaling, a crucial prerequisite for courtship (Lim et al. 2007).

Both sexes of the South American tree frog secrete the blue/green fluorescent (λ_{max} 450–470 nm

with a shoulder at λ_{max} 505–515 nm) dihydroisoquinolinone derivatives hyloin-L1, -L2 (lymph), and -G1 (glandular) (Taboada et al. 2017). Their fluorescence contributes 18.5–29.6% of the total emerging light (fluoresced + reflected photons) under twilight and nocturnal scenarios, enhancing brightness of the individuals (Taboada et al. 2017).

Recently, bone-based fluorescence was discovered in many chameleon species (Prötzel et al. 2018) and the Bibron's gecko (Sloggett 2018). In chameleons, the crests and tubercles protruding from the skull emit blue fluorescence under UV-A. For example, the excitation and emission spectra of chameleons *Calumma globifer* and *C. crypticum* showed their maxima at 353 nm and 433 nm, respectively (Prötzel et al. 2018). Constant fluorescent ornamentations have been proposed to provide chameleons with a means of visual communication (Prötzel et al. 2018).

In the ocean, the hydromedusa has green fluorescent protein (GFP)-derived fluorescent patches on the tips of tentacles, which attract the prey, the juvenile rockfishes (Haddock and Dunn 2015). Fluorescence emissions from many predators such as the siphonophores, mantis shrimp, and the triplefin blenny have been also proposed as prey attractants, as illuminated dots elicited aggressive responses from many fishes (Haddock and Dunn 2015; Mazel et al. 2004).

6.3. Plant-animal interactions

Fluorescence has been also found in many plants (García-Plazaola et al. 2015; Roschina and Melnikova 1999; Roschina 2003, 2012). Fluorescence is observed in the nectar of many melittophilous plant species, i.e., blue fluorescence in the almond and the onion and yellow fluorescence in the hollyleaf cherry (Thorp et al. 1975). Thorp et al. (1975, 1976) hypothesized that the fluorescence or UV-absorbing characteristics serve as a visual cue by which bees can evaluate the quantities of available nectar. The four o'clock flower bears a green fluorescent pattern on petals due to the emission from a mixture of betaxanthins (λ_{max} around 500 nm) and re-absorption of the emission by betanins (λ_{max} around 530 nm), which has been suggested as a visual cue for pollinators (Gandía-Herrero et al. 2005b). Green fluorescence of petals derived from betaxanthins is also found in yellow flowers of the moss rose and the purple ice plant (Gandía-Herrero et al. 2005a). Iriel and Lagorio (2010b) calculated the fluorescence quantum yield (Φ_f) for petals of several plant species, including the moss rose and the purple ice plant, according to the following equation

$$\Phi_f = \frac{\text{number of emitted photons}}{\text{number of absorbed photons}}$$

(Iriel and Lagorio 2010a). For example, Φ_f is <0.0001 for the moss rose and 0.003 for the purple ice plant; their petal fluorescence was concluded to be negligible by comparing the number of emitted photons to that of reflected photons (Iriel and Lagorio 2010b; Lagorio et al. 2015). However, the ability of their pollinators to perceive the fluorescence has not been tested.

Carnivorous plants, such as *Nepenthes ventricosa* and *Sarracenia purpurea*, display blue fluorescence from their pitcher peristome and trap fluid under UV-B irradiation (Kurup et al. 2013). As masking blue emission from the peristome of *N. khasiana* pitcher was found to drastically reduced prey capture, suggesting that this blue fluorescent guide works with other attractants such as nectar and visual and olfactory cues to attract arthropod prey towards the trap (Kurup et al. 2013).

7. Pollen fluorescence and its functions

Pollen fluorescence was first observed in three plant species over 90 years ago (Ruhland and Wetzel 1924), and subsequently in several other species (Baby et al. 2013; Berger 1934; Asbeck 1955; Thorp et al. 1975). Fukui et al. (2017) examined the floral fluorescence of over 580 plant species under UV irradiation, and found pollen fluorescence in most of them. The color of the pollen fluorescence varies with plant species, but most species fluoresce blue (Fig. 11). Linskens (1964) suspected that the pollen fluorescence functions in protection from solar UV-induced damage, and Thorp et al. (1975) proposed an additional function as a visual cue for pollinators. These possibilities are described in detail below.

Solar radiation at sea level comprises approximately 8% of UV radiation (200–400 nm), approximately 50% of visible radiation (400–700 nm), and approximately 40% of infrared (IR) radiation (700–1,000 nm) (Frederick 1993). UV radiation is divided into three different bands: UV-C (200–280 nm), -B (280–320 nm), and -A (320–400 nm) (Moan 2001). UV-C radiation is extremely harmful to organisms but completely filtered out by the Earth's atmosphere and does not reach the surface (Williamson et al. 2014). UV-B radiation is largely reduced due to the absorption by stratospheric ozone, but UV-A radiation passes through the atmosphere with little attenuation. UV-B and -A radiations constitute approximately 1.5% and 6.3% of the incoming solar radiation, respectively, at sea level (Hollósy 2002).

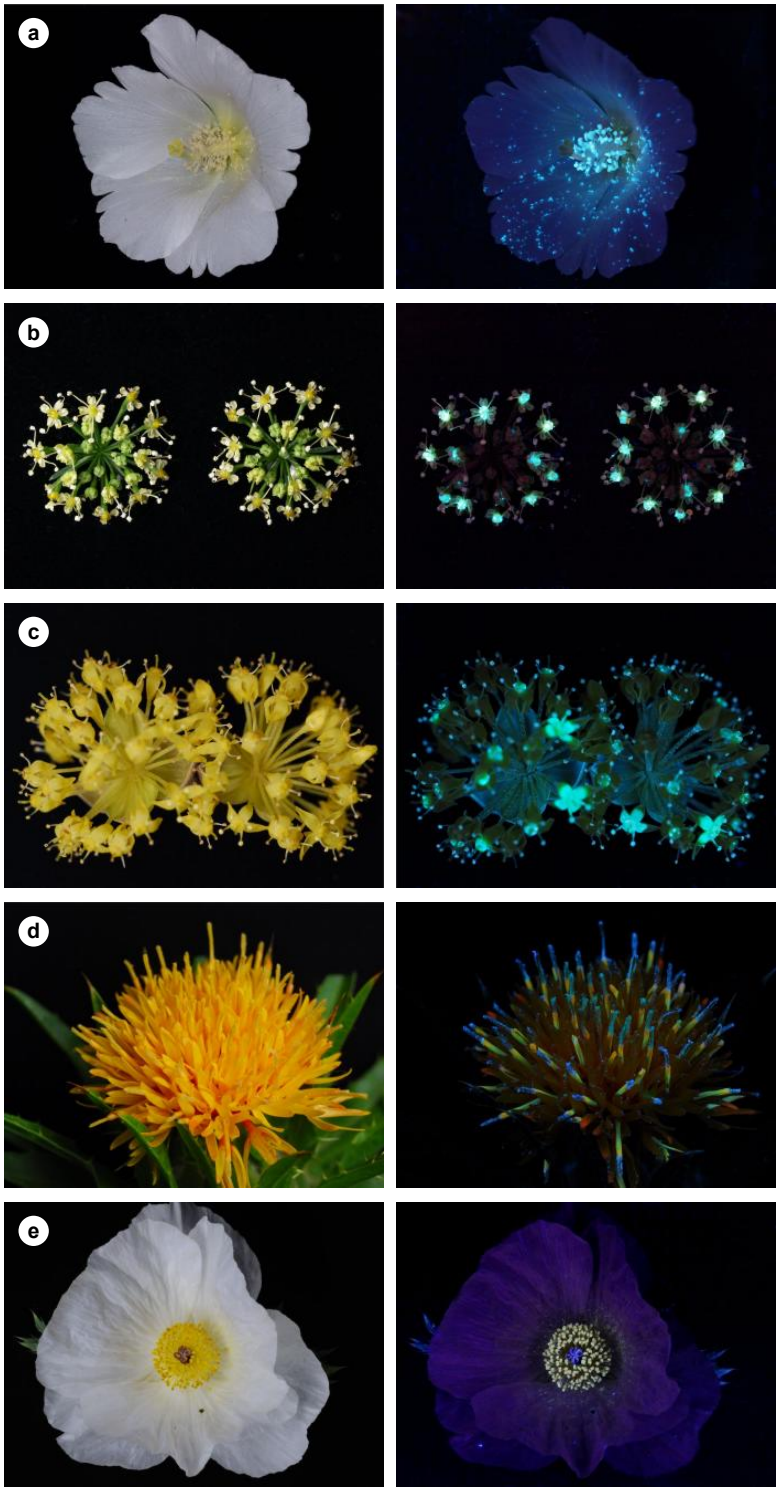

Fig. 8 Photographs of flowers under white light (*left*) and UV light (365 nm; *right*). (a) the confederate rose (*Hibiscus mutabilis*), (b) the garden parseley (*Petroselinum crispum*), (c) the Japanese cornel (*Cornus officinalis*), (d) the safflower (*Carthamus tinctorius*), and (e) the rough prickly poppy (*Argemone hispida*). Photographed by Hiroshi Fukui.

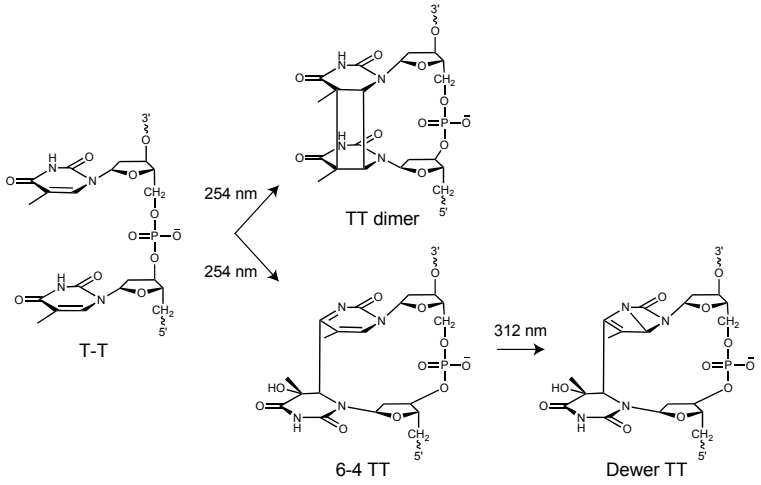

Fig. 9 Thymine dimer formation by UV radiation. T, thymine.

DNA is particularly susceptible to damage by UV radiation. Irradiation by UV-B induces photodimerization of adjacent pyrimidines such as cyclobutane pyrimidine dimers (75%) and pyrimidine (6-4) pyrimidinone dimers (25%) on the single strand of DNA (Britt 1996; Hollósy 2002). Pyrimidine (6-4) pyrimidinone dimers are further photoisomerized to Dewar isomers by UV-A (Fig. 12; Sinha and Häder 2002). These UV-induced photoproducts, if unrepaired, interfere with DNA transcription and replication, which may cause mutations (Jansen et al. 1998).

One potential mechanism by which UV-A radiation damages organisms is photosensitization (Hollósy 2002), wherein singlet oxygen ($^1O_2$), a singular reactive oxygen species (ROS), is generated via an energy transfer during a collision of the excited photosensitizer (i.e., tetrapyrroles, flavins, and reduced pyridine nucleotides) with triplet oxygen ($^3O_2$) (type II photosensitized oxidation reaction; Baptista et al. 2017). A variety of compounds can be a target of $^1O_2$, such as DNA bases, unsaturated fatty acids of membrane lipids, proteins, cellular thiols, and secondary metabolites such as terpenes (Triantaphylidès and Havaux 2009; Wright et al. 2002). $^1O_2$ adds to double bonds, leading production of dioxetane via the cycloaddition reaction, hydroperoxides via the ene reaction, and endoperoxides via the Diels-Alder reaction (Girotti 2001; Leach and Houk 2002).

In plants, there are two main detoxification mechanisms of $^1O_2$. The main mechanism is physical quenching. The physical quenchers (i.e., chlorophylls and carotenoids) deactivate $^1O_2$ through a transfer of excitation energy followed by thermal deactivation (Dickinson and Chang 2011; Triantaphylidès and Havaux 2009). The chemical quenching of $^1O_2$ is a reaction involving the oxidation of a quencher such as L-ascorbic acid and flavonoids (Larson 1988). Nevertheless, an increased level of $^1O_2$ is implicated in the signaling of programmed cell death (Triantaphylidès and Havaux 2009).

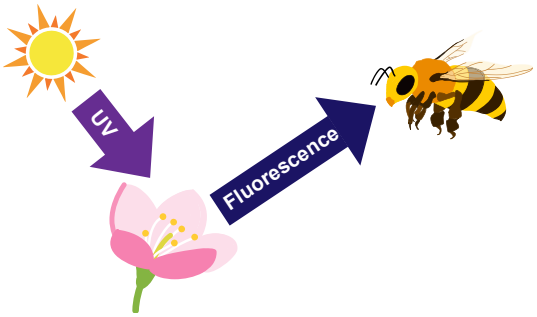

Fig. 10 Proposed function of pollen fluorescence.

Anthers usually extend beyond the corolla in angiosperms; thus, the DNA in pollen grains are exposed to the risk of UV-induced damage. Fluorescent compounds in pollen may protect the DNA from harmful UV energy through a transduction of absorbed UV energy to the fluorescence emission (Hoque and Remus 1999; Rozema et al. 2001).

The second function of pollen fluorescence may be the attraction of pollinators by highlighting pollen as their food (Fig. 13). Pollen fluorescence has been also proposed as a visual cue for insects (Section 6.3). Bees have a distinct ability in color discriminations (Dyer and Neumeyer, 2005), and an innate color preference for human-blue stimuli (Dyer et al. 2016; Giurfa et al. 1995; Gumbert 2000; Hempel de Ibarra et al. 2015; Section 5.2). This suggests that the blue fluorescence from pollen may be detectable by and attractive to them.

8. Research objectives

Plant-insect interactions have been addressed, and a number of studies demonstrated that flowers attract pollinators via olfactory, visual, and tactile cues (Lunau 2000). Despite great improvements in our understanding of plant-insect interactions, the factors influencing the foraging behavior of pollinating insects are poorly understood (Mayer et al. 2011). Several studies have contemplated the biocommunication between plants and pollinators through fluorescence (Gandía-Herrero et al. 2005a, b; Kevan 1976; Thorp et al. 1975, 1976), but the ability of insects to perceive fluorescence has not been examined by behavioral experiments, and an understanding of its functions remains rudimentary. Furthermore, the fluorescent compounds occurring in pollen grains and anthers have not been identified. The objectives of this thesis are to identify fluorescent compounds in pollen grains and anthers and to confirm the behavioral response of honeybees to the fluorescence. The results described here will open up a new aspect of biocommunication between plants and insects.

Chapter II
Identification of fluorescent compounds occurring in anthers and pollen

1. Introduction

Five species known to bear blue fluorescent pollen and/or anthers were selected from the 580 plants in the Floral Fluorescence Database (Fukui et al. 2017): the wild teasel, *Dipsacus fullonum* (Caprifoliaceae); the paperplant, *Fatsia japonica* (Araliaceae); the ribwort plantain, *Plantago lanceolata* (Plantaginaceae); the peach tree, *Prunus persica* cv. Akatsuki (Rosaceae); and the pincushion flower, *Scabiosa atropurpurea* cv. Snow Maiden (Caprifoliaceae) (Fig. 14).

D. fullonum is an herbaceous biennial plant native to Europe and Asia, and naturalized in North America (Jepsen Flora Project 2018). It forms a large basal rosette of leaves and grows to 1–2.5 m tall. Capitulums with massed pale violet flowers appear between July and August (Fig. 14a). The dried flower heads have been used as a natural comb for cleaning, aligning, and raising the nap on fabrics. Despite the limited quantities of nectar per capitulum (0.74 mg/capitulum/h), the flowers are

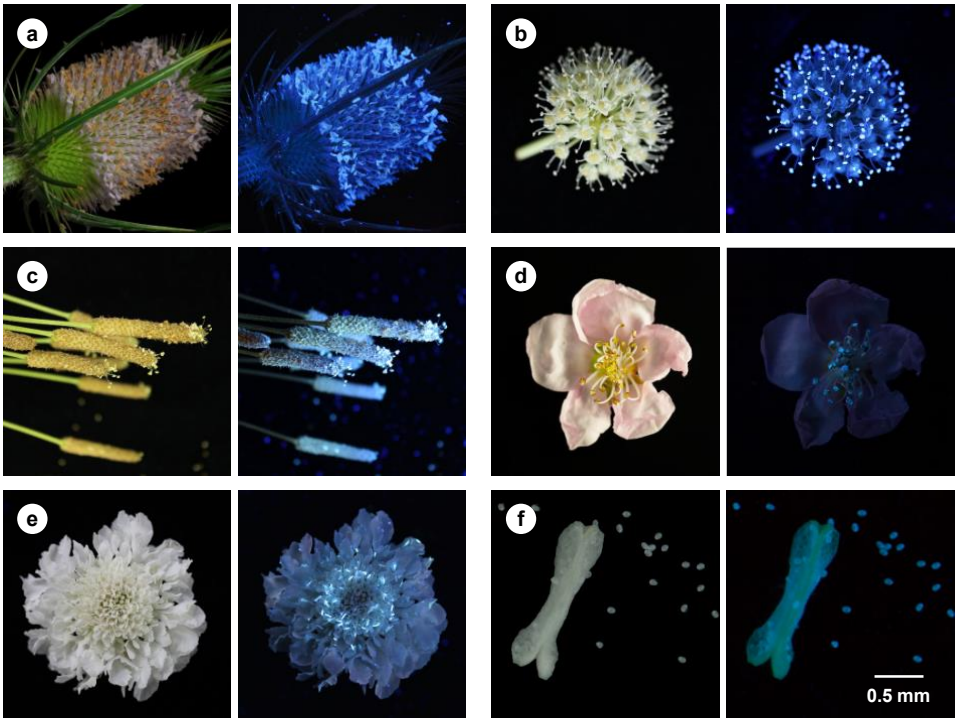

Fig. 1 Photographs of flowers under white light (*left*) and UV light (365 nm; *right*). Flowers of (a) *D. fullonum*, (b) *F. japonica*, (c) *Pl. lanceolata*, (d) *Pr. persica* cv. Akatsuki, and (e) *S. atropurpurea* cv. Snow Maiden. (f) Anther and pollen grains of *S. atropurpurea*.

frequently visited by many insects, such as hoverflies (*Episyrphus balteatus*, *Eristalis tenax*, and species of *Metasyrphus*, *Platycheirus* and *Melanostoma*) and bees (*Apis mellifera*, *Bombus lapidarius*, *B. pascuorum*, *B. terrestris*, and *Psithyrus* spp.) (Comba et al. 1999).

F. japonica is an evergreen shrub native to southern Japan, southern Korea, and Taiwan. The shrub grows to 1–3 m tall, with sparsely branched stems bearing palmately lobed leaves, and is a common garden plant in Japan. Axillary umbels of white flowers above foliage appear in October to December (Fig. 14b). It is an entomophilous plant visited by the Asian giant hornet (*Vespa mandarinia*), the pied hoverfly (*Scaeva pyrastri*), and the oriental latrine fly (*Chrysomya megacephala*) (Jun et al. 2011).

Pl. lanceolata is a rosette-forming perennial herb, with hairy stems (10–40 cm tall). Flowers appear along spikes between May and August (Fig. 14c). It is an invasive plant native to Europe, and estimated to have been introduced into Japan in the middle of the 19th century. Although most species of *Plantago* are self-compatible, *Pl. lanceolata* is self-incompatible (Ross 1973). *Pl. lanceolata* was previously regarded as anemophilous due to its morphology of stamens with long filaments, but is now regarded as ambophilic (Percival 1955; Clifford 1962). Frequent visitors are bees (*A. mellifera*, *A. dorsata*, and *A. florea*) and a few dipterans (Percival 1955; Saunders 2018; Sharma et al. 1993; Woodcock et al. 2014).

Pr. persica is a deciduous tree native to the eastern Asia (Jepsen Flora Project 2018). The tree blooms in April (Fig. 14d), and its fruits are harvested between July and August. The peach is one of largest fruit tree grown in temperate regions, in both hemispheres. Based on the statistics from the Ministry of Agriculture, Forestry and Fisheries of Japan (2018), the cultivation area and production of the peach in Japan reached approximately 9,700 ha and 124,900 t, respectively, in 2017. The 'Akatsuki' was developed in 1979 from the cross of 'Hakuto' × 'Hakuho' (Kanato et al. 1980), and is the most widely cultivated peach cultivar in Japan. The western honeybee (*A. mellifera*) is the principal pollinator of the peach followed by other bees (i.e., *Trigona spinipes* and *Xylocopa* sp.) and hummingbirds (da Mota and Nogueira-Couto 2002).

S. atropurpurea is an herbaceous annual plant native to southern Europe (Jepsen Flora Project 2018). The plant grows a basal rosette and flowers from June to October. The flower is composed of many small florets clustered together in a single head (Fig. 14e). Many cultivars with different colors are available as garden ornaments. *S. atropurpurea* offers 0.06 μL nectar (accumulated for 24 h) and 70 μg pollen per a flower, as rewards for visitors: honeybees, ants, other hymenopterans, mordellids, oedemerids, bruchids, dipterans, and lepidopterans (Bosch et al. 1997).

In this chapter, the fluorescence spectral properties of anthers and pollen of these entomophilous

plants were examined, and the fluorescent compounds responsible for their blue emission were isolated and identified. Distribution of the fluorescent compounds in pollen are also investigated.

2. Results

Both the pollen and anthers of these plants, except for *Pr. persica,* emitted blue fluorescence, whereas other parts including petals and pistils did not (Fig. 14). The anthers of *Pr. persica* exhibited blue fluorescence, but its pollen grains and other parts did not. The intrinsic fluorescence of the dehisced anthers with pollen exhibited excitation and emission maxima at around 350 nm and 450 nm for *D. fullonum*, *F. japonica*, *Pl. lanceolata*, and *S. atropurpurea*, respectively, and at 325 nm and 432 nm for *Pr. persica*, respectively (Fig. 15a).

Localization of the fluorescent compounds in the pollen grains of *S. atropurpurea* was examined. Two-photon excitation microscopy revealed that the fluorescence was emitted from the surface of pollen wall, not from the cytoplasm (Fig. 16a). After extraction with methanol, the fluorescence decreased in intensity but did not completely disappear (Fig. 16a). The extracts from pollen exhibited bright blue fluorescence under UV 365 nm light, suggesting that the fluorescent compounds were small molecules soluble in methanol. The pollen grains were observed with electron microscopies to clarify the alteration before and after extraction. Any detectable alteration was not observed by SEM (Fig. 16b), but by TEM (Fig. 16c). The surface of pollen grains was covered by pollen coat, as exemplified in the majority of entomophilous plants (Fig. 16c; Quilichini

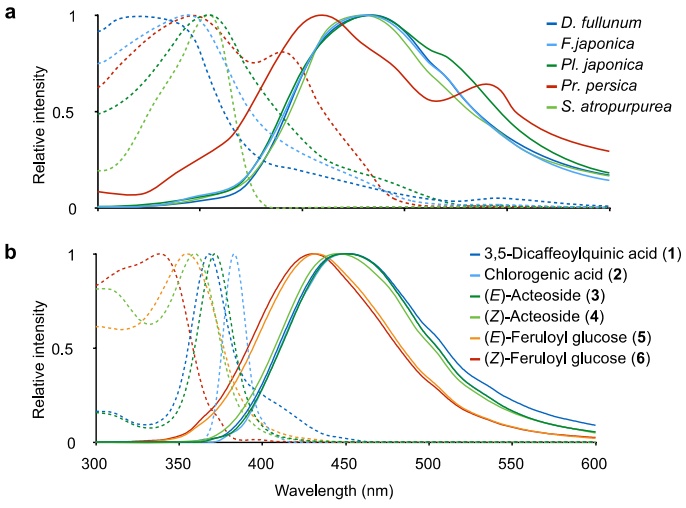

Fig. 2 Fluorescence spectra of (a) intrinsic dehisced anthers with pollen and (b) **1–6** from pollen and anthers. Excitation spectra (dotted line) and emission spectra (solid line).

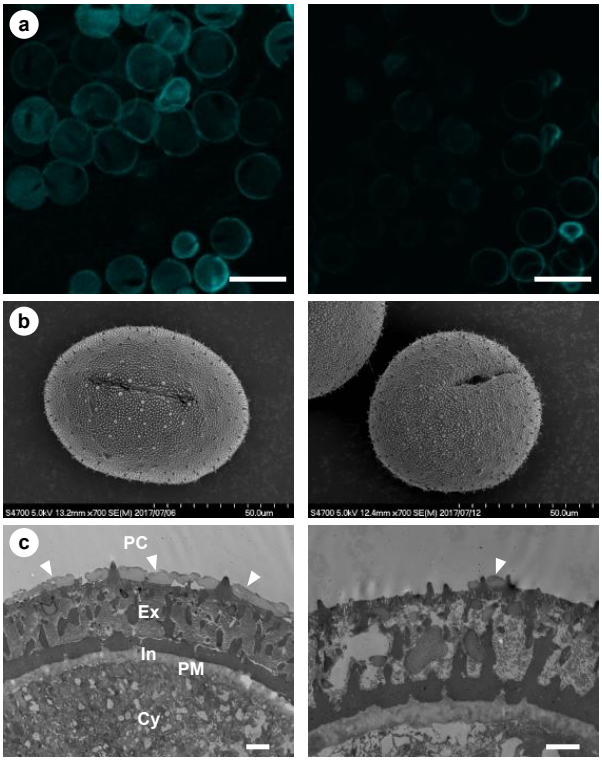

Fig. 3 Alteration of pollen grains of *S. atropurpurea* before (*left*) and after (*right*) extraction with methanol. (a) Two-photon excitation microscopic images of the pollen grains. (b) SEM images and (c) TEM images of the pollen walls. PC, pollen coat; Ex, exine; In, intine; PM, plasma membrane; Cy, cytoplasm. Arrowheads indicate the PC. Scale bars: 100 μm for (a); 2 μm for (c).

et al. 2015). The pollen coat was removed from underlying exine by extraction (Fig. 16c).

The major fluorescent compounds were isolated from the extracts, while monitoring the fluorescence on TLC. The following compounds were identified by ^{1}H NMR and LC-MS spectral data: 3,5-dicaffeoylquinic acid (**1**) (Scarpati and Guiso, 1964; Wald et al. 1989) and chlorogenic acid (**2**) (Fischer and Dangschat 1932; Cheminat et al. 1988) in *D. fulluonum*; **1** and **2** in *F. japonica*; (*E*)-acteoside (**3**) and its (*Z*)-isomer (**4**) in *Pl. lanceolata* (Birkofer et al. 1968; Nishimura et al. 1991); 1-*O*-(*E*)-feruloyl-β-D-glucose (**5**) (Birkofer et al. 1961; Bokern et al. 1987) and its (*Z*)-isomer (**6**) (Hixson et al. 2016) in *Pr. persica*, and **1** in *S. atropurpurea* (Fig. 17). The amounts of **1–6** in fresh pollen and anthers are shown in Table 1.

Fluorescence spectra of **1–6** corresponded well with those of the dehisced anthers with pollen, confirming that these fluorescent compounds are responsible for the fluorescence of the pollen and anthers (Fig. 15b). The excitation and emission wavelengths of **1–4** were almost coincident with those of methyl caffeate, indicating that the blue fluorescence of these compounds is derived from the caffeoyl moiety. The blue emission of **5** and **6** would be derived from a feruloyl moiety based on comparisons of their excitation and emission spectra with those of methyl ferulate (Fig. 15b).

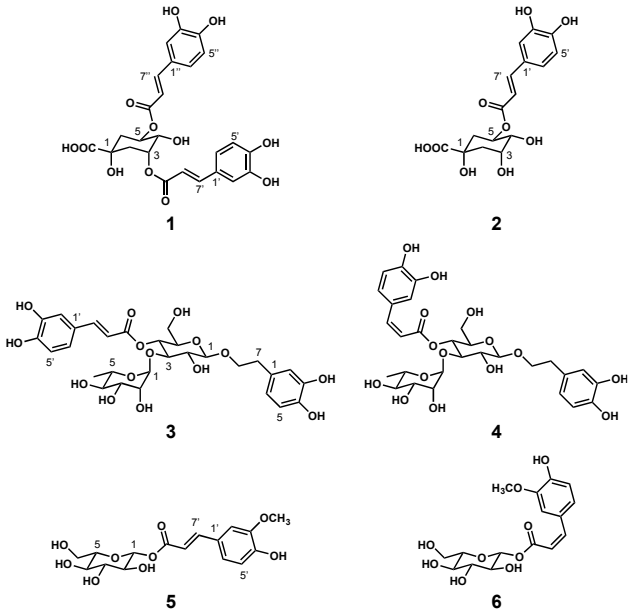

Fig. 4 Structures of **1–6**.

Table 1 Amounts of **1–6** in pollen and anthers.

Plant	Fluorescent compounds	Content (mg/g FW)		DPPH IC_{50} (μM)
		Anthers	Pollen	
D. fullonum	3,5-Dicaffeoylquinic acid (**1**)	29.8 ± 11.2	6.4 ± 2.5	10 Park et al. 2009
	Chlorogenic acid (**2**)	3.8 ± 1.7	0.3 ± 0.1	12 Kweon et al. 2001
F. japonica	3,5-Dicaffeoylquinic acid (**1**)	10.1 ± 2.1	3.4 ± 1.9	10 Park et al. 2009
	Chlorogenic acid (**2**)	2.2 ± 0.2	0.8 ± 0.3	12 Kweon et al. 2001
Pl. lanceolata	(*E*)-Acteoside (**3**)	14.4 ± 2.2	2.3 ± 0.7	6 Hung et al. 2012
	(*Z*)-Acteoside (**4**)	2.5 ± 0.8	0.4 ± 0.3	
Pr. persica	1-*O*-(*E*)-Feruloyl-β-D-glucose (**5**)	28.2	4.9	36 Hamerski et al. 2005
	1-*O*-(*Z*)-Feruloyl-β-D-glucose (**6**)	7.0	2.5	
S. atropurpurea	Chlorogenic acid (**2**)	3.5 ± 0.9	0.1 ± 0.03	12 Kweon et al. 2001

Amount values represent mean ± SE of three replications or mean of two replications.

3. Discussion

The anthers with pollen exhibited fluorescence with emission maxima in the range of 430–450 nm, corresponding to human-blue color. The emission spectra overlapped the spectral sensitivity curve of SWS and MWS class photoreceptors of hymenopterans (Fig. 8, 15a; Peitsch et al. 1992), indicating that hymenopterans including bees can perceive the blue fluorescence. The blue fluorescence from anthers and pollen may enhance their signaling to pollinators.

The fluorescent compounds **1–6** are known as antioxidants; the antioxidant activities of **1–6** are almost equal to those of L-ascorbic acid and caffeic acid (Table 1; Hamerski et al. 2005; Hung et al. 2012; Kweon et al. 2001; Park et al. 2009). The amounts of **1–6** in anthers and pollen were substantial, as shown in Table 1. This suggests their important function as protectants of the pollen grains and anthers from UV-induced damage. The fluorescent compounds may protect pollen DNA from UV-induced damage not only by transduction of absorbed energy to the fluorescence but also by scavenging ROS. The occurrence of caffeoyl and feruloyl esters in plants of four investigated families indicates their wide distribution as blue fluorophores in pollen and anthers.

Two-photon excitation microscopy and TEM revealed that the pollen fluorescence is emitted from the extracellular surface that is extractable with methanol. The extractable fluorescent compounds are presumed to be located in the pollen coat. As pollen coat is provided by the tapetum through tapetal programed cell death (Quilichini et al. 2015), the fluorescent compounds may be synthesized and accumulated in the tapetum at the maturation stage of microspores. Although the chemical composition of sporopollenin has not been elucidated due to its insolubility, ferulic acid has been identified as a component (Rozema et al. 2001). The remnant fluorescence after extraction is probably derived from a fluorophore such as a feruloyl moiety embedded in sporopollenin.

4. Materials and methods

Plant materials

Flowers of *Dipsacus fullonum* were collected at The Garden of Medicinal Plants, Kyoto Pharmaceutical University (Kyoto, Japan) in July 2013, *Fatsia japonica* at the North Campus of Kyoto University (Kyoto, Japan) from November 2013 to January 2014, and *Plantago lanceolata* at the riverside of Kamo River (Kyoto, Japan) in May 2013. Flowers of *Prunus persica* cv. Akatsuki

were collected at the Nagano Fruit-tree Experiment Station (Nagano, Japan) in April 2014. Flowers of *Scabiosa atropurpurea* cv. Snow Maiden were purchased from a local flower shop in Kyoto in April 2015.

Photography

Photographs of *D. fullonum* flowers were taken with a D200 camera (Nikon, Tokyo, Japan) equipped with an AF Zoom-Micro Nikkor ED 70–180 mm f/4.5–5.6D lens (Nikon). *F. japonica*, *Pr. persica*, and *S. atropurpurea* flowers were photographed with an EOS 60D camera (Canon, Tokyo, Japan) equipped with an EF-S60 mm F2.8 MACRO USM lens (Canon). *Pl. lanceolate* flowers were photographed with an EOS Kiss X4 camera (Canon) equipped with an EF-S 18–55 mm F3.5–5.6 IS II lens (Canon). The anther and pollen grains of *S. atropurpurea* were photographed with an E-510 camera (Olympus, Tokyo, Japan) connected to an SMZ-1500 stereomicroscope (Nikon). Photographs of filter papers were taken with the EOS 60D equipped with the EF-S 18–55 mm F3.5–5.6 IS II lens. Fluorescent lamps (HGX FHF32EX, 32 W; NEC lighting, Tokyo, Japan) were used for white light illumination, and two Handy UV Lamps (LUV-16, 365 nm, 16 W; ASONE, Osaka, Japan) were used for UV illumination.

Reagents

Reagents of analytical grade were purchased from Wako Pure Chemical Industries (Osaka, Japan). Methyl caffeate and methyl ferulate were prepared from caffeic acid and ferulic acid, respectively, by methylation with diazomethane. Wakogel® C-200 silica gel (Wako Pure Chemical Industries) was used for silica gel column chromatography. YMC*GEL ODS-AQ 12 nm S-50 μm (YMC, Kyoto, Japan) was used for ODS gel column chromatography.

TLC, HPLC, LC-MS, and NMR conditions

TLC Silica gel 60 F_{254} aluminum sheets (Merck, Darmstadt, Germany) were used for TLC analyses. The eluent was a mixture of MeOH, $CHCl_3$, and AcOH in the ratio of 15:5:1.

HPLC was performed on an L-7100 series equipment (Hitachi, Tokyo, Japan) consisting of an L-7100 pump and an L-7400 detector: a YMC-Pack ODS-AQ column (6.0 mm inner diameter × 100 mm; YMC, Kyoto, Japan); flow rate at 1.0 mL/min; and detection at 254 nm.

LC-MS analyses were performed on an LCMS-8040 mass spectrometer (Shimadzu, Kyoto, Japan) with a COSMOSIL-Pack 5C18-MS-II column (2.0 mm inner diameter × 150 mm; Nacalai tesque, Kyoto, Japan) for **1–4** and on an Acquity UPLC system H class and a Xevo G2-S QTof MS (Waters,

MA, USA) with an Acquity UPLC BEH C18 column (polar size 1.7 μm, 2.1 mm inner diameter × 50 mm; Waters) for **5** and **6**. The analyses were conducted under the following conditions for **1–4**: the eluent consisted of solvent A (100% ultrapure water containing 0.1% HCO_2H) and solvent B (100% MeCN) under the following gradient program: 10% B for 5 min and 10–50% B for 30 min at a flow rate of 0.2 mL/min. MS was operated in electron spray ionization (ESI) positive mode with the following parameters: column oven, 40°C; probe voltage, 4.5 kV; desolvation line temperature, 250°C; heat block temperature, 400°C. For analyses of **5** and **6**, the eluent consisted of solvent A (100% ultrapure water containing 0.1% HCO_2H) and solvent B (100% MeCN containing 0.1% HCO_2H) under the following gradient program: 10–50% B for 5 min at a flow rate of 0.3 mL/min. MS were operated in an ESI positive mode under the following parameters: capillary voltage, 3.0 kV; cone voltage, 40 V; source temperature, 150°C; and desolvation temperature, 500°C.

NMR spectra of methanol-d_4 (Sigma-Aldrich, MO, USA) solutions were measured with AVANCE III 400 and AVANCE III 500 spectrometers (Bruker, Rheinstetten, Germany).

Two-photon excitation laser scanning microscopy

Intact dehisced anthers with pollen grains of *S. atropurpurea* were observed with an upright microscope FV1200MPE-BX61WI (Olympus, Tokyo, Japan), equipped with a 25 × /1.05 water-immersion objective lens XLPLN 25XW-MP (Olympus), which was connected to an Insight DeepSee Ultrafast laser (Spectra Physics, Mountain View, CA, USA). An IR-cut filter BA685RIF-3 (Olympus), three dichroic mirrors (DM450, DM570, and DM505; all Olympus), and emission filters BA460-500 (Olympus) were used. The intrinsic fluorescence of anthers and pollen grains was examined at an excitation of 720 nm. Emission was captured in a GaAsP1 detector (460–500 nm, colored cyan). The anthers containing pollen after extraction with MeOH for 7 days were observed under the same conditions. Acquired images were processed with ImageJ version 2.0.0 (National Institutes of Health, MD, USA; Rueden et al. 2017; Schindelin et al. 2012).

Electron microscopy

Pollen grains of *S. atropurpurea* before and after extraction with methanol for 7 days were soaked in half Karnovsky's fixative at 4°C for 30 h. The fixed pollen grains were dehydrated in an ethanol series, soaked in *t*-butyl alcohol, and freeze-dried at −20°C. The dried anthers were mounted on stages and coated with platinum in an ion coater IB-3 (Eiko Engineering, Tokyo, Japan). The pollen grains were observed with a SEM S-4700 (Hitachi, Tokyo, Japan) at acceleration voltage 5.0 kV.

The fixed pollen grains were rinsed with 0.1 M phosphate buffer, followed by post-fixation with

1% osmium tetroxide at 4°C overnight. The samples were dehydrated in a graded ethanol series and then embedded in Plain resin (Nisshin EM, Tokyo, Japan) at 70°C for 5 days. Ultrathin sections were prepared by an ultramicrotome EM UC6 (Leica, Heidelberg, Germany) with a diamond knife and placed on copper grids. The sections were stained with 1% uranyl acetate and lead citrate and observed with a TEM H-7650 (Hitachi, Tokyo, Japan). Images were captured with an AMT XR-41C CCD camera system (Advanced Microscopy Techniques, MA, USA).

*Isolation and quantification of **1–6***

Anthers with pollen (0.7 g) of *D. fullonum* were extracted with 30 mL MeOH. The extract was partitioned between EtOAc and H_2O. The material from the organic layer was applied to a silica gel column and eluted with 20 mL of $CHCl_3$-MeOH for each fraction. The fraction eluting with 20% MeOH was subjected to preparative HPLC (eluent: 40% MeOH containing 0.1% TFA). The component eluting at *t*R 12.8 min was collected and concentrated to give 4 mg of **1**.

Anthers with pollen (2.6 g) of *F. japonica* were extracted with 30 mL MeOH. The extract was applied to a silica gel column and eluted with 30 mL of $CHCl_3$-MeOH for each fraction. The fraction eluting with 50% MeOH was subjected to preparative HPLC (eluent: 40% MeOH containing 0.1% AcOH). The component eluting at *t*R 10.6 min was collected and concentrated to give 1 mg of **1**. Another MeOH extract from the anthers containing pollen (1.0 g) was subjected to preparative HPLC (eluent: 40% MeOH containing 0.1% AcOH). The component eluting at *t*R 4.3 min was collected and concentrated to give 2 mg of **2**.

Anthers with pollen (3.7 g) of *Pl. lanceolata* were extracted with 30 mL MeOH. The extract was partitioned between EtOAc and H_2O. The material from the organic layer was applied to a silica gel column and eluted with 30 mL of $CHCl_3$-MeOH for each fraction. The fractions eluting with 20 and 30% MeOH were combined and then subjected to preparative HPLC (eluent: 40% MeOH containing 0.1% AcOH). The compounds eluting at *t*R 8.8 min and 15.0 min were separately collected and concentrated to give 7 mg of **3** and 0.8 mg of **4**, respectively.

Anthers with pollen (3.9 g) of *Pr. persica* were extracted with 30 mL MeOH. The extract was partitioned between EtOAc and H_2O. The material from the aqueous layer was partitioned between *n*-BuOH and H_2O. The material from the EtOAc and *n*-BuOH layers were combined, applied to an ODS gel column (0.5 mm inner diameter × 58 mm), and eluted with 75 mL of MeOH-H_2O for each fraction. The fraction eluting with 30% methanol was subjected to preparative HPLC (eluent: 23% MeOH containing 0.1% AcOH). The compounds eluting at *t*R 10.4 min and 11.4 min were collected and concentrated to give 1 mg of **5** and 0.3 mg of **6**, respectively.

Anthers with pollen (192 mg) of *S. atropurpurea* were extracted with 15 mL MeOH. The extract was applied to a silica gel column and eluted with 20 mL of $CHCl_3$-MeOH for each fraction. The material eluting with 70% MeOH was subjected to preparative HPLC (eluent: 25% MeOH containing 0.1% AcOH). The component eluting at *t*R 10.7 min was collected and concentrated to give 2 mg of **1**.

Quantification was carried out by using HPLC. Pollen grains were screened out from dehisced anthers with a wire mesh (opening, 0.5 mm), and pollen and anthers were separately extracted with MeOH. The amounts of **1–6** in the extracts were calculated with a calibration curve between weight and peak area, using isolated **1–6** as standards.

3,5-Dicaffeoylquinic acid (**1**): White powder; ESIMS *m/z* 517 $[M+H]^+$; ^1H NMR (400 MHz, methanol-d_4) δ 7.62 and 7.58 (each 1H, d, *J* = 16.0 Hz, H-7' and H-7''), 7.07 (2H, d, *J* = 2.1 Hz, H-2' and H-2''), 6.98 and 6.97 (each 1H, dd, *J* = 8.1 and 2.1 Hz, H-6' and H-6''), 6.78 (2H, d, *J* = 8.1 Hz, H-5' and H-5''), 6.34 and 6.27 (each 1H, d, *J* = 16.0 Hz, H-8' and H-8''), 5.43 (1H, m, H-5), 5.38 (1H, m, H-3), 3.98 (1H, dd, *J* = 7.3 and 3.2 Hz, H-4), 2.1–2.4 (4H, m, H-2 and H-6).

Chlorogenic acid (**2**): White powder; ESIMS *m/z* 355 $[M+H]^+$; ^1H NMR (400 MHz, methanol-d_4) δ 7.56 (1H, d, *J* = 15.9 Hz, H-7'), 7.05 (1H, d, *J* = 2.0 Hz, H-2'), 6.95 (1H, dd, *J* = 8.2 and 2.0 Hz, H-6'), 6.78 (1H, d, *J* = 8.2 Hz, H-5'), 6.27 (1H, d, *J* = 15.9 Hz, H-8'), 5.35 (1H, m, H-5), 4.16 (1H, m, H-3), 3.71 (1H, dd, *J* = 8.9 and 3.0 Hz, H-4), 2.19 (2H, m, H-6), 2.05 (2H, m, H-2).

(*E*)-Acteoside (**3**): White powder; ESIMS *m/z* 625 $[M+H]^+$; ^1H NMR (500 MHz, methanol-d_4) δ 7.60 (1H, d, *J* = 15.9 Hz, H-7'), 7.05 (1H, d, *J* = 2.1 Hz, H-2'), 6.96 (1H, dd, *J* = 8.3 and 2.1 Hz, H-6'), 6.78 (1H, d, *J* = 8.3 Hz, H-5'), 6.70 (1H, d, *J* = 2.2 Hz, H-2), 6.68 (1H, d, *J* = 8.0 Hz, H-5), 6.57 (1H, dd, *J* = 8.0 and 2.2 Hz, H-6), 6.28 (1H, d, *J* = 15.9 Hz, H-8'), 5.19 (1H, d, *J* = 1.7 Hz, Rha H-1), 4.9 (1H, m, Glc H-4), 4.38 (1H, d, *J* = 7.9 Hz, Glc H-1), 4.1–4.0 (1H, m, H-8a), 3.91 (1H, m, Rha H-2), 3.82 (1H, t, *J* = 9.1 Hz, Glc H-3), 3.72 (1H, m, H-8b), 3.7–3.5 (5H, m, Glc H-5, H-6a, H-6b, Rha H-3, H-5), 3.39 (1H, dd, *J* = 9.1 and 7.9 Hz, Glc H-2), 3.3 (1H, m, Rha H-4), 2.72 (2H, m, H-7), 1.10 (3H, d, *J* = 6.2 Hz, Rha H-6). Glc, glucose; Rha, rhamnose.

(*Z*)-Acteoside (**4**): White powder; ESIMS *m/z* 625 $[M+H]^+$; ^1H NMR (500 MHz, methanol-d_4) δ 7.53 (1H, d, *J* = 2.1 Hz, H-2'), 7.12 (1H, dd, *J* = 8.4 and 2.1 Hz, H-6'), 6.88 (1H, d, *J* = 12.9 Hz, H-7'), 6.74 (1H, d, *J* = 8.4 Hz, H-5'), 6.69 (1H, d, *J* = 2.5 Hz, H-2), 6.67 (1H, d, *J* = 8.0 Hz, H-5),

6.56 (1H, dd, *J* = 8.0 and 2.5 Hz, H-6), 5.77 (1H, d, *J* = 12.9 Hz, H-8'), 5.17 (1H, d, *J* = 1.7 Hz, Rha H-1), 4.9 (1H, m, Glc H-4), 4.36 (1H, d, *J* = 7.9 Hz, Glc H-1), 4.1–4.0 (1H, m, H-8a), 3.91 (1H, m, Rha H-2), 3.76 (1H, t, *J* = 9.2 Hz, Glc H-3), 3.72 (1H, m, H-8b), 3.7–3.5 (5H, m, Glc H-5, H-6a, H-6b, Rha H-3, H-5), 3.39 (1H, dd, *J* = 9.2 and 7.9 Hz, Glc H-2), 3.3 (1H, m, Rha H-4), 2.72 (2H, m, H-7), 1.17 (3H, d, *J* = 6.3 Hz, Rha H-6).

1-*O*-(*E*)-Feruloyl-β-D-glucose (**5**): White powder; ESIMS *m*/*z* 379 $[M+Na]^+$; ^1H NMR (400 MHz, methanol-d_4) δ 7.73 (1H, d, *J* = 15.9 Hz, H-7), 7.21 (1H, d, *J* = 2.0 Hz, H-2), 7.10 (1H, dd, *J* = 8.2 and 2.0 Hz, H-6), 6.82 (1H, d, *J* = 8.2 Hz, H-5), 6.40 (1H, d, *J* = 15.9 Hz, H-8), 5.58 (1H, d, *J* = 7.9 Hz, Glc H-1), 3.90 (3H, s, $-OCH_3$), 3.85 (1H, dd, *J* = 12.2 and 2.0 Hz, Glc H-6a), 3.69 (1H, dd, *J* = 4.8, 12.2 Hz, Glc H-6b), 3.5–3.3 (4H, m, Glc H-2, H-3, H-4, H-5).

1-*O*-(*Z*)-Feruloyl-β-D-glucose (**6**): White powder; ESIMS *m*/*z* 379 $[M+H]^+$; ^1H NMR data (400 MHz, methanol-d_4) δ 7.88 (1H, d, *J* = 1.9 Hz, H-2), 7.17 (1H, dd, *J* = 8.3 and 1.9 Hz, H-6), 6.94 (1H, d, *J* = 13.0 Hz, H-7), 6.77 (1H, d, *J* = 8.3 Hz, H-5), 5.82 (1H, d, *J* = 13.0 Hz, H-8), 5.56 (1H, d, *J* = 8.1 Hz, Glc H-1), 3.88 (3H, s, $-OCH_3$), 3.85 (1H, dd, *J* = 12.1 and 2.2 Hz, Glc H-6a), 3.68 (1H, dd, *J* = 12.1 and 5.0 Hz, Glc H-6b), 3.5–3.3 (4H, m, Glc H-2, H-3, H-4, H-5).

UV/Vis and fluorescence spectral analyses

UV/Visible spectra of MeOH solutions of **1–6** were measured in quartz cuvette (path length, 10 mm) with UV-2200AI and UV-1800 spectrophotometers (Shimadzu, Kyoto, Japan). Fluorescence spectra of MeOH solutions of **1–6** were measured in quartz cuvette (path length, 10 mm) with an FP-8300 spectrofluorometer (Jasco, Tokyo, Japan). An FUV-803 absorbance measurement cell block (Jasco) was used for MeOH solutions of **1–6**, and an FPA-810 powder sample cell block was used for intrinsic dehisced anthers with pollen. The absorption, excitation, and emission spectra were measured from 300 nm to 600 nm. Samples of the anthers with pollen were randomly divided into three sets. The measurements with each set were averaged.

Chapter III
Behavioral response of honeybees to pollen fluorescence

1. Introduction

The fluorescent compounds occurring in anthers and pollen have been identified as hydroxycinnamoyl derivatives including chlorogenic acid, as described in the previous chapter. A behavioral assay with chlorogenic acid was carried out to examine whether an important pollinator, the western honeybee (*A. mellifera*), can recognize the fluorescence under sunlight and, if so, exhibit a preference for it.

The honeybee is a social insect. Each colony consists of only one reproductive queen, about 20,000–50,000 functionally sterile worker bees, and a few male drones (Tautz 2008). Queens survive 3–5 years, and drones 2–4 weeks (Tautz 2008). Worker bees are usually replaced 4 weeks to 12 months, depending primarily on seasonal factors, and perform an age-dependent division of labor in their lives. Newly emerged bees cannot fly and therefore cell preparation, such as cleaning and removing the remnant of cocoons and larval excreta, is their first activity (Tautz 2008; Winston 1987). For about a week, from the age of about 4 days, these nursing caste workers use their hypopharyngeal and mandibular glands to feed a proteinaceous secretion to larvae (Winston 1987). Middle-aged bees (12–21 days old) have a broader task repertoire, such as nest building and maintenance, nectar receipt from foragers, nectar processing, and nest entrance guarding (Johnson 2010). Senior bees do not engage in tasks within the nest and focus on foraging propolis, water, nectar, and pollen (Johnson 2010). The Austrian ethologist Karl von Frisch discovered that forager honeybees communicate the spatial location of valuable resources (nectar, pollen, water, propolis, or a new nest site) to nestmates via a dance language (Couvillon 2012; von Frisch 1946). During the flight to the resource, foragers measure the direction relative to the sun and distance to the resource. The orientation of the waggling run and its duration encode the direction and distance to the resources (Winston 1987).

2. Results

The potential of fluorescence as a visual cue for free-flying honeybees was examined by a two-choice assay in the field under sunlight (Fig. 18a). The assay was based on the choice between a chlorogenic acid-containing filter paper and a plain filter paper, which were set on feeders consisting of a cup containing sucrose solution and a petri dish containing vanilla oil (Fig. 18b). Concentrations of chlorogenic acid from 0.3 to 100 mg/g were tested for the assay. Human eyes could not distinguish the chlorogenic acid-containing filter papers and plain filter paper under white light, although each were clearly distinguishable under UV light (Fig. 19a). The filter papers were sandwiched with quartz plates, and the edge was sealed to avoid any effect of volatilization of chlorogenic acid on the behavior of honeybees. The chlorogenic acid-containing filter papers showed absorption, excitation, and emission maxima at about 330 nm, 355 nm, and 430 nm, respectively (Fig. 19b). The intensities of absorption and emission of chlorogenic acid-containing filter papers were expressed as the area under the spectral curve (AUC). The AUC of absorption spectra (AUC_{Abs}) increased in an almost concentration-dependent manner (Fig. 19c). In contrast to the absorption, the AUC of emission spectra (AUC_{Em}) gradually increased from 0 to 10 mg/g but decreased from 30 to 100 mg/g due to the quenching of fluorescence by the inner-filter effect at higher concentrations (Fig. 19c; Parker and Rees 1962).

UV radiation is required for chlorogenic acid to emit fluorescence. Solar UV intensity changes depending on weather conditions (Williamson et al. 2014). Increased cloud coverage generally decreases the intensity of UV radiation reaching the surface of the Earth. The solar zenith angle also has a substantial impact on the UV intensity. Therefore, the solar UV intensity was monitored during each test to examine the relationship between the behavior of honeybees and UV intensity. Results of the assay were expressed as an excess proportion index (EPI; Sakuma and Fukami 1985),

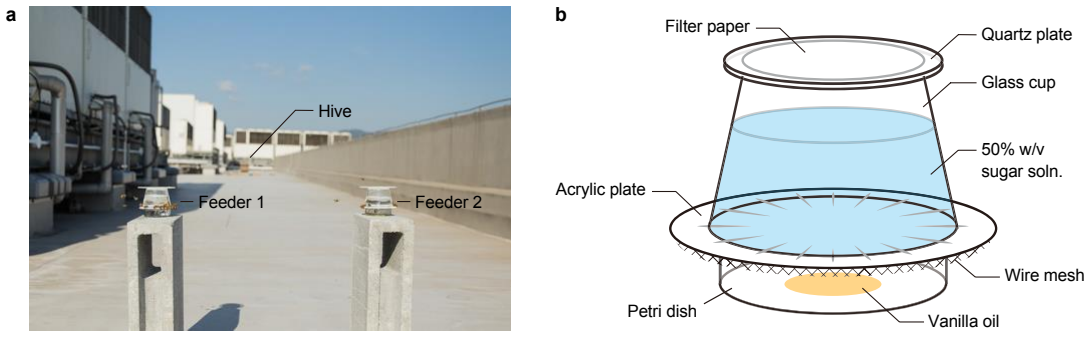

Fig. 1 Two-choice assay with honeybees. (a) Photograph of the two-choice assay. The chlorogenic acid-containing filter paper on the feeder 1 and the plain filter paper on the feeder 2. (b) Structure of the feeder with filter paper sandwiched with quartz plates.

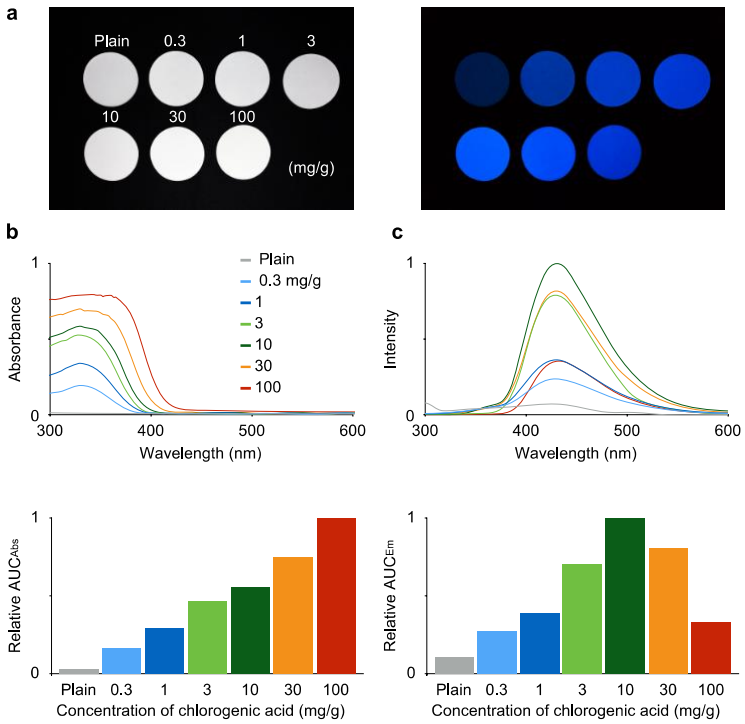

Fig. 2 Spectral profiles of tested filter papers. (a) Photographs of chlorogenic acid-containing filter papers under white light (*left*) and UV light (365 nm; *right*). (b) UV absorption spectra and AUC_{Abs}, and (c) emission spectra and AUC_{Em} of chlorogenic acid-containing filter papers.

representing the polarity of choice; the EPIs of all the tests against the UV intensity are shown in Fig. 20a. Matches with chlorogenic acid provided positive EPIs in almost all the tests under various UV intensities. This shows that honeybees prefer the chlorogenic acid-containing filter paper over the plain filter paper. Only two tests gave negative EPIs at 30 mg/g and 100 mg/g when the UV intensity were 70 μW/cm^2 and 210 μW/cm^2, respectively. The EPIs decreased prominently when the UV intensity was below 500 μW/cm^2. A UV intensity above 500 μW/cm^2 seemed to be necessary for the fluorescence to be effectively recognized by honeybees.

Chlorogenic acid and the UV intensity had significantly positive effects on the EPIs across the range of tested concentrations (Fig. 20a). Since the UV intensities were different among the tests, an analysis of covariance (ANCOVA) was performed to remove the effects of the UV intensity on the EPIs for comparisons among the concentrations. The least-square mean EPIs of matches with chlorogenic acid were positive, ranging from 0.0580 to 0.1823, whereas that of the control was −0.0087 (Fig. 20b). The values were highest at 10 mg/g and subsequently decreased. This change in the EPIs corresponded to that in AUC_{Em} rather than AUC_{Abs}. Photoisomerization of approximately 20% of (*E*)-chlorogenic acid to the (*Z*)-form on the filter paper occurred during the assay, but

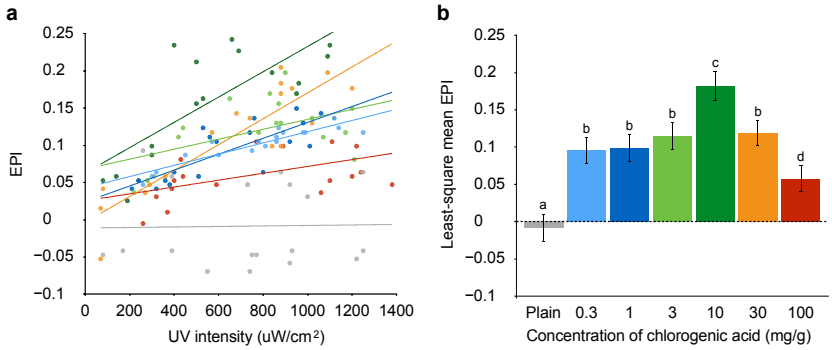

Fig. 3 Polarity of the choice by honeybees. (a) Relationship between EPI and UV intensity. Regression lines between EPIs and the UV intensity (ANCOVA: $R^2 = 0.736$; concentration of chlorogenic acid, $F_{6,112} = 2.21$, $P = 0.047$; UV intensity, $F_{1,112} = 74.81$, $P < 0.0001$; interaction between two factors, $F_{6,112} = 5.86$, $P < 0.0001$). (b) Least-square mean EPIs with a Bonferroni correction for tested concentrations of chlorogenic acid. Different letters denote significant differences among the concentrations (post-hoc test, $P < 0.05$). Error bars represent 95% fiducial intervals of each least-square mean.

decomposed products were not detected, suggesting that the fluorescence characteristics of the filter paper did not change during the assay. These results clearly revealed that honeybees perceive and prefer the fluorescence from chlorogenic acid under sunlight.

3. Discussion

Our two-choice assay demonstrated that honeybees preferred blue fluorescent filter paper over the non-fluorescent filter paper. The EPIs had a higher correlation with AUC_{Em} than with AUC_{Abs}. This indicates that honeybees preferred the emission rather than the UV absorption, although the absorption may be also informative. The blue fluorescence emitted from pollen and anthers may be attractive to flower-visiting honeybees and other insects by providing additional photons to their reflection. An artificial blue light might be also attractable for them. Further experiments are required in order to clarify, whether pollinators use the fluorescence of pollen, anthers, and other floral structures under sunlight. The quantification of fluorescence quantum yields from pollen and anthers and an experimental approach in which the emission is quenched would be necessary.

For long-distance vision, honeybees rely on a contrast signal provided by their green receptors between the target and background, rather than on color signals (Giurfa et al. 1996; Dötterl and Vereecken 2010). Visual cues for bees appear to be more effective in close proximity to flowers, in

contrast to olfactory cues (Giurfa et al. 1996; Dafni et al. 1997; Dötterl and Vereecken 2010), and honeybees may use the fluorescence from pollen and anthers when they approach flowers. Fluorescences from nectars and other floral structures may also contribute to pollination by enhancing foraging efficiency in association with other cues. Pitcher peristomes of some carnivorous plants emit UV-induced blue fluorescence, which has been considered to function as a possible attractant to capture prey (Kurup et al. 2013). Fluorescent cues probably serve in mutualistic and commensal interactions between plants and insects.

Fluorescent pollen grains are found not only in entomophilous but also in anemopilous plants. The pollen of primitive gymnosperms such as the dawn redwood (*Metasequoia glyptostroboides*) and the red pine (*Pinus densiflora*) also show blue fluorescence under UV light (Fukui et al. 2017), although they do not require pollinating animals. The original function of fluorescent compounds could be the direct protection of DNA in pollen grains from UV light by absorption and subsequent emission of energy, and indirect protection by scavenging radicals from reactive oxygen species caused by UV radiation. Pollinating insects might later have begun to employ the fluorescent compounds as a guide to food sources. Pollinators exert selective pressures on floral characteristics and vice versa. The fluorescence from pollen and anthers could be a possible factor attracting pollinators toward flowers, and the mutualism between plants and pollinators through fluorescence might contribute to their co-evolution.

4. Materials and methods

Behavioral two-choice assay

The western honeybees (*A. mellifera*) were purchased from Higuchi Yohoen (Kyoto, Japan). The hive was placed on the rooftop of the building of the Graduate School of Agriculture, Kyoto University (Kyoto, Japan), and the honeybees were bred in the hive with 9 frames (Fig. 18a).

The feeder, designed by von Frisch (1967), was modified as illustrated in Fig. 18b. The modified feeder consisted of a glass cup (70 mm diameter, 45 mm height) filled with a 50% aqueous white sugar solution (w/v) and a circular acrylic plate SUMIPEX® (white and non-fluorescent, 85 mm diameter, 2 mm thickness; Sumitomo Chemical, Tokyo, Japan). The glass cup was inverted over an acrylic plate with 16 grooves (1 × 1 × 10 mm), cut in a radial arrangement on the surface. A petri dish (60 mm diameter, 15 mm height) containing 0.5 mL of vanilla oil (My Essence Vanilla,

MEIDI-YA, Tokyo, Japan) was put beneath the acrylic plate. A wire screen (80 mm diameter) was placed between the acrylic plate and the petri dish for ventilation.

White filter paper (ADVANTEC No. 2 Filter paper Qualitative 70 mm, Toyo Roshi Kaisha, Tokyo, Japan) was used for the behavioral assay. Fluorescent filter paper was prepared by adsorbing chlorogenic acid onto the filter paper. A MeOH solution of chlorogenic acid was uniformly applied onto a filter paper, and the filter paper was dried in air. The chlorogenic acid concentrations tested were 0.3, 1, 3, 10, 30, and 100 mg/g weight of the filter paper. The filter papers were sandwiched between two Labo-USQ quartz glass plates (90 mm diameter, 1 mm thickness; Daiko MFG, Kyoto, Japan), having light transmission rates of more than 90% in the range from 180 nm to 1200 nm, and the edge was sealed with Parafilm M® (Bemis, WI, USA).

The behavioral two-choice assay was carried out on the rooftop during November and December 2016 to avoid the flowering season. The assay was performed between 10:30 am and 4:00 pm. The solar UV intensity between 290 nm and 390 nm was measured with an UV light meter UV-340A (Lutron Electronic Enterprise, Taipei, Taiwan) during each test. Honeybees were trained to forage from the feeder placed just in front of the hive entrance before the assay. Once visits of foraging honeybees to the feeder were confirmed, the feeder was moved gradually to 1, 3, 10, 15, and 20 m away from the hive entrance (Seeley 1995). After the training, the feeder was taken off, and two feeders were newly placed at 20 m away from the hive. Two filter papers were set on the top of the feeders at the same time. The distance between two feeders was 0.5 m. The honeybees had a choice at a distance of 20 m away from the hive between filter papers on the feeders under the following conditions: a filter paper containing chlorogenic acid on feeder 1 vs a plain filter paper on feeder 2 for the test matches, and plain filter papers on both feeders for the control match.

The number of honeybee landings on both feeders was counted. One test was finished when the number of landings at either feeder reached 100. Tests were repeated 18 times for each match. The positions of feeders 1 and 2 were switched after every 3 tests. The feeders were cleaned with detergent every 3 tests. The numbers of honeybee landings at each feeder were converted into an excess proportion index (EPI) (Sakuma and Fukami, 1985), according to the following equation

$$\mathrm{EPI} = \frac{\mathrm{NF1} - \mathrm{NF2}}{\mathrm{NF1} + \mathrm{NF2}}$$

where NF1 and NF2 are the numbers of honeybee landings at feeders 1 and 2, respectively. EPI values range from +1 to −1 and simply express polarity of the choice. Positive values indicate a positive approach response to feeder 1.

UV/Vis and fluorescence spectral analyses

UV/Visible absorption spectra of chlorogenic acid-containing filter papers were measured with a V-670 spectrometer (Jasco, Tokyo, Japan) equipped with an integrating sphere unit ISN-723 (Jasco). Fluorescence spectra of the filter papers were measured with an FP-8300 spectrofluorometer (Jasco). An FPA-810 powder sample cell block (Jasco) was used for both measurements. The absorption, excitation, and emission spectra were measured from 300 nm to 600 nm. Areas under the spectral curves (AUC) of absorbance (AUC_{Abs}) and of emission (AUC_{Em}) were integrated to compare the intensities among the concentrations.

Statistics

Statistical analysis was performed using a general linear model with SAS® Studio version 3.6 (SAS Institute, NC, USA). The polarity of the choice of honeybees for each match under various UV intensities was analyzed by using two-way analysis of covariance (ANCOVA) on the assumption of a Gaussian distribution of EPIs. The analysis employed the EPI as a dependent variable and the concentration of chlorogenic acid as an independent variable. The UV intensity was included as the covariate. Interaction between the concentration of chlorogenic acid and UV intensity was also included in the model. The least-square means were assessed with post-hoc tests to disentangle the differences among the concentrations for multiple comparisons. The significance levels of the post-hoc tests were corrected for multiple comparisons by applying a Bonferroni correction. The 95% fiducial limits of the least-square mean EPIs were also calculated.

Chapter IV
Fluorescence from abnormally developed pollen of the Japanese apricot

1. Introduction

The Japanese apricot tree, *Prunus mume* Siebold & Zucc. (Rosaceae), is a deciduous tree native to China, and is considered to have been introduced into Japan ca. 2,000 years ago (Hayashi et al. 2008). A wide variety of cultivars is cultivated for ornamental and commercial purposes, and their fruits are usually consumed in pickles and liqueurs. The annual yield of *P. mume* fruit fluctuated between 546.7 and 763.6 kg/10a in 2007–2016, based on statistics from the Ministry of Agriculture, Forestry and Fisheries of Japan (2018). These yields are at the poorest level among major fruit trees in Japan. The low and fluctuating yield is considered to be due to the self-incompatibility and male-sterility of major cultivars and the occurrence of imperfect flowers (Burgos et al. 2004; Tao et al. 2002; Yaegaki et al. 2003). The imperfect flowers are characterized by pistil abortions. These flowers usually show withered, short, and/or curved pistils, or in serious cases, absence of pistils (Hou et al. 2011; Nakanishi 1982; Sharma and Nayyar 2016; Sun et al. 2016; Zinn et al. 2010). Furthermore, in the flowering period between February and March, temperatures often drop below 15°C, which deteriorates the foraging activity of pollinating insects. Pollination of *P. mume* is predominantly achieved by the western honeybee, *Apis mellifera* L., introduced into orchards, so that the foraging activity of honeybees is critical for ensuring fruit sets (Nakanishi and Ishii 1978; Potts et al. 2016). The pollen of *P. mume* is a valuable source for honeybees after winter clustering in early spring. The floral characteristics of *P. mume* in relation to the foraging activity of honeybees remain rudimentary.

Nakanishi (1982) examined the visual difference of flowers between male-fertile and -sterile cultivars of *P. mume*, and observed that the anthers of sterile cultivars 'Shirokaga', 'Gyokuei', and 'Gojiro' fluoresce under UV irradiation, while those of fertile cultivars 'Koshusaisho', 'Oshuku', and 'Aogiku' do not. Recently, we have found that the most cultivated male-fertile cultivar 'Nanko' bears two types of flowers in individual trees: those with anthers with pollen that fluoresce under UV irradiation, and those with anthers with pollen that do not. The difference may be implicated in their development, and may influence the foraging behavior of honeybees. The difference in development

between the non-fluorescent and fluorescent pollen of *P. mume* cv. Nanko was examined in relation to the foraging behavior of honeybees.

2. Results

Morphology and viability of pollen grains

The two types of flowers of *Prunus mume* cv. Nanko are shown in Fig. 21a: flowers with anthers bearing pollen that emit blue fluorescence under UV irradiation, and those that do not. Approximately 33% of flowers in individual trees bore the fluorescent pollen at the time of blooming (n = 2). Under white light, while the non-fluorescent pollen appeared yellow (Fig. 21b), the fluorescent pollen appeared white (Fig. 21c). The anthers with white pollen had relatively lighter

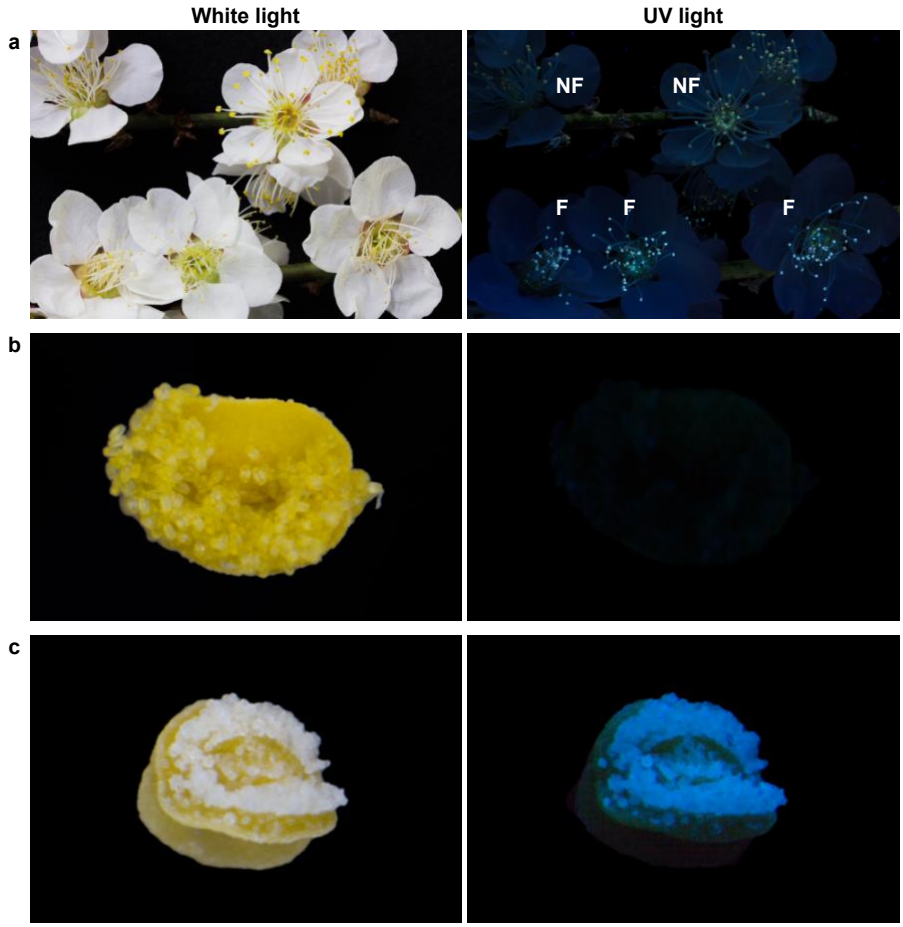

Fig. 1 Photographs of the two types of flowers of *Prunus mume* cv. Nanko under white light (*left*) and UV light (365 nm; *right*). (a) Flowers with anthers bearing non-fluorescent pollen (NF) and those bearing fluorescent pollen (F). Dehisced anthers of (b) NF and (c) F.

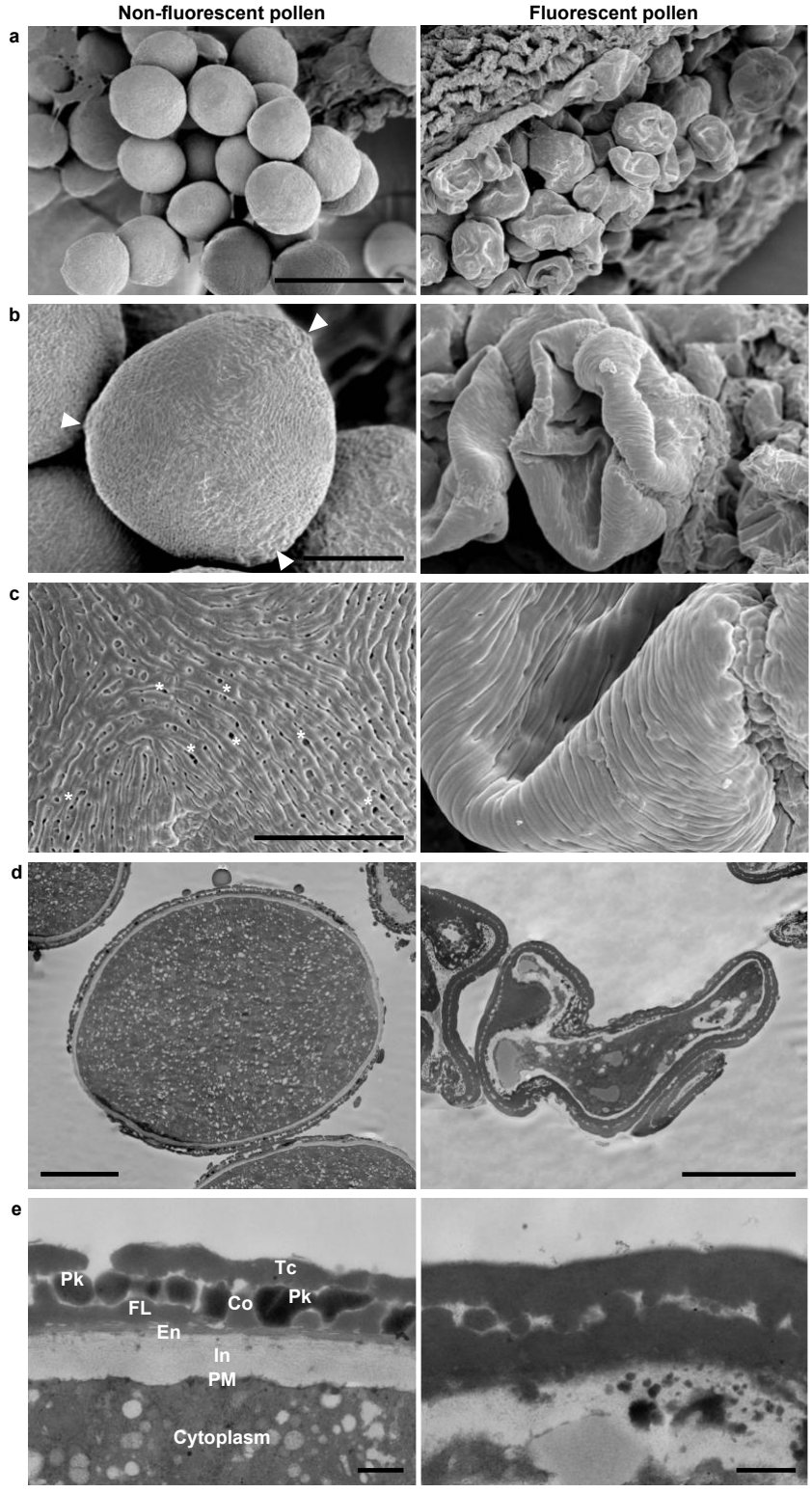

Fig. 2 Electron microscopic images of non-fluorescent pollen (*left*) and fluorescent pollen (*right*) at the bicellular pollen stage. SEM micrographs of (a) pollen, (b) whole grains, and (c) its magnified views. Arrowheads and asterisks indicate the tectal perforations and apertures, respectively. TEM micrographs of the sections of the pollen: (d) whole grains and (e) details of the pollen wall. Scale bars: (a) 50 μm, (b) 10 μm, (c) 5 μm, (d) 10 μm, and (e) 500 nm. In, intine; PM, plasma membrane; En, endexine; FL, foot layer; Co, collumera; Tc, tectum; Pk, pollenkitt.

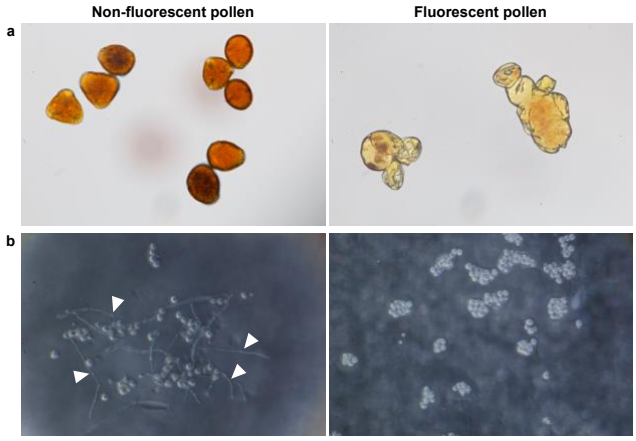

Fig. 3 Viabilities of non-fluorescent pollen (*left*) and fluorescent pollen (*right*). (a) Pollen after 2 min cultivation in Lugol's solution. (b) Pollen after 12 h cultivation on 1% agar medium with 15% sucrose and 0.01% boric acid. Arrowheads indicate pollen tubes.

yellow anther walls. The yellow pollen and the anther walls did not emit fluorescence. The color difference between the two types of anthers is discussed in the section on colorimetry. The anthers bearing fluorescent pollen were slightly smaller than those with the non-fluorescent pollen (Fig. 21b, c). There appeared to be no difference between the two types of flowers in other floral structures such as the pistil, petal, and sepal.

SEM indicated that the non-fluorescent pollen grains were elliptical and triaperturate with germinal furrow extending almost the full length of the grains (Fig. 22a). On the other hand, the fluorescent pollen grains were abnormally collapsed and firmly fixed to the anther wall. The sexine of the non-fluorescent pollen grains had a striate ornamentation pattern with perforated tectum (Fig. 22b, c). Although the fluorescent pollen grains showed a similar pattern to the non-fluorescent ones, no tectal perforations were observed. Cross-sectional ultrastructures of these pollen grains were examined by TEM, which confirmed plasmolysis of the fluorescent pollen (Fig. 22d). The non-fluorescent pollen showed a pollen wall consisting of intine, continuous thin endexine, foot layer, columella, tectum, and pollenkitt filling the sculptured cavities of exine (Fig. 22e; Punt et al. 2007). The striate ornamentation pattern and exine stratification structure of the non-fluorescent pollen are mostly consistent with other Rosaceae species (Song et al. 2016, 2017). The fluorescent pollen grains exhibited densely and nonuniformly arranged exine, and lacked pollenkitt and intine.

The non-fluorescent pollen accumulated starch granules, as confirmed by staining with Lugol's solution (Fig. 23a). However, the fluorescent pollen grains were almost devoid of starch granules. The pollen germination rate of the non-fluorescent pollen was 60.5 ± 4.8% in *in vitro* cultivations, whereas that of the fluorescent pollen was 0 ± 0% (Fig. 23b).

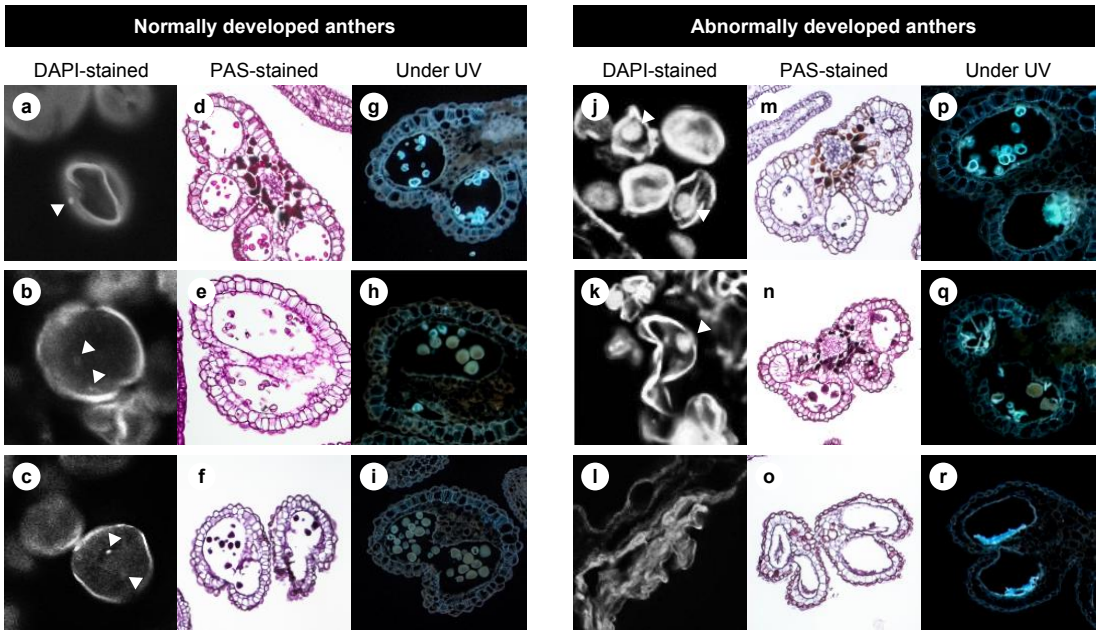

Fig. 4 Sections of normally developed anthers with pollen (a–i) and abnormally developed ones (j–r) at the unicellular microspore stage (a, d, g, j, m, and p), interphase (b, e, h, k, n, and q), and the bicellular pollen stage (c, f, i, l, o, and r). Arrowheads indicate nuclei.

Pollen development within anthers

Development of anthers and pollen was investigated using floral buds at different developmental stages to disclose how the fluorescent pollen grains occurred. The pollen development was classified into three stages according to the number of DAPI-stained pollen nuclei: unicellular microspore stage, bicellular pollen stage, and interphase containing both unicellular and bicellular pollen (Fig. 24). At the unicellular microspore stage, all anthers contained microspores surrounded by tapetum, middle layer, endothecium, and epidermis (Fig. 24d, m; Sanders et al. 1999). In the normally developed anthers, a tapetal programmed cell death was initiated between the unicellular microspore stage and interphase (Fig. 24d, e; Quilichini et al. 2015), and the tapetum completed the degeneration by the bicellular pollen stage (Fig. 24f).

Several anthers displayed abnormally vacuolated tapetal cells at the unicellular microspore stage and interphase (Fig. 24m, n). At further developed stages, the vacuolated tapetum disappeared, and all pollen were collapsed (Fig. 24o). Although the anthers, such as in Fig. 24o, appeared to be at the bicellular pollen stage according to the degenerated tapetum, nuclei were not detected in the pollen.

Under UV 365 nm irradiation, both the normally and abnormally developed microspores emitted bright blue fluorescence at the unicellular microspore stage (Fig. 24g, p). While the fluorescence of the normally developed microspores disappeared at interphase (Fig. 24h), that of the abnormally developed microspores remained until the bicellular pollen stage (Fig. 24p–r).

Colorimetry of the anthers with pollen grains

The visible spectrum of honeybees, *Apis mellifera* L., ranges from approximately 300 nm to 650 nm based on trichromatic vision with the maxima of peak sensitivities at UV (344 nm), blue (436 nm), and green (544 nm), whereas that of human beings ranges from approximately 400 nm to 700 nm (Bowmaker and Dartnall 1980; Peitsch et al. 1992). The color difference of petals and anthers with pollen between the two types of flowers were analyzed to examine whether honeybees can distinguish between them. The diffuse reflectance spectrum of the anthers with fluorescent pollen showed 1.0–9.3% higher reflectance than those of the anthers with non-fluorescent pollen across the range of 350 nm to 700 nm (Fig. 25a). The petals of both types of flowers displayed almost the same reflectance spectra, so the averaged reflectance spectrum of the petals was applied as a background of the anthers for the calculations.

The color loci of the anthers with pollen in a color hexagon space were calculated, considering the spectral sensitivity of the honeybee photoreceptors (Fig. 25b; Chittka 1992; Peitsch et al. 1992). The color loci of both types of anthers with pollen were classified as bee-UV-Green. A color distance from the center, representing the background petal, to the anthers with non-fluorescent pollen was 0.236 hex units, and that to the anthers with fluorescent pollen was 0.218 hex units. The pairwise distance between the color loci of the two types of anthers with pollen was 0.024 hex units.

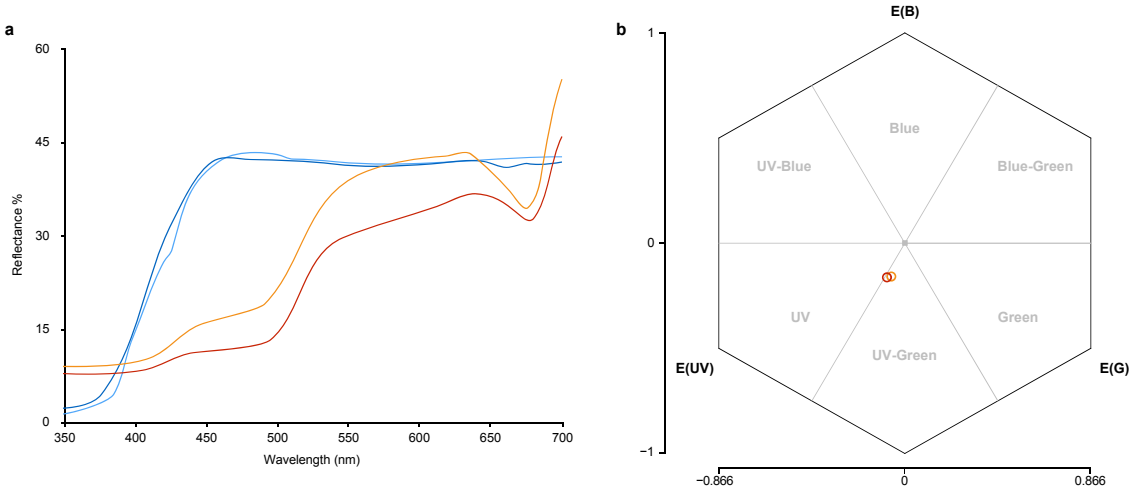

Fig. 5 Reflectance characteristics of anthers with pollen and petals. (a) Diffuse reflectance spectra of anthers with pollen (*red*) and petals (*blue*) from the flowers with anthers bearing non-fluorescent pollen, and those (*orange* and *light blue*, respectively) from the flowers with anthers bearing fluorescent pollen. (b) Color loci of anthers with non-fluorescent pollen (*red*) and those with fluorescent pollen (*orange*) plotted in the bee color hexagon (Chittka 1992). E_{UV}, E_B, E_G: excitation of the UV-, blue-, and green-sensitive photoreceptors, respectively.

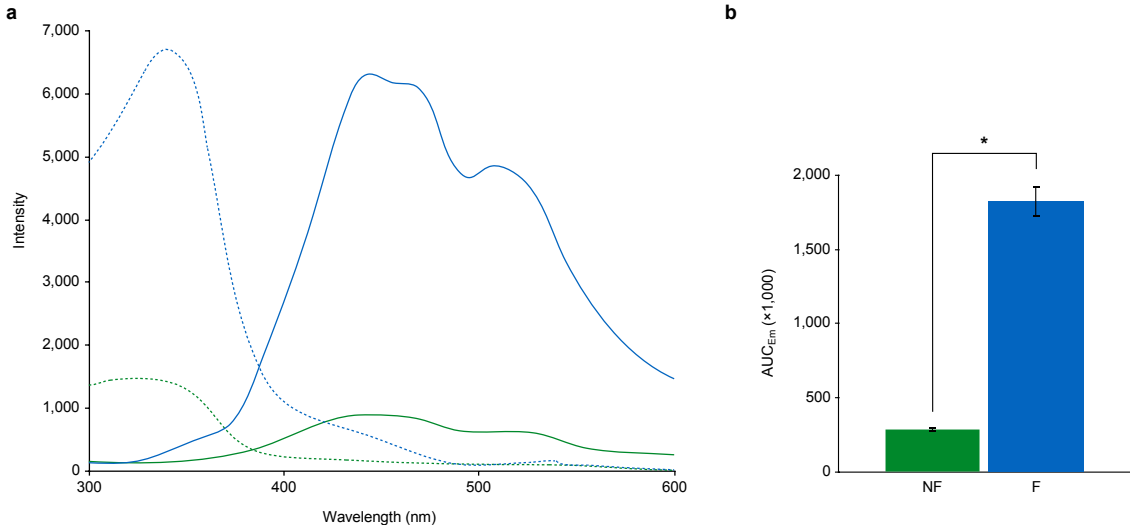

Fig. 6 Fluorescence characteristics of anthers with pollen and petals. (a) Excitation spectra (*dashed lines*) and emission spectra (*solid lines*) of anthers with non-fluorescent pollen (*green*) and those with fluorescent pollen (*blue*). (b) AUC_{Em} of the two types of anthers with pollen. NF, Anther with non-fluorescent pollen; F, those with fluorescent pollen. AUC_{Em} represents the intensity of emission between 350 to 600 nm. Error bars indicate SE. * $p < 0.001$.

Since the diffuse reflectance spectra do not include fluoresced photons, the fluorescence characteristics of the anthers with pollen were examined with the fluorescence spectra (Fig. 26a), and their intensities were evaluated by areas under the curves of emission spectra, AUC_{Em} (Fig. 26b). The anthers with non-fluorescent pollen displayed excitation maxima (λ_{Ex}) at 324 nm and emission maxima (λ_{Em}) at 439 nm, and those with fluorescent pollen displayed λ_{Ex} and λ_{Em} at 340 nm and 444 nm, respectively. The AUC_{Em} of the anthers with fluorescent pollen was significantly higher than those with the non-fluorescent pollen (Fig. 26b; 6.3-fold, t (4) = 21.59, $p < 0.001$).

Isolation and identification of major constituents from anthers and pollen grains

The chemical constituents of the non-fluorescent anthers and of the fluorescent anthers were analyzed by HPLC. The extracts from the anthers with non-fluorescent pollen yielded three fluorescent compounds (**2**, **5**, and **6**), one yellow pigment (**7**), and eight non-fluorescent UV-absorbing compounds (**8–15**) as major constituents (Fig. 27a). In the extract from the anthers with fluorescent pollen, **2**, **5**, **6**, **8**, and a limited amount of **9–11** were detected, but **12–15** were not (Fig. 27b). The yellow pigment **7** isolated from the extract of the anthers with non-fluorescent pollen was identified as quercetin 3-*O*-β-D-glucoside (**7**) (Bennini et al. 1992; Perkin 1909), based on its ^{1}H NMR and LC-MS spectral data. The LC-MS analysis of the mixture of **8–15** showed that they all had the same molecular formula $C_{34}H_{37}N_3O_6$ (Fig. 28). A ^{1}H NMR spectrum of this mixture

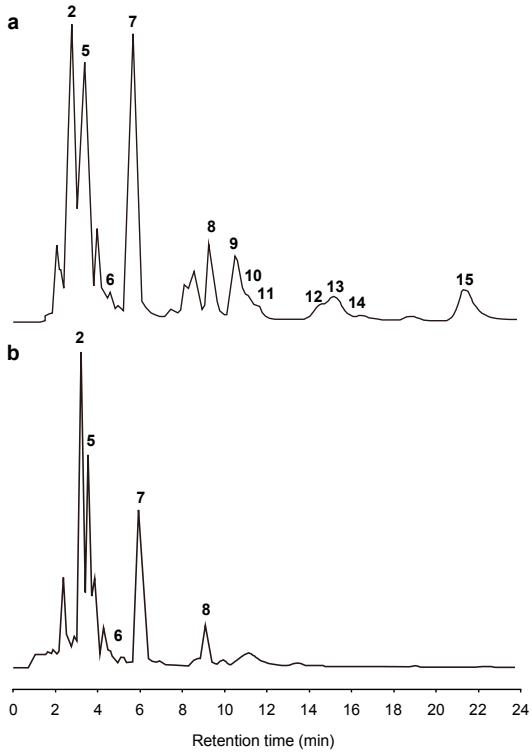

Fig. 7 HPLC chromatograms of an extract from anthers with pollen. (a) Extract from anthers with non-fluorescent pollen and (b) those with fluorescent pollen. Operating conditions: column, ODS; solvent, 0.1% AcOH in 39% MeOH (1 mL/min); detection, UV 254 nm.

exhibited clusters of signals at around 7.6–5.7 ppm and 3.7–1.5 ppm, corresponding to olefinic / aromatic and methylene protons, respectively. These spectral data suggest that **8**–**15** are the eight possible *E*-*Z* isomers of N^1,N^5,N^{10}-tri-*p*-coumaroylspermidine (*EEE*, *EEZ*, *EZE*, *ZEE*, *EZZ*, *ZEZ*, *ZEE*, and *ZZZ*), wherein double bonds are present in each of the three *p*-coumaroyl moieties. As the isomerization of olefinic double bonds is catalyzed by light (Kahnt 1967), further separation of **8**–**15** by HPLC was conducted in the dark. The HPLC chromatogram of the mixture of **8**–**15** is shown in Fig. 29. The peaks corresponding to **9**–**11** and **12**–**14** partially overlapped, and thus they were separated by a peak shaving method (Bidlingmeyer 1993). The ^{1}H NMR chemical shifts of the olefinic proton signals of **8**–**15** are summarized in Table 2. Compounds **8**, **10**–**12**, and **15** were identified as N^1,N^5,N^{10}-tri-*p*-(*ZZZ*)-, (*EZZ*)-, (*ZZE*)-, (*EZE*)-, and (*EEE*)-coumaroylspermidine, respectively, by comparison of their ^{1}H NMR spectra with literature data (Fig. 30; Jiang et al. 2008; Li et al. 2013; Ma et al. 2001; Strack et al. 1990; Zhao et al. 2010). Each isomer of N^1,N^5,N^{10}-tri-*p*-coumaroylspermidine showed pairs of proton signals due to the rotamers caused by a hindered rotation of N^5-*p*-coumaroyl amide (Ma et al. 2001; Meurer et al. 1988b). Undescribed

isomers (**9**, **13**, and **14**) were obtained as mixtures of **9–11** and **12–14** (Fig. 29). The *E*-*Z* configurations of **9**, **13**, and **14** were elucidated by comparing their ^{1}H NMR spectra with those of **1** and **8**, as follows.

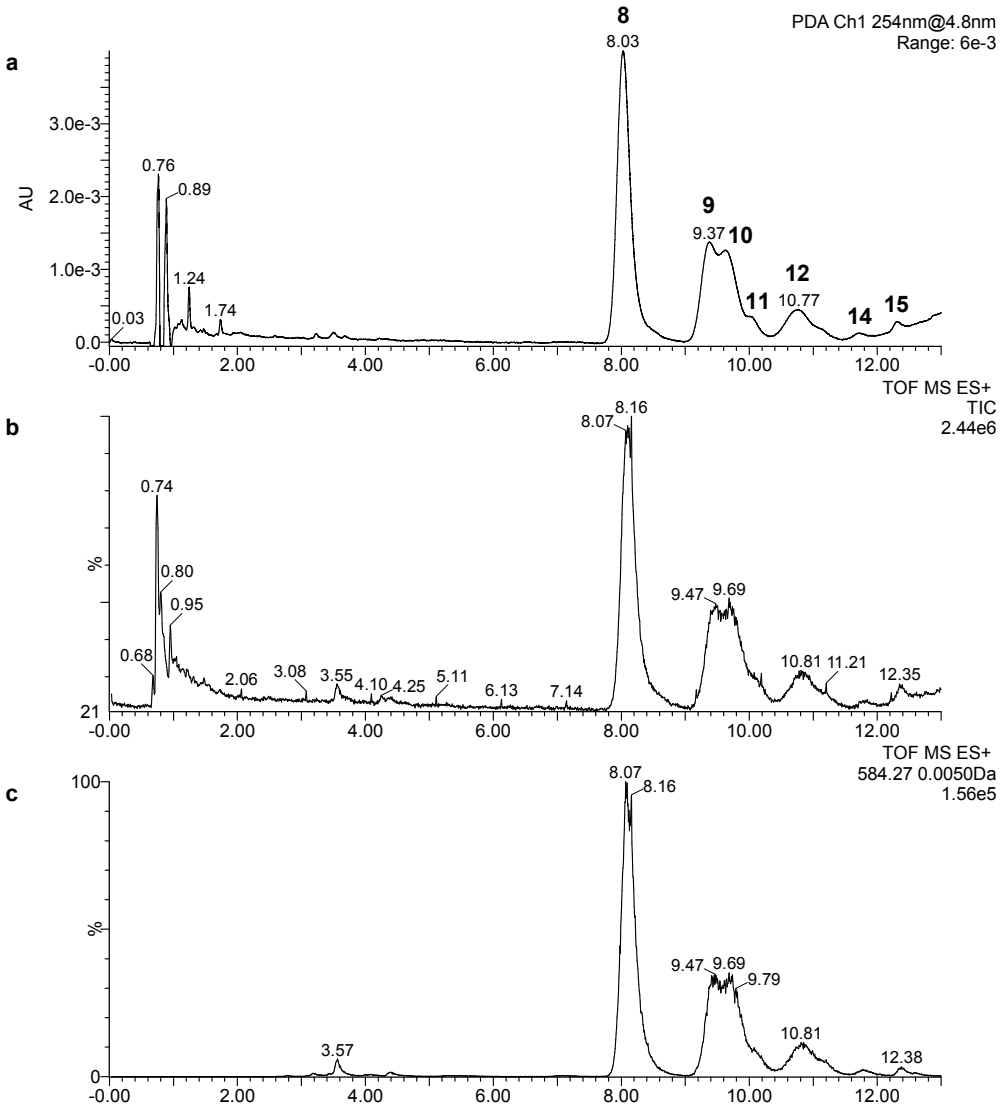

Fig. 8 LC-MS analysis of the mixture of **8–15**. (a) UPLC chromatogram detected at 254 nm. (b) Total ion chromatogram. (c) MS chromatogram for *m*/*z* 584.27. Continued on the next page.

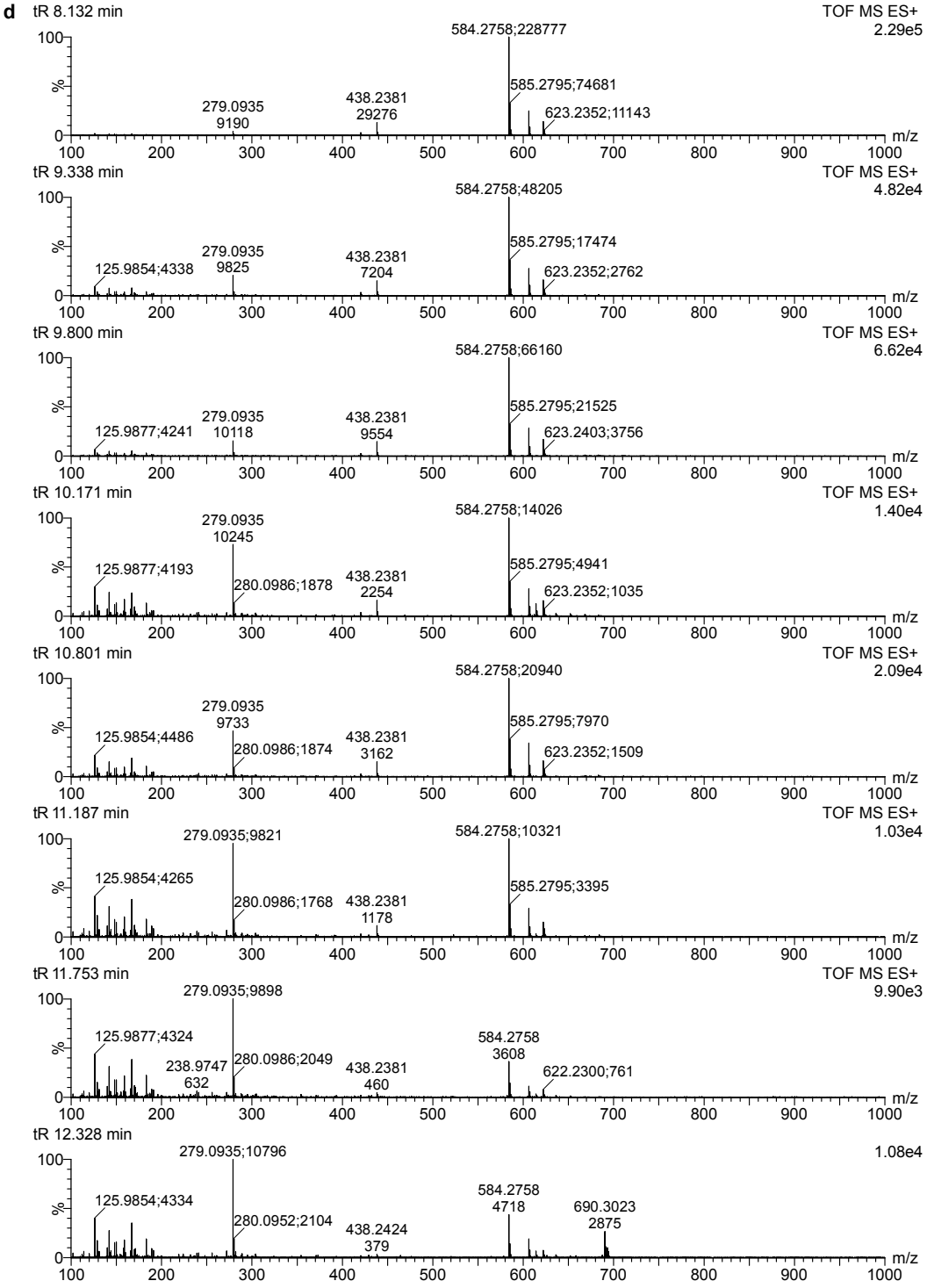

(d) Mass spectra for **8** (*t*R 8.132 min), **9** (*t*R 9.338 min), **10** (*t*R 9.800 min), **11** (*t*R 10.171 min), **12** (*t*R 10.801 min), **13** (*t*R 11.187 min), **14** (*t*R 11.753 min), and **15** (*t*R 12.238 min).

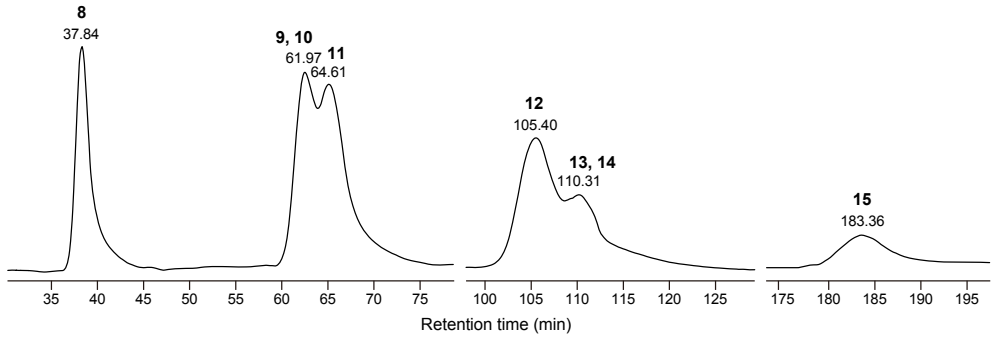

Fig. 9 HPLC chromatogram of N^1,N^5,N^{10}-tri-*p*-coumaroylspermidine isomers. *t*Rs: **8** (37.84 min), **9** and **10** overlapped (61.97 min), **11** (64.61 min), **12** (105.40 min), **13** and **14** overlapped (110.31 min), and **15** (183.36 min). Operating conditions: column, ODS; solvent, 0.1% AcOH in 39% MeOH (1 mL/min); detection, UV 254 nm.

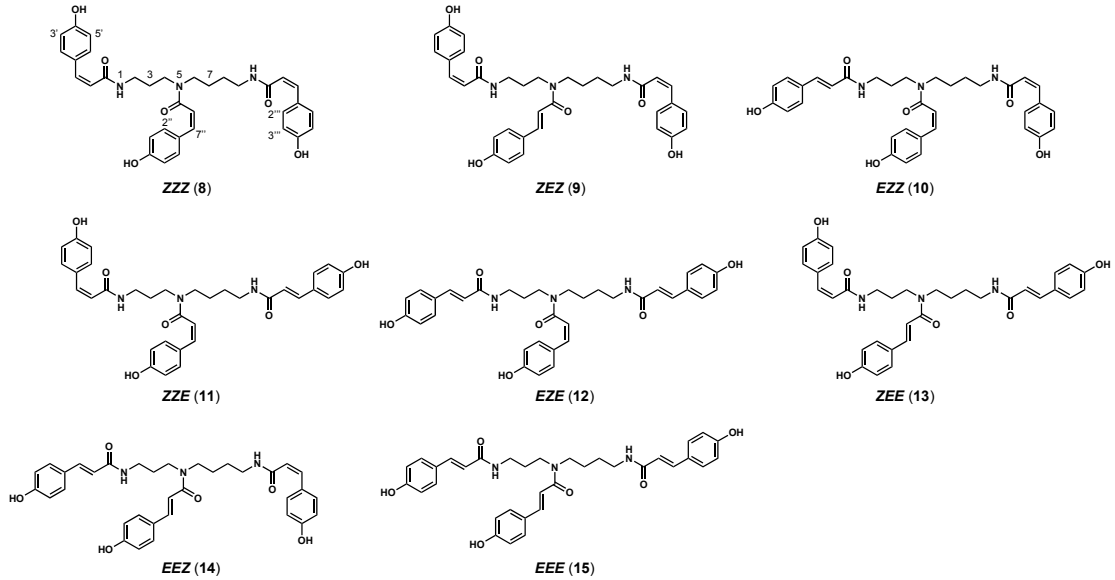

Fig. 10 Structures of **8–15**.

Table 1 Olefinic signals of **8–15** in ^{1}H NMR (400 MHz, methanol-d_4). OL indicates that the signals were overlapped with other signals. Asterisks denote that the signals of two rotamers overlapped.

	δ_H (*J* in Hz)							
	***ZZZ* (8)**	***ZEZ* (9)**	***EZZ* (10)**	***ZZE* (11)**	***EZE* (12)**	***ZEE* (13)**	***EEZ* (14)**	***EEE* (15)**
H-7'	6.63 / 6.61 (12.7)	OL	7.46 / 7.42 (15.8)	6.62 / 6.60 (12.5)	7.43 (15.7)*	6.62 / 6.60 (12.5)	7.44 / OL (16.3)	7.45 / 7.44 (16.0)
H-8'	5.85 / 5.84 (12.7)	5.83 / OL (12.1)	6.41 / 6.35 (15.8)	5.84 / 5.78 (12.5)	6.36 / 6.35 (15.7)	5.83 / 5.80 (12.5)	6.41 / 6.37 (16.3)	6.41 / 6.37 (16.0)
H-7''	6.58 / 6.53 (12.8)	7.51 / 7.45 (15.4)	6.53 / 6.58 (12.7)	6.59 / 6.55 (12.5)	6.59 / 6.55 (12.6)	7.54 / 7.51 (15.6)	7.52 / 7.50 (16.0)	7.54 / 7.52 (15.3)
H-8''	5.92 / 5.90 (12.8)	6.81 / 6.80 (15.4)	5.95 / 5.90 (12.7)	5.94 / 5.93 (12.5)	5.97 / 5.93 (12.6)	6.85 / 6.79 (15.6)	6.84 / 6.79 (16.0)	6.87 / 6.82 (15.3)
H-7'''	6.65 / 6.63 (12.7)	6.65 / OL (12.7)	6.64 / 6.62 (12.6)	7.46 / 7.43 (15.8)	7.46 (15.8)*	7.48 / 7.47 (15.6)	6.64 (12.8)*	7.48 / 7.47 (16.2)
H-8'''	5.79 / 5.78 (12.7)	5.80 / OL (12.7)	5.85 / 5.79 (12.6)	6.42 / 6.36 (15.8)	6.43 / 6.41 (15.8)	6.42 (15.6)*	5.84 / 5.83 (12.8)	6.42 (15.7)*

Compound **9** was obtained as a major compound in a mixture with **10** and **11** (**9**:**10**:**11** = 47:26:27). The ^{1}H NMR spectrum of this mixture showed three (*Z*)-olefinic proton signals of **9** at δ 6.65 (1H, d, *J* = 12.7 Hz, H-7'''), 5.83 (1H, d, *J* = 12.1 Hz, H-8'), and 5.80 (1H, d, *J* = 12.7 Hz, H-8'''), corresponding to the protons of the N^1- and N^{10}-(*Z*)-coumaroyl moieties of **8**. A pair of (*E*)-olefinic proton signals of **9** at δ 7.51 (1H, d, *J* = 15.4 Hz, H-7''), 7.45 (1H, d, *J* = 15.4 Hz, H-7''), 6.81 (1H, d, *J* = 15.4 Hz, H-8''), and 6.80 (1H, d, *J* = 15.4 Hz, H-8'') corresponded to those of a N^5-coumaroyl moiety of **15**. The other olefinic proton signals of H-8', H-7''', and H-8''', a signal pair of H-7', and signals of aromatic and spermidine moieties of **9** overlapped each other or with signals derived from *p*-coumaroyl moieties of **10** and **11**. These assignments allowed the identification of **9** as N^1,N^5,N^{10}-tri-*p*-(*ZEZ*)-coumaroylspermidine.

Compound **13** was obtained as a mixture with **14** (**13**:**14** = 76:24). The ^{1}H NMR spectrum of this mixture showed a pair of (*Z*)-olefinic proton signals of **13** at δ 6.62 (1H, d, *J* = 12.5 Hz, H-7'), 6.60 (1H, d, *J* = 12.5 Hz, H-7'), 5.83 (1H, d, *J* = 12.5 Hz, H-8'), and 5.80 (1H, d, *J* = 12.5 Hz, H-8'), corresponding to those of a N^1-*p*-(*Z*)-coumaroyl moiety of **8**, and two pairs of (*E*)-olefinic proton signals at δ 7.54 (1H, d, *J* = 15.6 Hz, H-7''), 7.51 (1H, d, *J* = 15.6 Hz, H-7''), 7.48 (1H, d, *J* = 15.6 Hz, H-7'''), 7.47 (1H, d, *J* = 15.6 Hz, H-7'''), 6.85 (1H, d, *J* = 15.6 Hz, H-8''), 6.79 (1H, d, *J* = 15.6 Hz, H-8''), and 6.42 (2H, d, *J* = 15.6 Hz, two rotamers overlapped, H-8'''), corresponding to those of N^5- and N^{10}-*p*-(*Z*)-coumaroyl moieties of **15**. The signals of aromatic and spermidine moieties of **13** overlapped each other or with signals of **14**. Compound **13** was identified as N^1,N^5,N^{10}-tri-*p*-(*ZEE*)-coumaroylspermidine, based on these signal assignments.

Compound **14** was obtained as a mixture with **12** (**12**:**14** = 41:9). The ^{1}H NMR spectrum of this mixture showed a pair of (*Z*)-olefinic proton signals of **14** at δ 6.64 (2H, d, *J* = 12.8 Hz, two rotamers overlapped, H-7'''), 5.84 (1H, d, *J* = 12.8 Hz, H-8'''), and 5.83 (1H, d, *J* = 12.8 Hz, H-8'''), corresponding to those of a N^{10}-*p*-(*Z*)-coumaroyl moiety of **8**, and two pairs of (*E*)-olefinic proton signals at δ 7.52 (1H, d, *J* = 16.0 Hz, H-7''), 7.50 (1H, d, *J* = 16.0 Hz, H-7''), 7.44 (partially overlapped, d, *J* = 16.3 Hz, H-7'), 6.84 (partially overlapped, d, *J* = 16.0 Hz, H-8''), 6.79 (partially overlapped, d, *J* = 16.0 Hz, H-8''), 6.41 (1H, partially overlapped, d, *J* = 16.3 Hz, H-8'), and 6.37 (1H, partially overlapped, d, *J* = 16.3 Hz, H-8'), corresponding to those of N^1- and N^5-*p*-(*E*)-coumaroyl moieties of **15**. The other olefinic proton signal H-7' of **14** overlapped with other signals of *p*-coumaroyl moieties of **12**. Compound **14** was identified as N^1,N^5,N^{10}-tri-*p*-(*EEZ*)-coumaroylspermidine, based on these signal assignments.

These structure elucidations confirmed that the isomers of N^1,N^5,N^{10}-tri-*p*-coumaroylspermidine were eluted from the ODS column in the following order: *ZZZ* (**8**), *ZEZ* (**9**), *EZZ* (**10**), *ZZE* (**11**),

Table 2 Amounts of **8–15** in anthers with pollen.

Compounds	Amount (mg/g DW)		*t* (4), *P*
	NF	F	
Chlorogenic acid (**2**)	3.2 ± 0.1	21.6 ± 0.7	20.00, < 0.01
1-*O*-(*E*)-Feruloyl-β-D-glucose (**5**)	2.0 ± 0.2	1.3 ± 0.3	
1-*O*-(*Z*)-Feruloyl-β-D-glucose (**6**)	0.1 ± 0.0	0.3 ± 0.0	
Total amount of **5** + **6**	2.1 ± 0.2	1.6 ± 0.2	1.60, 0.18
Quercetin 3-*O*-β-D-glucoside (**7**)	17.1 ± 0.5	11.2 ± 0.2	8.91, < 0.01
N^1,N^5,N^{10}-Tri-*p*-(*ZZZ*)-coumaroylspermidine (**8**)	4.2 ± 0.3	3.0 ± 0.2	
(*ZEZ*)-isomer (**9**)			
(*EZZ*)-isomer (**10**)	3.2 ± 0.2	0.2 ± 0.1	
(*ZZE*)-isomer (**11**)			
(*EZE*)-isomer (**12**)			
(*ZEE*)-isomer (**13**)	1.4 ± 0.1	ND	
(*EEZ*)-isomer (**14**)			
(*ZZZ*)-isomer (**15**)	3.4 ± 0.1	ND	
Total amount of **8–15**	12.2 ± 0.5	3.2 ± 0.4	14.47, < 0.01

Values represent means ± SE from three replications. NF, anthers with non-fluorescent pollen; F, anthers with fluorescent

EZE (**12**), *ZEE* (**13**), *EEZ* (**14**), and *EEE* (**15**) (Fig. 29). The difficulties encountered in the separation of the (*EZZ*/*ZEZ*/*ZZE*)- and (*EZE*/*EEZ*/*ZEE*)-isomers may be due to their structural similarities.

Amounts of **2** and **5–15** in the anthers with pollen are summarized in Table 3. The amount of **2** was 3.2 mg/g DW in the anthers with non-fluorescent pollen, whereas it was significantly higher in the anthers with fluorescent pollen (21.6 mg/g DW; 6.8-fold). The amount of **7** was significantly higher in the anthers with fluorescent pollen, compared to the anthers with non-fluorescent pollen (17.1 vs 11.2 mg/g DW; 1.5-fold). In contrast, the total amount of *E*-*Z* isomers **8–15** was significantly higher in the anthers with non-fluorescent pollen than that in the anthers with fluorescent pollen (12.2 vs 3.2 mg/g DW; 3.8-fold). There was no significant difference in the total amount of *E*-*Z* isomers **5–6** between the two types of anthers with pollen (2.1 vs 1.6 mg/g DW).

*Fluorescence and UV/Vis absorption spectral profiles of **2** and **5–12***

Fluorescence spectra of the methanol solution of **2**, **5**, and **6** showed their λ_{Ex} and λ_{Em} as follows: 383 nm and 453 nm (**2**); 355 nm and 433 nm (**5**); and 339 nm and 431 nm (**6**), respectively (see Chapter II). UV/Vis absorption spectra of **7**, **8**, mixtures of **9–11** (**9**:**10**:**11** = 47:26:27) and **12–14** (**12**:**13**:**14** = 59:12:29), and **15** are shown in Fig. 31. The absorption spectrum of **7** displayed its absorption maxima λ_{Abs} at 358 nm. Compound **8** exhibited a λ_{Abs} at 274 nm, the shortest among the

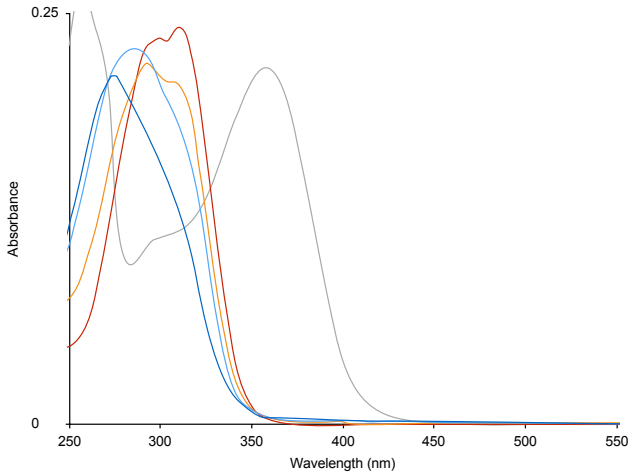

Fig. 11 UV/Vis absorption spectra of **7** (*gray*), **8** (*blue*), a mixture of **9–11** (*light blue*), a mixture of **12–14** (*orange*), and **15** (*red*).

isomers. The λ_{Abs} were at 286 nm for the mixture of **9–11**, at 293 nm for the mixture of **12–14**, and at 310 nm for **15**. Compounds **8–15** exhibited absorption maxima at wavelengths proportional to the number of (*Z*)-double bonds in the molecule (the shorter the wavelength, the greater the number of (*Z*)-double bonds). These characteristics of **8–15** would be attributed to the nonplanarity of the (*Z*)-form (Beale and Roe 1953), as described in Chapter V.

*Distributions of **2** and **8–15** in anthers and pollen*

The amounts of **2** and **8–15** were largely different between the two types of anthers with pollen (Table 3). MALDI-MS/MS imaging analyses were performed on-tissue to examine the distributions of **2** and **8–15** at the bicellular pollen stage. Compound **2** was detected by a fragment ion at *m*/*z* 191.04, corresponding to $[M-H-\text{caffeoyl}]^-$ (Fig. 32a). The peak intensity of **2** in the MS imaging was approximately 3.3-fold higher in the anthers with fluorescent pollen compared to those with non-fluorescent pollen. In the anthers with fluorescent pollen, **2** was distributed throughout the entire anther and pollen, with the highest concentrations in the endothecium and pollen grains (Fig. 32b).

Compounds **8–15** (isomers not distinguished) were detected by a fragment ion at *m*/*z* 420.22, corresponding to $[M+2H-H_2O-\text{coumaroyl}]^{2+}$ (Fig. 32c). The peak intensity of **8–15** in the MS imaging was approximately 14.3-fold higher in the anthers with fluorescent pollen compared to the anthers with non-fluorescent pollen. Compounds **8–15** were distributed evenly across the anther and non-fluorescent pollen grains (Fig. 32d), with the highest abundance in the pollen. Only a limited amount of **8–15** was detected in the anthers with non-fluorescent pollen.

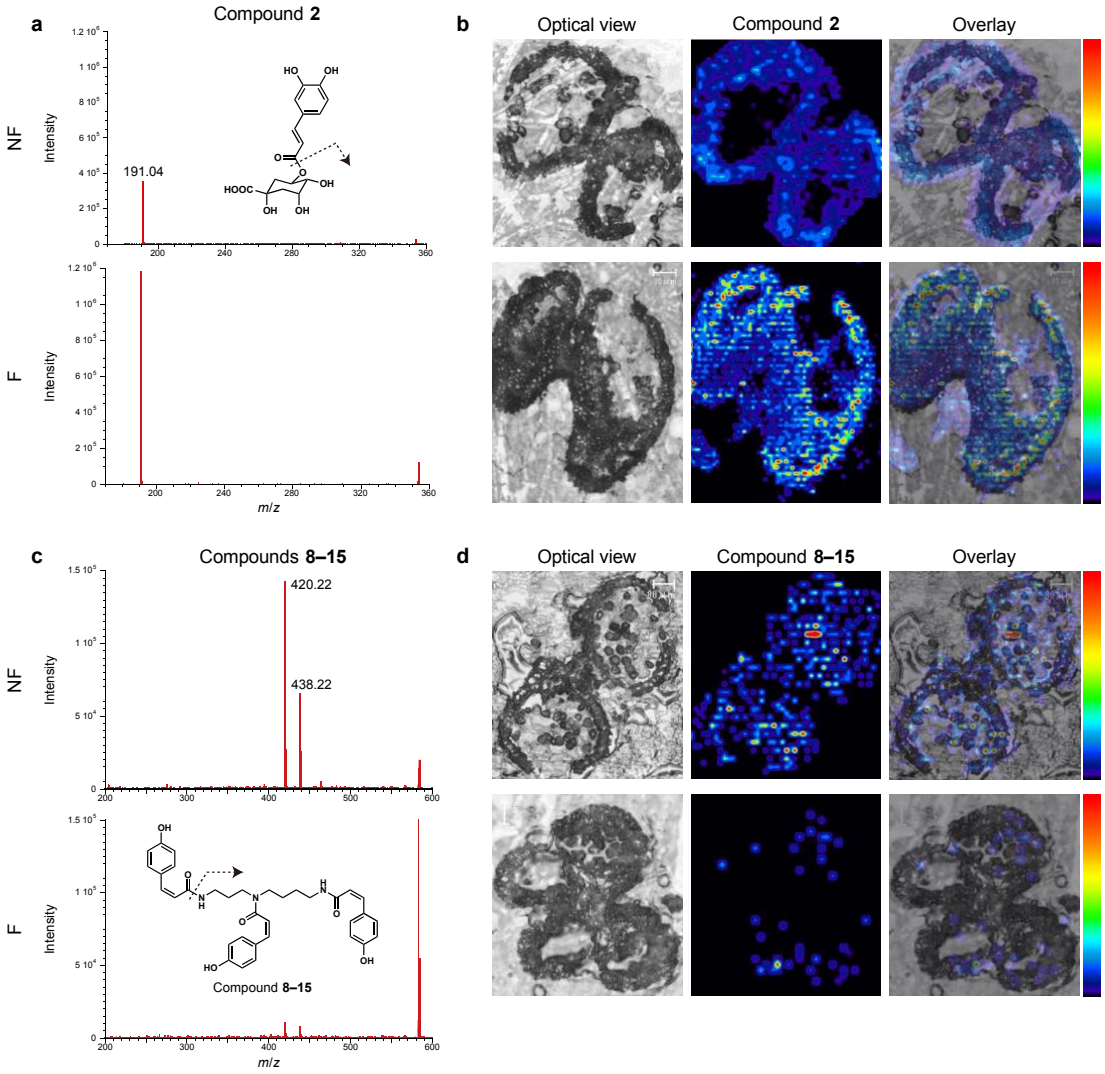

Fig. 12 Distributions of **2** and **8–15** in anthers and pollen at the bicellular pollen stage. (a) MS chromatograms and (b) distributions of **2** (*m*/*z* 191.04) in anthers with non-fluorescent pollen (NF; *upper*) and anthers with fluorescent pollen (F; *lower*), and (c and d, respectively) those of **8–15** (*m*/*z* 420.22; isomers not distinguished).

3. Discussion

The pollen viability test showed that the fluorescent pollen grains were completely sterile (Fig. 23b). The occurrence of fluorescent pollen in 33% of flowers in individual trees indicates that these flowers underwent abnormal development to be sterile. The electron microscopic observations confirmed that the sterile pollen was abnormally collapsed and devoid of pollenkitt and intine (Fig. 22). Intine development begins at the unicellular microspore stage, and pollenkitt is provided through tapetal programmed cell death at the bicellular pollen stage (Carrizo García et al. 2017; Sanders et al. 1999). In the abnormally developed anthers, tapetal cells were vacuolated at the

unicellular microspore stage, even filling the anther locule (Fig. 24). The absences of pollenkitt and intine and the vacuolated tapetum suggest a failure in the development of the anther and pollen at the early unicellular microspore stage (Fig. 22d). Male reproductive development is the most sensitive stage to various environmental stresses. Similar tapetal vacuolation has been observed in cold-stressed rice anthers (Mamun et al. 2006, 2010; Oda et al. 2010).

The anthers with sterile pollen contained a significantly higher amount of fluorescent compound **2**, compared to those with fertile pollen. Phenylpropanoids, including **2**, are induced in response to environmental stresses, including low temperature (Dixon and Paiva 1995; Koeppe et al. 1970). This is consistent with tapetal vacuolation at the unicellular microspore stage. Low temperature stress during the early unicellular microspore stage may cause the abortion of pollen development in *P. mume* cv. Nanko. MALDI-MS/MS imaging suggested that a substantial amount of **2** exists on the surface of sterile pollen grains. Compound **2** may have been accumulated in the abnormally vacuolated tapetum, and then deposited onto the surface of sterile pollen by tapetal degradation.

N^1,N^5,N^{10}-Tri-*p*-coumaroylspermidine isomers **8**, **10–12,** and **15** have been previously isolated from the flowers and anthers of several plant species (Bokern et al. 1995; Jiang et al. 2008; Sobolev et al. 2008; Werner et al. 1995; Zhao et al. 2010). However, **9**, **13,** and **14** have not been previously described. The anthers and pollen are exposed to sunlight, so the isomers may arise from photoisomerization under the sun *in vivo*, considering their high photosensitivity. Hydroxycinnamic acid amide (HCAA) derivatives including N^1,N^5,N^{10}-tri-*p*-coumaroylspermidine constitute a major group of specialized metabolites resulting from the conjugation of hydroxycinnamic acid with polyamines (i.e., putrescine, spermidine, and spermine), present in plant seeds, roots, and reproductive organs (Buta and Izac 1972; Cabanne et al. 1981; Fu et al. 2008; Hedberg et al. 1996; Luo et al. 2009; Mbadiwe 1973; Meurer et al. 1988a, b; Yang et al. 2012; Yoshihara et al. 1981). Polyamines are essential for life due to their diverse physiological functions in organogenesis, embryogenesis, floral initiation and development, leaf senescence, fruit development and ripening, and (a)biotic stress responses (Alcázar et al. 2010; Martin-Tanguy 2001; Moschou et al. 2012). Recently, polyamines were implicated in plant hormone biosynthesis and/or signaling (Alcázar et al. 2010; Anwar et al. 2015; Bassard et al. 2010; Bitrián et al. 2012; Morant et al. 2007b; Wimalasekera et al. 2011). Although the precise functions of HCAAs have yet to be elucidated (Fellenberg and Vogt 2015), HCAAs have been implicated in growth and developmental processes, and protection from UV-induced damage, microbial infection, and insect herbivory (Aloisi et al. 2016; Bassard et al. 2010; Facchini et al. 2002; Kaur et al. 2010; Walters et al. 2001). Previously, HCAAs were regarded as end products; more recently, their involvement in polyamine homeostasis and phenolic

metabolism has been proposed (Matsuno et al. 2009; Vogt 2010).

MALDI-MS/MS imaging on anthers with fertile pollen showed that **8–15** were distributed entirely within the anther and pollen, with the highest amount in the pollen. This indicates that the pollenkitt of fertile pollen contains **8–15**, as exemplified in *Arabidopsis thaliana* (Brassicaceae; Grienenberger et al. 2009) and the apple tree, *Malus domestica* (Rosaceae; Elejalde-Palmett et al. 2015). Compounds **8–15** are synthesized by a spermidine hydroxycinnamoyltransferase (SHT) (Elejalde-Palmett et al. 2015; Grienenberger et al. 2009). Since the *sht* knockout mutants show the abnormally crushed phenotype of pollen grains, hydroxycinnamoylspermidines, including N^1,N^5,N^{10}-tri-*p*-coumaroylspermidine, have been considered to be the components of sporopollenin (Elejalde-Palmett et al. 2015; Grienenberger et al. 2009). The deficiency of **8–15** in the anthers with sterile pollen is consistent with the morphological abnormality of exine and suggests that the flowers were exposed to stresses.

Pollenkitt of entomophilous plants typically contains pigments, such as flavonoids and carotenoids (Ferreres et al. 1989; Jiang et al. 2012), that are extractable from underlying exine with methanol (see Chapter II). After extraction with methanol, the fertile pollen grains became colorless and exhibited blue fluorescence (data not shown). Furthermore, in the normally developed anthers, the fluorescence of microspores disappeared as the pollenkitt deposited on the exine (Fig. 24). These are indicative that the absence of pollenkitt is responsible for the colorlessness and fluorescence. Ferulic acid has been demonstrated as a precursor of sporopollenin (Rozema et al. 2001; Xu et al. 2017), although the chemical structure of sporopollenin has not been elucidated (Mackenzie et al. 2015; Quilichini et al. 2015). The remnant fluorescence after extraction may be emitted from fluorophores such as caffeoyl and feruloyl moieties embedded in sporopollenin. The UV-absorbing compounds **7–15** in the pollenkitt would prevent UV light from reaching the underlying exine; thus, the pollenkitt-covered fertile pollen may not display fluorescence. The anthers with fertile pollen contained relatively small amounts of fluorescent compounds **2**, **5**, and **6**. As the absorption spectra of **7–15** overlap with the excitation and emission spectra of **2**, **5**, and **6**, the high amounts of **7–15** may quench the fluorescence of **1–3** through the primary and secondary inner-filter effects (Parker and Rees 1962). The emission spectra of **2**, **5**, and **6** corresponded well with that of the anthers with sterile pollen, suggesting that the fluorescence of sterile pollen is derived from these compounds. After extraction with methanol, the blue fluorescence of sterile pollen remained, so the embedded fluorophore may also contribute to the total fluorescence.

Bees discriminate human-gray from -yellow, with approximately 75–80% accuracy, when their color distance is 0.025 hex units (Dyer and Neumeyer 2005). The color distance from the anthers

with fertile pollen and background petal, representing the contrast between them, was 0.236 hex units, and that to the anthers with sterile pollen was 0.218 hex units. Both types of anthers may be easily detectable by honeybees against the petal background. The color distance between the two loci was 0.024 hex units, suggesting that honeybees distinguish between the two types of anthers by their reflection. Furthermore, the emission spectra of the anthers with pollen overlap the sensitivity curve of honeybee photoreceptors, implying that honeybees can perceive blue emission (Peitsch et al. 1992). The fluorescence emitted from the sterile pollen would contribute to the total emerging light (fluoresced + reflected photons), enhancing the visual signaling to pollinators. As honeybees prefer the blue fluorescence of chlorogenic acid (see Chapter III), the fluorescence may have an influence on their foraging behavior.

One possible cause of low and fluctuating yield of *P. mume* is abnormal sterile pollen, likely caused by low temperature stress at the male reproductive stage. Another is the foraging efficiency of honeybees introduced into orchards. The sterile pollen was devoid of starch granules, so the fertile pollen may be more nutritious for honeybees. However, if pollinating honeybees preferred the sterile pollen, the cross-pollination efficiency of *P. mume* might deteriorate.

4. Materials and methods

Plant material

Flowers and buds of the Japanese apricot, *Prunus mume* Siebold & Zucc. cv. Nanko (Rosaceae) were collected at The Garden of Medicinal Plants, Kyoto Pharmaceutical University (Kyoto, Japan) and the experimental farm of Kyoto University (Kyoto, Japan) from February to March 2017.

Photography

Photographs of flowers were taken with an EOS 60D camera (Canon, Tokyo, Japan) equipped with an EF-S60 mm F2.8 MACRO USM lens (Canon). The anthers and pollen were photographed with the camera EOS 60D connected to an SMZ-1500 stereomicroscope (Nikon, Tokyo, Japan). Fluorescent lamps HGX FHF32EX (32 W; NEC lighting, Tokyo, Japan) were used for white light illumination, and two Handy UV lamps LUV-16 (365 nm, 16 W; ASONE, Osaka, Japan) for UV illumination.

Reagents

9-Aminoacridine was purchased from Tokyo Chemical Industry (Tokyo, Japan). Other reagents were purchased from Wako Pure Chemical Industries (Osaka, Japan). Wakogel® C-200 silica gel (Wako Pure Chemical Industries) was used for silica gel column chromatography. Ultrapure water was obtained by Genpure UV-TOC xCAD PLUS (Thermo Fisher Scientific, MA, USA). All reagents were of analytical grade.

Pollen viability test

The anthers were incubated to be dehisced at 20°C for 10 h in an IC800 incubator (Yamato Scientific, Osaka, Japan). The non-fluorescent and fluorescent pollen were collected under UV illumination. The two types of pollen grains were separately cultivated on the mediums containing 1% agar (w/v), 15% sucrose (w/v), and 0.01% boric acid (w/v) for 12 h in the dark. Temperature and humidity were maintained at 20°C and 85%, respectively, during the tests. The tests were replicated three times for both types of pollens, and germination rates were presented as mean ± SE. Images were captured with the EOS 60D camera connected to the SMZ-1500 stereomicroscope.

The non-fluorescent and fluorescent pollen grains were stained for 5 min with Lugol's solution (Johansen 1940). Images were captured with the EOS 60D camera attached to a BX50 upright light microscope (Olympus, Tokyo, Japan).

Electron microscopies

The dehisced anthers containing pollens were collected from fresh opened flowers. The anthers were soaked in FAA fixative (63% EtOH, 5% AcOH, and 5% HCHO) at 4°C overnight. The fixed anthers were dehydrated in a graded ethanol series and in *t*-butyl alcohol, and then freeze-dried at −20°C. The dried anthers were mounted on stages and coated with platinum in an ion coater IB-3 (Eiko Engineering, Tokyo, Japan). The anthers were observed by a SEM S-4700 (Hitachi, Tokyo, Japan) at an acceleration voltage of 5.0 kV.

The dehisced anthers were soaked in half Karnovsky's fixative for 30 h. The fixed anthers were rinsed with 0.1 M phosphate buffer, followed by post-fixation with 1% osmium tetroxide at 4°C overnight. The anthers were dehydrated in a graded ethanol series, and embedded in Plain resin (Nisshin EM, Tokyo, Japan) at 70°C for 5 days. Ultrathin sections were prepared by an EM UC6 ultramicrotome (Leica, Heidelberg, Germany) using a diamond knife. The sections were stained with 1% uranyl acetate and then with lead citrate. The prepared sections were placed on copper grids and observed with a TEM H-7650 (Hitachi, Tokyo, Japan). Images were captured with an

AMT XR-41C CCD camera system (Advanced Microscopy Techniques, MA, USA).

Cytohistological analyses

The floral buds and opened flowers were soaked in the FAA fixative at 4°C overnight. Tissue fixation and paraffin embedding were performed with a LabPulse H2850 microwave processor (Energy Beam Sciences, CT, USA), according to Osaka et al. (2013), with minor modifications. All samples were embedded in Paraplast X-TRA paraffin (Fisher Scientific, Hampton, NH, USA). The paraffin blocks were stored at 4°C until observation. The samples were cut into 10 μm-thick sections using a microtome RV240 (Yamato Koki, Saitama, Japan). The sections were placed on glass slides (Matsunami Glass, Osaka, Japan) and baked at 50°C overnight. The paraffin was removed with Histo-Clear II (National Diagnostics, GA, USA). After rehydration by an ethanol series, the sections were stained with Periodic acid-Schiff (PAS) stain kit (Muto Pure Chemicals, Tokyo, Japan). The stained sections were placed in a Multimount480 mounting medium (Matsunami Glass). The prepared sections were stained with DAPI (4',6-diamidino-2-phenylindole) staining solution (Watanabe et al. 1991), and then mounted in 70% glycerol medium. All section images were obtained with a SteREO Discovery V20 stereomicroscope (Carl Zeiss, Jena, Germany).

Colorimetry

Diffuse reflectance spectra of the intrinsic anthers and petals were measured from 350 nm to 700 nm, using a V-670 spectrometer (Jasco, Tokyo, Japan) equipped with an ISN-723 integrating sphere unit (Jasco). The dehisced anthers with pollen and fresh petals were used for the measurements. The spectra were measured in an FPA-810 powder sample cell (Jasco). Spectralon (Labsphere, NH, USA) was used as a white standard for calibration. Data were processed using Spectra Manager version 2.10.01 (Jasco).

The color loci of the anthers with pollen in the color hexagon space (Chittka 1992) were calculated in R (R Core Team 2016) using a package 'pavo' version 1.3.2 (Maia et al. 2013) with the reflectance spectra from 350 nm to 650 nm, considering the spectral sensitivity of honeybees, *Apis mellifera* L. (Peitsch et al. 1992). The daylight irradiance spectrum of CIE D65 was applied as a model of daylight irradiance. The reflectance of petals was assumed as the background of the anthers. The hexagon was divided into six categories, UV, UV-Blue, Blue, Blue-Green, Green, and UV-Green, which refer to the stimulation of honeybee photoreceptors. Chromatic contrasts were evaluated by the Euclidian distances (hex units) (Chittka 1992).

UV/Vis absorption and fluorescence spectral analyses

The UV/Vis spectra of MeOH solutions of **7–15** were measured with a UV-1800 spectrometer (Shimadzu, Kyoto, Japan). Fluorescence spectra were measured with an FP-8300 spectrofluorometer (Jasco, Tokyo, Japan). An FUV-803 absorbance measurement cell block (Jasco) was used for solutions of **7**–**15**, and an FPA-810 powder sample cell block for the intrinsic dehisced anthers with pollens. The ratios of compounds **9–11** and of compounds **12–14** in the mixtures were determined with ^{1}H NMR by calculating based on the integrated areas under signals of each isomers. The absorption spectra **7–15** were measured from 250 nm to 550 nm, and the excitation and emission spectra of the anthers with pollen from 300 nm to 600 nm. The samples of anthers with pollen were randomly divided into three sets. The spectra with each set were averaged. The fluorescence spectral data were processed with Spectra Manager version 2.10.01 (Jasco). The areas under spectral curves of emission, AUC_{Em}, of anthers and pollen were integrated.

HPLC, LC-MS, and NMR analyses

HPLC was performed on L-7100 series (Hitachi, Tokyo, Japan) consisting of an L-7100 pump (Hitachi) and an L-7400 detector (Hitachi) on the following conditions: column, a YMC-Pack ODS-AQ (6.0 mm inner diameter × 100 mm; YMC, Kyoto, Japan); eluent, H_2O-MeOH-AcOH; flow rate, 1.0 mL/min; and detection, UV 254 nm.

LC-MS analyses were performed on an Acquity UPLC system H class and a Xevo G2-S QTof MS (Waters, MA, USA) with an Acquity UPLC BEH C18 column (polar size 1.7 μm, 2.1 mm inner diameter × 100 mm; Waters). The analyses were conducted on the following conditions: eluent, 22% MeCN containing 0.1% HCO_2H for 10 min and 50% MeCN containing 0.1% HCO_2H for 10–15 min; flow rate, 0.3 mL/min; detection, UV 254 nm. MS was operated in electron spray ionization (ESI) of positive mode under the following parameters: column oven, 35°C; capillary voltage, 3.0 kV; cone voltage, 40 V; source temperature, 150°C; desolvation temperature, 500°C; cone gas, 50 L/h; desolvation gas, 800 L/h. Data processing was performed using MassLynx version 4.1 (Waters).

^{1}HNMR spectra were measured in methanol-d_4 (Sigma-Aldrich, MO, USA) at 25°C with an AVANCE III 400 spectrometer (Bruker, Rheinstetten, Germany). Data processing was performed using TopSpin version 3.0 (Bruker).

*Isolation and quantification of **2** and **5–15***

The non-fluorescent anthers with pollen (1.4 g fresh weight) were soaked in 30 mL of MeOH at 4°C for 5 days. The extract was filtered and concentrated *in vacuo* to give an oily residue (136 mg).

The residue was partitioned with EtOAc and H_2O three times. The material from the organic layer was applied to a silica gel column (10 mm inner diameter × 70 mm) with eluent of $CHCl_3$-MeOH (5 mL for each fraction). The materials eluted with 10% (fraction 1) and 20% MeOH (fraction 2) were subjected to further separations, and that eluted with 30% MeOH was concentrated to give **2**. Further purifications were carried out in the dark.

Fraction 1 was analyzed by LC-MS (Fig. 28) and subjected to preparative HPLC (eluent: 0.1% AcOH in 50% MeOH) to give the following fractions: *t*R 7.1 min (fraction 3), 10.8 min (fraction 4), 12.0–15.0 min (fraction 5), and 18.4 min (fraction 6). The materials in fractions 3 and 6 were concentrated to give **8** (0.3 mg) and **15** (trace), respectively. Fraction 4 was concentrated and then purified with preparative HPLC (eluent: 0.1% AcOH in 39% MeOH). The materials eluted at *t*R 60.4, 62.0, and 63.0 min were separately collected and concentrated to give **9** (trace), **10** (trace), and **11** (trace) as major compounds in each, respectively. Fraction 5 was concentrated and then subjected to preparative HPLC (eluent: 0.1% AcOH in 39% MeOH). The materials eluted at *t*R 105.4, 110.3, and 111.5 min were collected and concentrated to give **12** (trace), **13** (trace), and **14** (trace), as major compounds in each, respectively. The ratios of **9–11**, of **12** and **13**, and of **12** and **14** in the mixtures were determined with ^{1}H NMR by calculation based on the integrated areas of signals of each isomer.

Fraction 2 was subjected to preparative HPLC (eluent: 0.1% AcOH in 40% MeOH) to give two fractions at *t*R 0–11.4 min (fraction 7) and 14.2 min (fraction 8). Fraction 7 was subjected to preparative HPLC (eluent: 0.1% AcOH in 20% MeOH), and the materials eluted at *t*R 17.3 min and 20.1 min were collected and concentrated to give **5** (0.2 mg) and **6** (trace), respectively. Fraction 8 was concentrated to give **7** (1 mg).

Quantification was performed with HPLC. The amounts of **2** and **5–12** in the extracts were calculated with a calibration curve between the weight and peak area, using isolated **2** and **5–12** as standards.

Quercetin 3-*O*-β-D-glucoside (**7**): yellow powder; ESIMS *m*/*z* 463.1 $[M-H]^-$; ^{1}H NMR data (400 MHz, methanol-d_4) δ 7.73 (1H, d, *J* = 2.2 Hz, H-2'), 7.61 (1H, dd, *J* = 8.5 and 2.2 Hz, H-6'), 6.89 (1H, d, *J* = 8.5 Hz, H-5'), 6.40 (1H, d, *J* = 2.1 Hz, H-8), 6.22 (1H, d, *J* = 2.1 Hz, H-6), 5.26 (1H, d, *J* = 7.6 Hz, Glc H-1), 3.74 (1H, dd, *J* = 11.9 and 2.4 Hz, Glc H-6), 3.60 (1H, dd, *J* = 11.9 and 5.3 Hz, Glc H-6), 3.20–3.55 (4H, Glc H-2, 3, 4, and 5).

N^1,N^5,N^{10}-tri-*p*-coumaroylspermidine isomers (**8–15**): white powder; HRESIMS *m*/*z* 584.2758 $[M+H]^+$ (calcd. for $C_{34}H_{38}N_3O_6$, 583.2761); see Table 3 for ^1H NMR data (400 MHz, methanol-d_4).

MALDI-MS/MS imaging analyses

For sample treatment, the anthers with non-fluorescent pollen and those with fluorescent pollen were collected individually and embedded in 4% carboxymethyl cellulose (CMC; Leica, Wetzlar, Germany). The embedment was performed on base-mold (7 mm × 7 mm × 5 mm) (FALMA, Tokyo, Japan). The anthers were slowly mixed to disperse in the CMC. After dispersion, the molds were stored in a deep freezer at −80°C until complete freezing. Before making tissue sections, the blocks of CMC with anthers were put in a cryomicrotome CM1950 (Leica) at −20°C for 10 minutes. The blocks were put on the tissue-holder, fixed with optimum cutting temperature polymer (Leica), and sliced at 10 μm-thickness. The tissue sections were collected onto cryofilm (Leica). The obtained section on the film was mounted onto Indium-tin-oxide (ITO)-coated glass slides (100 Ω/m^2 without anti-peeling coating; Matsunami Glass, Osaka, Japan) via double-sided adhesive conductive tape (3M, MN, US). The glass slides were dried at room temperature in 50 mL conical tubes with silica gel.

9-Aminoacridine was applied to the tissue sections by the recrystallization method, a method combining sublimation and exposing 5% methanol vapor. For sublimation, 9-aminoacridine was heated at 220°C and deposited on the surface of the tissue sections in iMLayer (Shimadzu, Kyoto, Japan) until the thickness of the matrix reached 0.5 μm. After covering the sections with a 9-aminoacridine layer, 5% methanol with H_2O vapor was provided for three seconds, and then they were dried at room temperature.

Imaging mass spectrometry was performed with iMScope TRIO (Shimadzu, Kyoto, Japan). Both optical images and ion distribution could be obtained within the same instrument under atmospheric pressure. Nd:YAG laser (λ = 355 nm, 1 kHz) was used as the MALDI laser source, and laser irradiation was repeated 80 times on each data point with a laser power of 45.0 (arbitrary unit in iMScope TRIO). Negative and positive ion modes were used to detect **2** and **5–12**, respectively. To enhance the specificity, MS/MS imaging was performed using the transition of *m*/*z* 353.08 > 191.04 for **2** and of *m*/*z* 584.28 > 420.22 for **5–12**. The voltages of the sample stage and detector were 3.0 kV and 2.1 kV, respectively. Imaging data was reconstructed using BioMap 3.8 (Mass Spectrometry Imaging Society, https://ms-imaging.org/wp/).

Chapter V
Unusual conformational preference of N^1,N^5,N^{10}-tri-*p*-coumaroylspermidine

1. Introduction

In the isolation process of N^1,N^5,N^{10}-tri-*p*-coumaroylspermidine *E*-*Z* isomers (**8**–**15**; Fig. 30), they were found to show a characteristic photoisomerization, which the (*ZZZ*)-isomer (**8**) predominated over the (*EEE*)-isomer (**15**). This unusual preference for (*Z*)- over (*E*)-geometry double bonds has also been observed in *N*,*N*'-di- and *N*-mono-*p*-coumaroylspermidines (Hu et al. 1998; Sobolev et al. 2008; Werner et al. 1995), but its causes were previously unknown. Under UV irradiation, the photoequilibrium ratio of the (*E*):(*Z*) isomers of N^5-*p*-coumaroylspermidine is 4:96, and 33:67 for N^1- and N^{10}-*p*-coumaroylspermidines (Hu et al. 1998), reflecting the relative stability of the (*Z*)-geometry of these molecules, compared to the (*E*). However, *p*-coumaric acid reaches a photoequilibrium in the ratio of (*E*):(*Z*) = approximately 90:10 (Hartley and Jones 1975). The unusual stability of *N*-*p*-(*Z*)-coumaroylspermidine compared to *N*-*p*-(*E*)-coumaroylspermidine seems to arise from intramolecular interactions between the coumaroyl and spermidine moieties, which are only possible in the (*Z*)-isomer.

For *N*,*N*'-di-*p*-coumaroylspermidines, the photoequilibrium ratio of (*EE*):(*EZ*/*ZE*):(*ZZ*) isomers is approximately 15:49:36 for N^1,N^{10}-di-*p*-coumaroylspermidine, and approximately 3:37:60 for N^1,N^5- and N^5,N^{10}-di-*p*-coumaroylspermidines, according to the HPLC chromatograms in Hu et al. (1998). One hypothesis for the higher photoequilibrium ratios of the N^1,N^5- and N^5,N^{10}-di-*p*-(*ZZ*)-coumaroylspermidines compared to N^1,N^{10}-di-*p*-(*ZZ*)-coumaroylspermidine is that the N^5-*p*-(*Z*)-coumaroyl moiety interacts with the adjacent *p*-coumaroyl moiety, stabilizing their (*ZZ*)-forms. However, in N^1,N^{10}-di-*p*-(*ZZ*)-coumaroylspermidine, the intramolecular distance between the N^1- and N^{10}-*p*-(*Z*)-coumaroyl moieties is much longer than that between N^1 and N^5, which may preclude their mutual interaction. The relative stability of N^1-acetyl-N^5,N^{10}-di-*p*-(*ZZ*)-coumaroylspermidine over its (*EE*)-isomer also suggests a role for the N^5-*p*-(*Z*)-coumaroyl moiety in stabilizing the (*ZZ*)-form (Sobolev et al. 2008). These studies imply that the intramolecular interactions between the *p*-(*Z*)-coumaroyl and spermidine moieties; and between the *p*-(*Z*)-coumaroyl and *p*-(*Z*)-coumaroyl moieties, are responsible for the relative stability of **8**. The N^5-*p*-(*Z*)-coumaroyl moiety may be important to enhance the stability of **8**, **10, 11**, and **12**.

The photoisomerization characteristics of **8–15** and the intramolecular interactions that give rise to the unusual preference for **8** were examined.

2. Results and discussion

*Photoequilibrium ratio of **8–15***

Exposure of a pure sample of **15** to UV light (254 nm) caused it to rapidly isomerize to **8–14**. No degradation or photodimerization was observed. After 10 min, 40% of **15** had isomerized. Equilibrium had been reached after 120 min, and the final ratio of compounds was **8**:**9–11**:**12**:**13** and **14**:**15** = 33:45:12:8:2 (Fig. 33; by HPLC analysis of the sample solution). This result indicates that the thermodynamic stability of N^1,N^5,N^{10}-tri-*p*-coumaroylspermidine increases as the number of (*Z*)-coumaroyl moieties in the molecule increases. The photoequilibrium ratio of **12** was higher than that of the mixture of **13** and **14** (12 vs 8), suggesting the importance of N^5-*p*-(*Z*)-coumaroyl moiety for the stability. The relative instability of the N^5-*p*-(*E*)-coumaroyl moiety is probably responsible for the very limited quantities of **9** that were observed.

*Conformational analyses of compounds **8–15***

The conformation of **8** was investigated by ^{1}H NMR spectroscopy and NOESY, in order to elucidate the intramolecular interactions responsible for the preference for the (*ZZZ*)-form of **8** over the (*EEE*)-form (**15**). Major NOESY correlations are shown in Fig. 34. The methylene proton

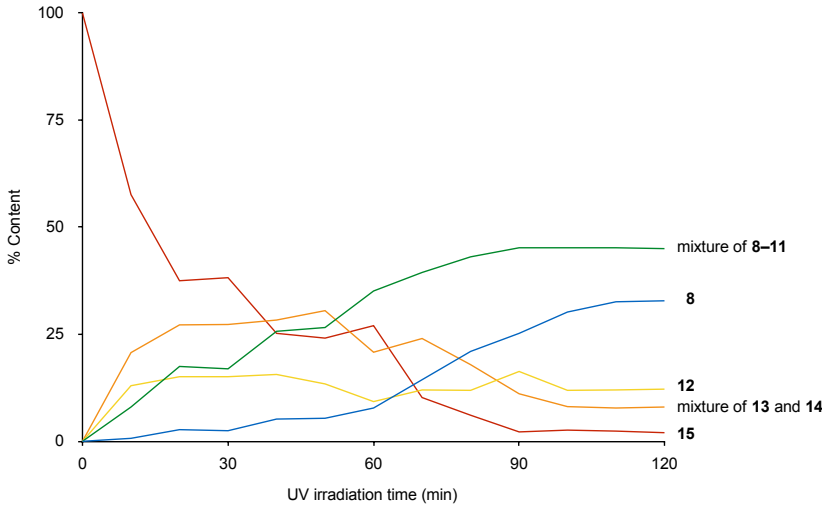

Fig. 1 Photoisomerization of **15** under UV 254 nm.

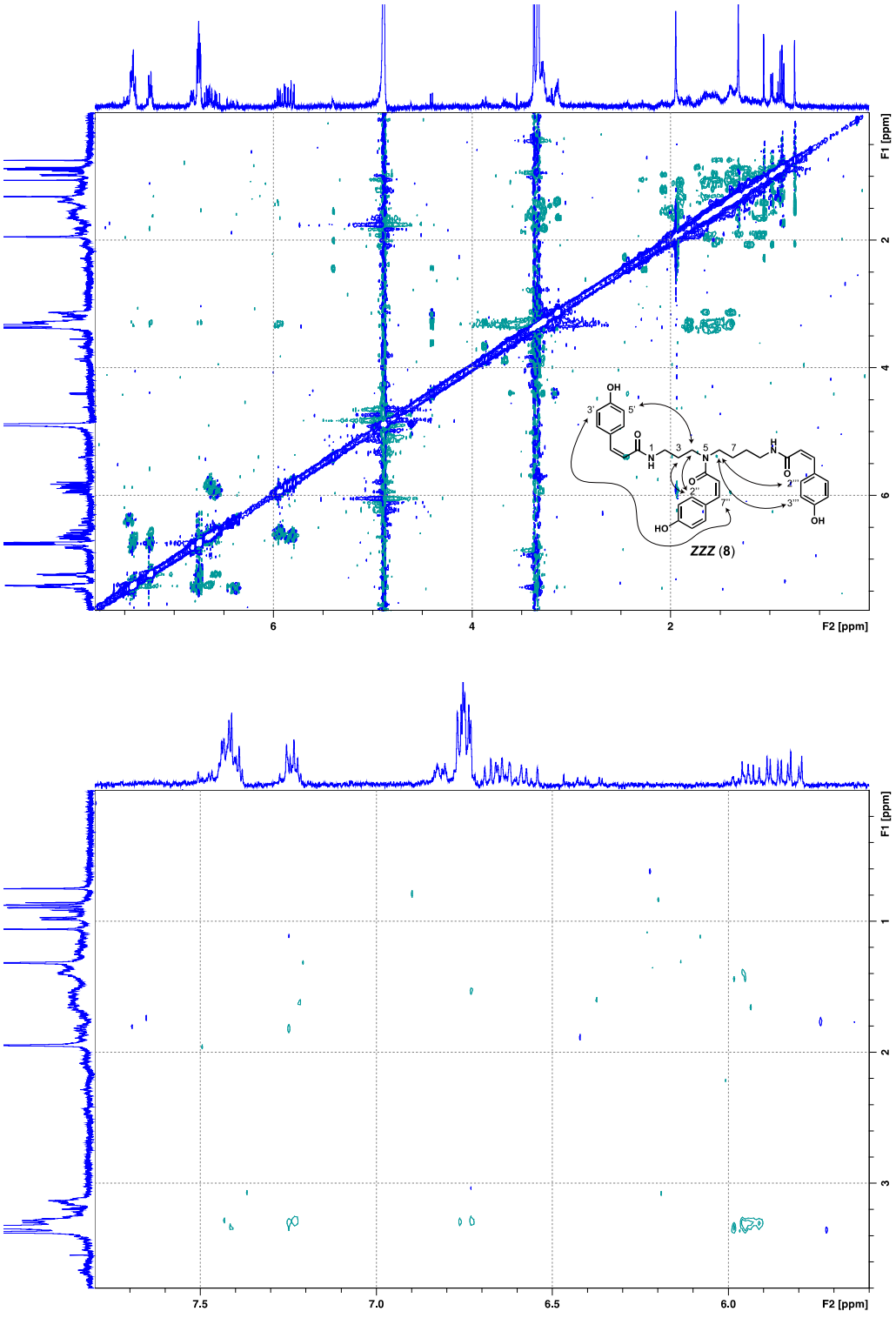

Fig. 2 NOESY spectrum of **8** of whole region (*upper*) and an expanded region (*lower*).

signals of **8** were observed at higher field than those of **15**; for example, the H-3 and H-4 signals were shifted approximately 0.1 ppm and 0.3 ppm upfield, respectively. The methylene signals at δ 3.3 (m, H-4 and 6, overlapped) showed NOEs with aromatic signals at 7.4 (m, H-2', 6', 2''', and 6''', overlapped) and at 6.7 (m, H-3', 5', 3''', and 5''', overlapped). These upfield shifts and the NOEs suggest that the N^1- and N^{10}-*p*-(*Z*)-coumaroyl moieties are folded back toward the center of spermidine moiety, and that the methylene bridges lie in the shielding region of aromatic rings (Johnson and Bovey, 1958). The N^5-*p*-coumaroyl aromatic signal at δ 7.2 (m, H-2'' and 6'') showed NOE interactions with the signals at 3.3 (m, H-4 and 6, overlapped) and at 1.9 (quintet, H-3), suggesting that the N^5-*p*-(*Z*)-coumaroyl moiety is folded toward the N^1-side. The signals of N^5-*p*-(*Z*)-coumaroyl H-2'' and H-6'' (overlapped) of **8** also appeared at higher field comparing with **15** (7.2 ppm vs 7.4 ppm), implying that H-2'' or H-6'' is located in the shielding region of the N^1-*p*-(*Z*)-coumaroyl aromatic ring. The similarity in chemical shifts of H-3'' and H-5'' for compounds **1** and **8** suggest a T-shaped π/π interaction between the N^1- and N^5-*p*-(*Z*)-coumaroyl aromatics, not one based upon parallel and parallel displaced π/π arrangements (Martinez and Iverson, 2012). The calculated π/π interaction energy for the T-shaped benzene dimer is approximately −12.43 kJ/mol at the MP2/cc-pVTZ level, when the distance between the two aromatic centroids is 5.0 Å (Tsuzuki et al., 2002). Aromatic signals at δ 6.7 (m, H-3', 5', 3'', 5'', 3''', and 5''', overlapped) showed an NOE with signals at 6.58/6.53 (d, H-7''). The N^5-*p*-coumaroyl H-7'' is spatially separate from H-3'', H-5'', H-3''', and H-5'''. This suggests that the NOE is derived from H-7'' and H-3' or H-5', which supports the T-shaped geometry. These NMR spectral data indicate that three *p*-(*Z*)-coumaroyl aromatics and spermidine moiety are close in space, likely causing intramolecular CH/π and T-shaped π/π interactions to stabilize (Suzuki et al. 1959; Oki and Mutai 1965; Nishio and Hirota 1989; Tsuzuki et al. 2002; Tsuzuki and Fujii 2008; Nishio 2011). Furthermore, as the N^{10}-*p*-coumaroyl moiety is folded back to the center of spermidine moiety, the N^{10}-*p*-coumaroyl hydroxy group may approach the N^5-*p*-coumaroyl carbonyl group to form an OH...O=C hydrogen bond.

Ab initio molecular orbital calculations were performed to examine the possibility of the intramolecular hydrogen bond in **8**, using simplified model compounds **16–18** of the N^1-, N^5-, and N^{10}-*p*-coumaroylamide moieties, respectively (Fig. 35). The enone s-*trans*/*cis* configurations of the *E*/*Z* forms were optimized for each model compound at MP2/cc-pVTZ level to include dispersion interaction (Dunning 1989; Møller and Plesset 1934; Tsuzuki et al. 2000a, b). The optimized conformations are illustrated in Fig. 35, and their energies are summarized in Table 4. The geometry optimizations of s-*trans*/*cis* (*E*)-**16–18** yielded almost planar conformations. S-*trans* (*Z*)-**16–18** and

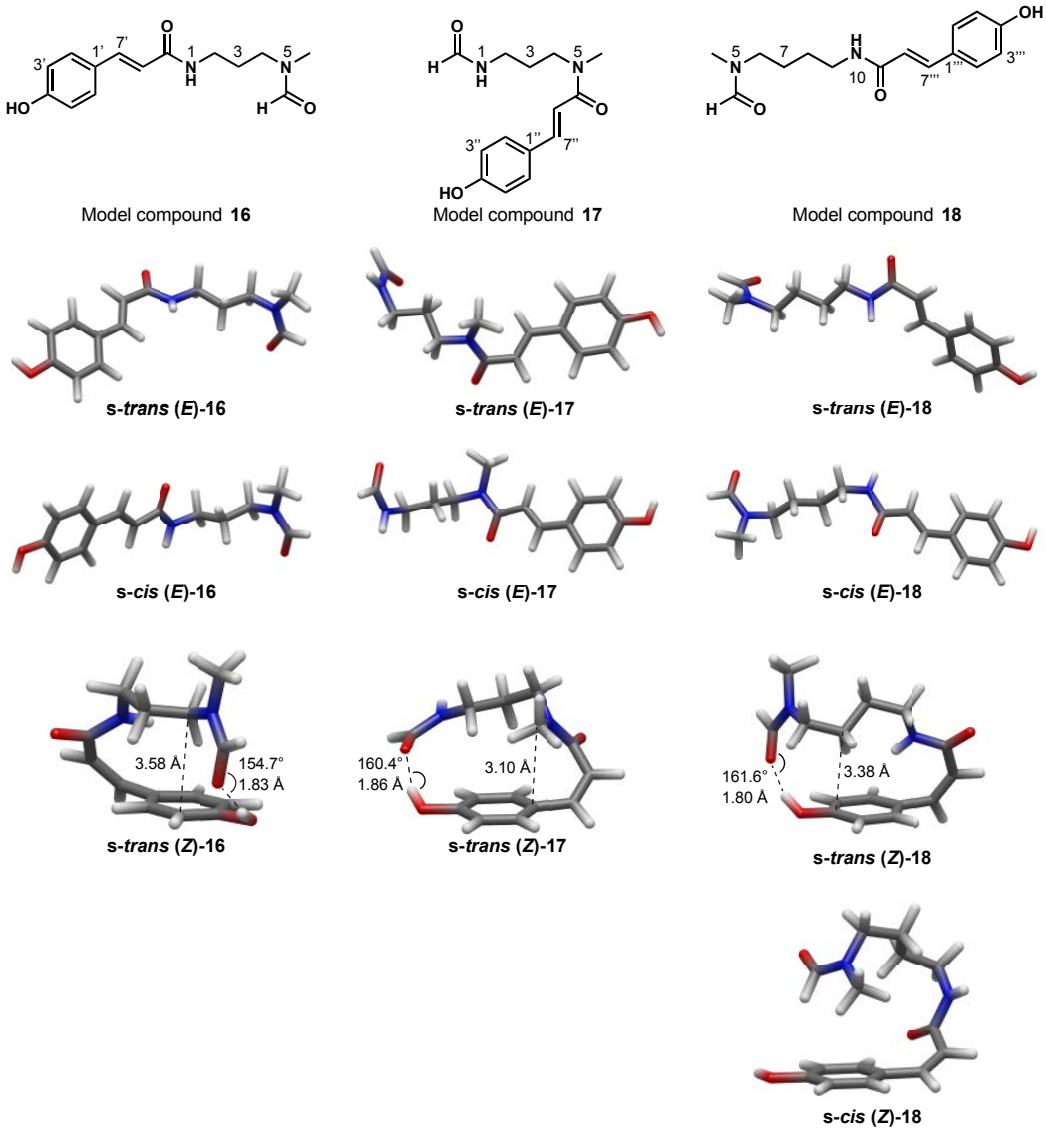

Fig. 3 Structures and optimized conformations of model compounds **16–18** at the MP2/cc-pTVZ level.

s-*cis* (*Z*)-**18** were optimized to highly nonplanar conformations; for example, the optimized geometry of s-*trans* (*Z*)-**16** has dihedral angles of 46.6° between phenyl and vinylene groups, and of 46.5° between vinylene and amide groups (Fig. 35). The geometry optimizations of s-*cis* (*Z*)-**16** and (*Z*)-**17** resulted in conversion into their s-*trans* conformation (data not shown), implying the instability of the s-*cis* (*Z*)-forms. The intramolecular molecular interactions in compounds (*Z*)-**16–18** are discussed below.

S-*cis* (*E*)-**16–18** were calculated to have lower energies than their s-*trans* forms (Table 4), suggesting that the (*E*)-isomers predominantly exist in their s-*cis* form, presumably to minimize steric hindrances. (*Z*)-**18** is 21.26 kJ/mol lower in energy in its s-*trans* form than in the s-*cis* form (Table 4). In contrast to the (*E*)-isomers, (*Z*)-**16–18** may predominantly exist in the s-*trans* form.

These configurational preferences of model *p*-coumaroylamides deduced from the theoretical calculations are consistent with previous results of NOE experiments for simple cinnamamides (Lewis et al. 1991). The unusual preferences of (*E*)-cinnamamides for their s-*cis* forms and of the (*Z*)-isomers for their s-*trans* forms are attributed to intramolecular charge transfer from aromatic to amide functionality (Lewis et al. 1991). Additionally, stabilization through CH/π interactions may also contribute to this preference, as discussed below. The optimized conformations of **16–18** suggest that **8–11** are highly nonplanar, but relatively planar for **12–15**. The nonplanar conformational distortion of s-*trans* (*Z*)-form would reduce the π orbital conjugation, which causes a hypsochromic shift (Beale and Roe 1953). The distortion may be responsible for shorter UV absorption maxima of **8–14** than that of **15** (Fig. 31). This may account also for similar UV spectral differences among the isomers of N^1-acetyl-N^5,N^{10}-di- and N^1,N^5-di-*p*-coumaroylspermidine and N^1,N^5,N^{10},N^{14}-tetra-*p*-coumaroylspermine (Lewis et al. 1991; Park et al. 2017; Sobolev et al. 2008; Werner et al. 1995).

The energy differences between the s-*trans* (*Z*)- and s-*cis* (*E*)-forms, $\Delta E_{\text{s-}trans\ (Z)\ -\ \text{s-}cis\ (E)}$, are −19.05 kJ/mol for **16**, −29.85 kJ/mol for **17**, and −24.31 kJ/mol for **18**, reflecting the higher stability of s-*trans* (*Z*)-**16–18** than their s-*cis* (*E*)-form. In the optimized conformations of s-*trans* (*Z*)-**16** and (*Z*)-**18**, the methylene C-4 and C-7 atoms locate above the *p*-coumaroyl aromatic C-3' and C-4''' atoms, respectively (Fig. 35). The intramolecular distances are 3.58 Å between C-4 and C-3' atoms, and 3.38 Å between C-7 and C-4''' atoms. These spatial arrangements and intramolecular distances suggest that the methylene C-H bonds interact with the π system to stabilize s-*trans* (*Z*)-**16** and (*Z*)-**18** (Bloom et al. 2012; Tsuzuki et al. 2000a). The CH/π interaction energies of the methane-benzene complex at the MP2/cc-pVTZ level are approximately −4.2 kJ/mol and −3.6 kJ/mol when the methane carbon atom is above the aromatic carbon atom at the distances of 3.6 Å

Table 1 Energies of s-*trans*/*cis* *E*-*Z* isomers of **16–18** at the MP2/cc-pVTZ level.

Compound	MP2/cc-pVTZ Energy (kJ/mol)	Δ*E*
s-*trans* (*E*)-**16**	-2304675.22	+32.92
s-*cis* (*E*)-**16**	-2304689.09	+19.05
s-*trans* (*Z*)-**16**	-2304708.14	0
s-*cis* (*Z*)-**16**	*	*
s-*trans* (*E*)-**17**	-2304659.32	+46.62
s-*cis* (*E*)-**17**	-2304676.09	+29.85
s-*trans* (*Z*)-**17**	-2304705.94	0
s-*cis* (*Z*)-**17**	*	*
s-*trans* (*E*)-**18**	-2407654.79	+36.72
s-*cis* (*E*)-**18**	-2407667.20	+24.31
s-*trans* (*Z*)-**18**	-2407691.51	0
s-*cis* (*Z*)-**18**	-2407670.25	+21.26

*Asterisks indicate that the optimizations resulted in conversion into their s-*trans* conformations.

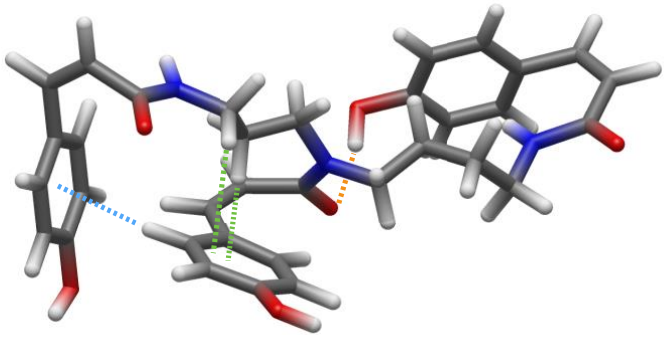

Fig. 4 Putative conformation of **8** in MeOH. Dotted lines: blue, T-shaped π/π interaction; green, CH/π interaction; orange, OH...O=C hydrogen bonding interaction.

and 3.4 Å, respectively, with little dependence on the orientation of C-H bond (Tsuzuki et al. 2000a, 2006). Although, in the optimized conformation of s-*trans* (*Z*)-**17**, the methylene C-6 atom locates above the aromatic C-1" atom at the distance of 3.10 Å, too short for a favorable CH/π interaction (Fig. 35; Tsuzuki et al. 2000a). Besides the CH/π interactions, the hydroxy group approaches the carbonyl group in the optimized conformation of s-*trans* (*Z*)-**16–18**. The intramolecular distance between the hydroxy hydrogen and carbonyl oxygen atoms is 1.83 Å, and the O-H-O bond angle 154.7° for s-*trans* (*Z*)-**16** (Fig. 35). For s-*trans* (*Z*)-**17**, those same measurements are 1.86 Å and 160.4°, and 1.80 Å and 161.6° for s-*trans* (*Z*)-**18** (Fig. 35). These distances and angles coincide almost exactly with the 1.79 Å and 160.1° of the optimized geometry of a formamide-phenol complex, wherein the hydrogen bond (OH...O=C) energy of the optimized complex was calculated to be approximately −36.82 kJ/mol at the MP2/cc-pVTZ level (Kaur and Kaur 2015). These theoretical characteristics of **16–18** establish the stabilizing capability of OH...O=C hydrogen bonds among *N*-*p*-(*Z*)-coumaroyl moieties (Arunan et al. 2011; Kaur and Kaur 2015; Liu et al. 2008).

The conformation of **8** in methanol was estimated based on these ^{1}H NMR and NOESY spectral analyses and *ab initio* calculations (Fig. 36). The close proximities of *N*-*p*-(*Z*)-coumaroyl moieties to methylene bridges indicated by the spectral analyses are consistent with the results of calculations (Fig. 35). The spectral analyses suggest that N^{1}-*p*-(*Z*)-coumaroyl and N^{5}-*p*-(*Z*)-coumaroyl aromatics exist in T-shaped π/π geometry, and the calculations with model compound **18** suggest an OH...O=C hydrogen bond between N^{10}-*p*-(*Z*)-coumaroyl hydroxy and N^{5}-*p*-(*Z*)-coumaroyl carbonyl groups. The N^{1}-*p*-(*Z*)-coumaroyl moiety may not form the OH...O=C hydrogen bonds with N^{5}-*p*-(*Z*)-coumaroyl moiety, since their hydroxy and carbonyl groups locate far from each other in T-shaped π/π geometry. The CH/π, T-shaped π/π, and OH...O=C hydrogen bonding interactions may provide the energies to overcome the photoisomerization barriers from (*E*)- to (*Z*)-isomer of N^{1},N^{5},N^{10}-tri-*p*-coumaroylspermidine. The methanol solvent may also affect the unusual

configurational preference (Nagy 2014).

These intramolecular interactions are probably responsible also for the stabilities of N^1,N^5-di-*p*-(*ZZ*)-, N^5,N^{10}-di-*p*-(*ZZ*)-, and N^1-acetyl-N^5,N^{10}-di-*p*-(*ZZ*)-coumaroylspermidines (Hu et al. 1998; Sobolev et al. 2008; Werner et al. 1995). The calculations with the model compounds **16** and **17** suggest that N^1-acetyl-N^5,N^{10}-di-*p*-(*ZZ*)-coumaroylspermidine forms two OH...O=C hydrogen bonds between the N^1-acetyl carbonyl and N^5-*p*-(*Z*)-coumaroyl hydroxy groups, and between N^{10}-*p*-(*Z*)-coumaroyl hydroxy and N^5-*p*-(*Z*)-coumaroyl carbonyl groups. Although *N*-mono-*p*-(*Z*)-coumaroylspermidines are also unexpectedly stable (Hu et al. 1998), this cannot be due to T-shaped π/π and OH...O=C hydrogen bonding interactions because of the absence of adjacent *N*-*p*-coumaroyl moieties.

Conformational analyses of N-mono-p-coumaroylspermidine

The intramolecular interactions between *N*-*p*-coumaroyl and spermidine moieties in N^1-, N^5-, and N^{10}-*p*-coumaroylspermidines were also investigated by *ab initio* molecular orbital calculations with simplified model compounds **19–21**, respectively (Fig. 37). The geometry optimizations of s-*trans*/*cis* (*E*)-**19–21** at the MP2/cc-pVTZ level provided the planar conformations, whereas the optimizations resulted in nonplanar conformations for their s-*trans* (*Z*)-forms, as well as compounds **16–18** (Fig. 37). The s-*cis* (*Z*)-forms of **19** and **20** were optimized to their s-*trans* conformations (data not shown), indicating the instabilities of their s-*cis* configurations. The lower energies of s-*cis* (*E*)-**19–21** compared to their s-*trans* forms indicate that (*E*)-**19–21** predominantly exist in the s-*cis* form (Table 5). S-*trans* (*Z*)-**21** had 27.64 kJ/mol lower energy than its s-*cis* form. (*Z*)-**19–21** may be more stable in the s-*trans* forms than in the s-*cis* form (Table 5). The $\Delta E_{\text{s-}trans\ (Z)\ -\ \text{s-}cis\ (E)}$ are −3.16 kJ/mol for **19**, −6.77 kJ/mol for **20**, and −13.25 kJ/mol for **21** (Table 5), suggesting that **19–21** prefer the s-*trans* (*Z*)-form over the s-*cis* (*E*)-form. The predominance of nonplanar s-*trans* (*Z*)-**19–21** may be responsible for the UV spectral difference in *E*-*Z* isomers of N^5- and N^{10}-*p*-coumaroylspermidines (Hu et al. 1998).

In the optimized conformations of s-*trans* (*Z*)-**19–21**, the methylene bridges and amino group are located above the aromatic ring, in close proximity to one another. For s-*trans* (*Z*)-**19**, the intramolecular distance between the N^5-amino nitrogen and aromatic C-4' atoms is 3.46 Å. The NH/π interaction energy of the ammonia-benzene complex at the MP2/cc-pVTZ level is approximately −7.5 kJ/mol, when the ammonia nitrogen atom locates above the aromatic carbon atom at the distance of 3.5 Å (Tsuzuki et al. 2000a). In the optimized conformations of s-*trans* (*Z*)-**20** and of (*Z*)-**21**, the distance between methylene C-2 and aromatic C-3'' atoms is 3.43 Å, and

that between C-7 and C-3''' atoms is 3.53 Å. The CH/π interaction energies of methane-benzene complex at the MP2/cc-pVTZ level are approximately −3.7 kJ/mol and −4.2 kJ/mol, when the methane carbon atom is above the aromatic carbon atom at the distance of 3.4 Å and of 3.5 Å, respectively (Tsuzuki et al. 2000b). The amino group of s-*trans* (*Z*)-**20** and (*Z*)-**21** do not lie above the aromatic ring, in contrast to those of s-*trans* (*Z*)-**19**. These geometries and distances imply that the NH/π and CH/π interactions contribute to the unusual stability of s-*trans* *N*-*p*-(*Z*)-coumaroylspermidine (Fig. 37; Table 5; Bloom et al. 2012; Hu et al. 1998; Tsuzuki et al. 2000a, b). The results for **19** suggest that N^1-*p*-(*Z*)-coumaroylspermidine was stabilized by the NH/π interaction between N^1-*p*-(*Z*)-coumaroyl aromatic and N^5-amino group. According to the results for **20** and **21**, the stability of N^5- and N^{10}-*p*-(*Z*)-coumaroylspermidines may be derived from the CH/π interaction between their aromatics and the C-H bonds at C-2 and C-7, respectively.

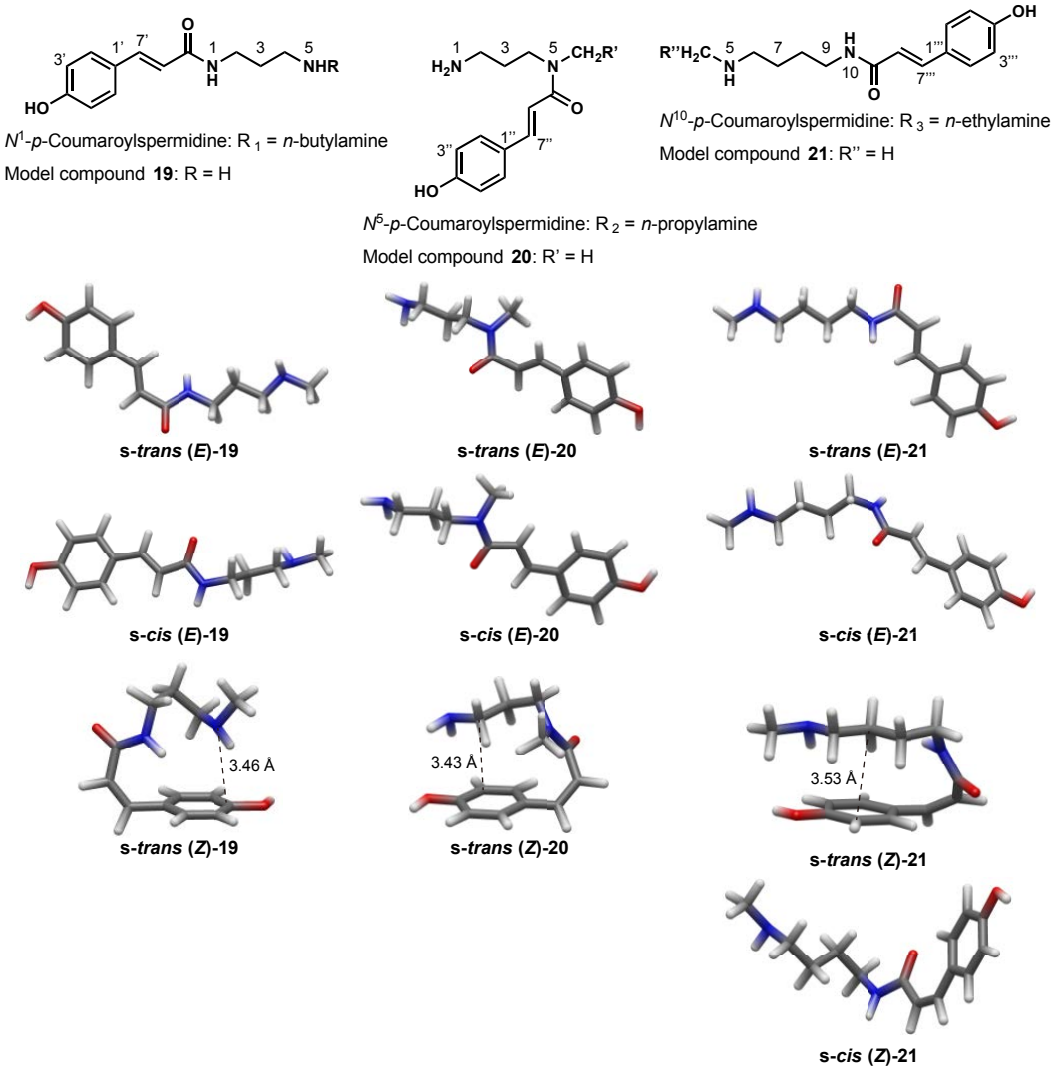

Fig. 5 Structure and optimized conformations of model compounds **19–21** at the MP2/cc-pVTZ level.

Table 2 Energies of s-*trans*/*cis* *E*-*Z* isomers of **19–21** at the MP2/cc-pVTZ level.

Compound	MP2/cc-pVTZ Energy (kJ/mol)	Δ*E*
s-*trans* (*E*)-**19**	-2007561.05	+12.23
s-*cis* (*E*)-**19**	-2007570.13	+3.16
s-*trans* (*Z*)-**19**	-2007573.29	0
s-*cis* (*Z*)-**19**	*	*
s-*trans* (*E*)-**20**	-2007560.14	+13.95
s-*cis* (*E*)-**20**	-2007567.32	+6.77
s-*trans* (*Z*)-**20**	-2007574.09	0
s-*cis* (*Z*)-**20**	*	*
s-*trans* (*E*)-**21**	-2110538.96	+21.98
s-*cis* (*E*)-**21**	-2110547.69	+13.25
s-*trans* (*Z*)-**21**	-2110560.94	0
s-*cis* (*Z*)-**21**	-2110533.30	+27.64

*Asterisks indicate that the optimizations resulted in conversion into their s-*trans* conformations.

N^5-*p*-(*Z*)-Coumaroylspermidine has higher thermodynamic stability compared to N^1- and N^{10}-*p*-(*Z*)-coumaroylspermidine (Hu et al. 1998). However, the intramolecular interaction energy of s-*trans* (*Z*)-**20** is implied to be not lowest among those of s-*trans* (*Z*)-**19–21** (Tsuzuki et al. 2000a, b). The notable stability of N^5-*p*-coumaroylspermidine may be not caused only by the single CH/π interaction (Hu et al. 1998). For N^5-*p*-(*Z*)-coumaroylspermidine, the N^5-*p*-(*Z*)-coumaroyl moiety may be able to form the CH/π interaction regardless of whether 4-aminopropyl or 4-aminobutyl groups approach. As the entropy of an *n*-alkyl chain increases with increasing number of carbons (Parks et al. 1930), the spermidine moiety is expected to have a higher entropy than the 4-aminopropyl or 4-aminobutyl groups. Loss of conformational entropy (Δ*S*) upon the CH/π formation may be lower in N^5-*p*-(*Z*)-coumaroylspermidine than in N^1- and N^{10}-*p*-coumaroylspermidines (Carroll et al. 2011). Formation of the CH/π interaction is probably entropically advantageous for N^5-*p*-coumaroylspermidine over N^1- and N^{10}-*p*-(*Z*)-coumaroylspermidines, and this advantage impart the prominent stability to N^5-*p*-(*Z*)-coumaroylspermidine; the enthalpic contribution ($-T\Delta H$) derived from the intramolecular CH/π interaction is not thought to be significant.

3. Materials and methods

Plant materials

Flowers of *Prunus mume* Siebold & Zucc. cv. Nanko (Rosaceae) were collected at The Garden of Medicinal Plants (34°56'15.0"N 135°49'03.3"E), Kyoto Pharmaceutical University (Kyoto, Japan) in the spring, March 2016.

Reagents

Reagents of analytical grade were purchased from Wako Pure Chemical Industries (Osaka, Japan) and used without further purification.

NMR spectroscopy

^{1}H NMR and NOESY spectra were measured in methanol-d_4 (Sigma-Aldrich, MO, USA) at 24°C with an AVANCE III 400 spectrometer (Bruker, Rheinstetten, Germany). Sample preparations were carried out in the dark. Data processing was performed using TopSpin version 3.0 (Bruker).

Photoisomerization

A methanol solution of **15** (2 mM) was put into a quartz cuvette (10 mm width × 40 mm height × 45 mm depth; Jasco, Tokyo, Japan), and the cuvette was covered with a Labo-USQ quartz glass plate (1 mm thickness; Daiko MFG, Kyoto, Japan). The cuvette was placed inside a dark box (ASONE, Osaka, Japan) equipped with a Handy UV Lamp SLUV-8 (254 nm, 8 W; ASONE). The distance between the UV lamp and the solution surface was 125 mm. The solution was irradiated by the UV light at 25°C. The UV intensity reaching the solution surface was 32 μW/cm^2. The solution was analyzed with the HPLC (eluent: 0.1% AcOH in 50% MeOH) every 10 min until the isomers reached a photoisomerization equilibrium. The ratio of **8–15** was calculated by each peak area on an assumption of the same molar extinction coefficient of **8–15**. The ratios of **9–11**, and of **13** and **14** were calculated with respective mixtures.

Molecular modeling

Ab initio molecular orbital calculations were carried out with simplified model compounds **16–21**. The structure construction of the model compounds was conducted with a SYBYL-X version 2.1.1 (Certara, NJ, USA). The s-*cis* structures of (*E*)-**16–21** were constructed by modifying the X-ray crystallographic data of s-*cis* *N*,*N*-dimethyl-*p*-(*E*)-bromocinnamamide (BCINAM; Meester and Schenk 1971) obtained from the Cambridge Crystallographic Data Centre (CCDC, https://www.ccdc.cam.ac.uk). The s-*cis* structures of (*Z*)-**16–21** were constructed by inverting the olefinic bond of s-*cis* (*E*)-**16–21**. The s-*trans* (*E*)- and (*Z*)-**16–21** were constructed by inverting the enone single bond between two double bonds of the respective s-*cis* structures. All structures were subjected to a systematic search of possible conformations by rotating all rotatable bonds in steps of 15°, and their minimum energy conformations were selected as starting structures from results of the search. Further calculations were performed with Spartan '16 version 2.0.7 (Wavefunction, CA,

USA; Shao et al. 2006). All starting structures were subjected to geometry optimizations using a Møller-Plesset second order perturbation theory (MP2; Møller and Plesset 1934) with a cc-pVTZ basis set (Dunning 1989). Dihedral angles and intramolecular distances were measured with the Spartan '16 using the optimized conformations. The construction of putative conformation of **8** was performed with the Spartan '16. The optimized conformations and putative conformation of **8** were illustrated with Avogadro 2 version 1.90.0 (Hanwell et al. 2012).

Summary

Anthers and pollen fluoresce under UV irradiation, which has been proposed as a visual cue for pollinating insects. Fluorescent compounds occurring in anthers and pollen may attract pollinating insects, while protecting DNA from UV-induced damage. Biocommunication between plants and insects through fluorescence has been discussed for decades, but the perceptive capability of insects for the fluorescence and the fluorescent compounds in anthers and pollen has not been investigated. This thesis describes the identification of fluorescent compounds and the behavioral response of honeybees to fluorescence. The major findings described below will open up new aspect of biocommunication between plants and insects.

Chapter II. Intact anthers with the pollen of six plant species displayed human-blue fluorescence under UV excitation. The pollen fluorescence was emitted from pollenkitt. The fluorescent compounds were identified as six hydroxycinnamoyl acid derivatives: 3,5-dicaffeoylquinic acid, chlorogenic acid, (*E*)-acteoside and its (*Z*)-isomer, and 1-*O*-(*E*)-feruloyl-β-D-glucose and its (*Z*)-isomer. These compounds may protect DNA not only by the transduction of absorbed UV energy to emission but also by antioxidant activity.

Chapter III. A behavioral assay on the western honeybee (*A. mellifera*) revealed that they perceived and preferred the fluorescence from chlorogenic acid under the sun. This result suggests that the fluorescence from anthers and pollen functions in attracting pollinators.

Chapter IV. The author found that *Pr. mume* bears two types of flowers in individuals: flowers with pollen grains that fluoresce under UV irradiation and those that do not. The fluorescent pollen abnormally developed to be sterile, likely by low temperature stress. The abnormal development and preference of honeybees for the fluorescence from sterile pollen may cause the low yield of *Pr. mume* fruit. The anthers with non-fluorescent pollen contained eight isomers of N^1,N^5,N^{10}-tri-*p*-coumaroylspermidine as major constituents; whereas the anthers with fluorescent pollen contained only a limited amount of the isomers, but relatively large amounts of the fluorescent chlorogenic acid. These differences may be responsible for the fluorescence of the sterile pollen. The photoisomerization of N^1,N^5,N^{10}-tri-*p*-coumaroylspermidine may have occurred *in vivo*

since the anthers and pollen are exposed to the sunlight.

Chapter V. N^1,N^5,N^{10}-Tri-*p*-coumaroylspermidine isomers showed an unusual photoequilibrium ratio, wherein the (*ZZZ*)-isomer predominated over the (*EEE*)-isomer. NMR spectroscopy, NOESY, and *ab initio* molecular orbital calculations indicated that multiple intramolecular CH/π, T-shaped π/π, and OH...O=C hydrogen bonding interactions can provide the unusual thermodynamic stability of the (*ZZZ*)-isomer.

Acknowledgements

This work was carried out in the Laboratory of Comparative Agricultural Science, Division of Environmental Science and Technology, Graduate School of Agriculture, Kyoto University, from 2012 to 2014 and 2015 to 2018. The author would like to thank Dr. Nobuhiro Hirai, Dr. Miki Akamatsu, Dr. Takeshi Miyake, and Dr. Hitoshi Shinjo of this laboratory, for their advice and encouragement throughout this study; as well as the late Dr. Hiroshi Fukui (Professor Emeritus of Kagawa University); Dr. Masayuki Sakuma, Mr. Masanori Oishi, and Ms. Mari Kawakami (Graduate School of Agriculture, Kyoto University); the late Mr. Katsumi Goto and Ms. Junko Tsukioka (The Garden of Medicinal Plants, Kyoto Pharmaceutical University); Dr. Shuichi Shimma (Graduate School of Engineering, Osaka University); Dr. Tetsu Nakanishi (Professor Emeritus of Kobe University); Dr. Masao Watanabe and Ms. Hiromi Masuko-Suzuki (Graduate School of Life Sciences, Tohoku University) for their contributions to this study. The author is also grateful to Mr. Masao Kaneko (Nagano Vegetable and Ornamental Crops Experiment Station) for supplying peach flowers; Dr. Makio Takeda (Graduate School of Agricultural Science, Kobe University) for supplying honeybees; Dr. Masatoshi Murai and Dr. Mizuho Hanaki (Graduate School of Agriculture, Kyoto University) and Dr. Katsutoshi Nishino (Graduate School of Biostudies, Kyoto University) for the mass spectral measurements; Mr. Tetsuhito Suzuki (Graduate School of Agriculture, Kyoto University) for the diffuse reflectance spectral measurements; Ms. Keiko Okamoto-Furuta and Mr. Haruyasu Kohda (Center for Anatomical, Pathological and Forensic Medical Researches, Graduate School of Medicine, Kyoto University) for their technical assistance with electron microscopy; Ms. Kanako Takakura (Fluorescent Live Imaging Core Facility of the Medical Research Support Center, Graduate School of Medicine, Kyoto University) for the technical assistance with the two-photon excitation microscopy; Dr. Kentaro Arikawa (School of Advanced Sciences, Graduate University for Advanced Studies) and Dr. Masami Sasaki (Professor Emeritus of Tamagawa University) for valuable discussion on the behavioral experiments with honeybees. The author thanks Dr. Kazuhiro Irie, Dr. Kazuma Murakami, Dr. Yusuke Hanaki, Dr. Masahiro Osakabe, Dr. Ryutaro Tao, Dr. Hisayo Yamane, and Dr. Takashi Akagi (Graduate School of Agriculture, Kyoto University), Dr. Akira Murakami (School of Human Science and Environment, University of Hyogo), and Dr. Yuto Kitamura (Japanese Apricot Research Laboratory, Wakayama Research Center) for valuable comments on this study. This research was not funded by any specific grant from funding agencies

in either the public, commercial, or not-for-profit sectors.

The author also thanks to all members of the Laboratory of Comparative Agricultural Science and the Laboratory of Organic Chemistry in Life Science, Division of Food Science and Biotechnology, Graduate School of Agriculture, Kyoto University, Ms. Yoko Fukui, Mr. Yoshiaki Higuchi, Ms. Yoko Yamamoto, Ms. Kirie Watanabe, Ms. Sakiko Imaeda, Mr. Takeshi Yoneda for their encouragement. The author is grateful to the funding received through the TOBE MAKI Scholarship Foundation. Finally, the author expresses special thanks to his family for their love and encouragement.

References

1. Aarts MGM, Hodge R, Kalantidis K, Florack D, Wilson ZA, Mulligan BJ, Stiekema WJ, Scott R, Pereira A (1997) *Plant J* **12**, 615–623.
2. Abrol DP (2012) Pollination Biology: Biodiversity conservation and agricultural production. Springer, Heidelberg.
3. Ackerman JD (2000) *Plant Syst Evol* **222**, 167–185.
4. Acquaah G (2012) Principles of Plant Genetics and Breeding, 2nd edition. John Wiley & Sons, New York.
5. Aguilar R, Ashworth L, Galetto L, Aizen MA (2006) *Ecol Lett* **9**, 968–980.
6. Ahlers F, Bubert H, Steuernagel S, Wiermann R (2000) *Z Naturforsch C* **55**, 129–136.
7. Ahlers F, Lambert J, Wiermann R (2003) *Z Naturforsch C* **58**, 807–811.
8. Aizen MA, Garibaldi LA, Cunningham SA, Klein AM (2009) *Ann Bot* **103**, 1579–1588.
9. Albersheim P, Darvill A, Roberts K, Sederoff R, Staehelin A (2010) Plant cell walls: From chemistry to biology. Garland Science, New York.
10. Alcázar R, Altabella T, Marco F, Bortolotti C, Reymond M, Koncz C, Carrasco P, Tiburcio AF (2010) *Planta* **231**, 1237–1249.
11. Aloisi I, Cai G, Serafini-Fracassini D, Del Duca SD (2016) *Front Plant Sci* **7**, 155.
12. Amador GJ, Matherne M, Waller D, Mathews M, Gorb SN, Hu DL (2017) *Bioinspir Biomim* **12**, 026015.
13. Andersson J, Borg-Karlson AK, Wiklund C (2000) *Proc R Soc Lond B* **267**, 1271–75.
14. Andrews K, Reed SM, Masta SE (2007) *Biol Lett* **3**, 265–267.
15. Anwar R, Matoo A, Handa AK (2015) Polyamine interactions with plant hormones: crosstalk at several levels. in: Kusano T, Suzuki H (Eds), Polyamines: a universal molecular nexus for growth, survival, and specialized metabolism. Springer Verlag, New York, pp. 267–302.
16. Ariizumi T, Hatakeyama K, Hinata K, Inatsugi R, Nishida I, Sato S, Kato T, Tabata S, Toriyama K (2004) *Plant J* **39**, 170–181.
17. Ariizumi T, Hatakeyama K, Hinata K, Sato S, Kato T, Tabata S, Toriyama K (2005) *Sex Plant Reprod* **18**, 1–7.
18. Ariizumi T, Toriyama K (2007) *Int J Plant Dev Biol* **1**, 106–115.
19. Ariizumi T, Toriyama K (2011) *Annu Rev Plant Biol* **62**, 437–460.
20. Arikawa K (2003) *J Comp Physiol A* **189**, 791–800.
21. Arikawa K, Inokuma K, Eguchi E (1987) *Naturwissenschaften* **74**, 297–298.
22. Arikawa K, Mizuno S, Kinoshita M, Stavenga DG (2003) *J Neurosci* **23**, 4527–4532.
23. Arikawa K, Stavenga DG (2014) Insect Photopigments: Photoreceptor Spectral Sensitivities and Visual Adaptations. in: Hunt DM, Hankins MW, Collin SP, Marshall NJ (Eds) Evolution of Visual and Non-Visual Pigments. Springer, New York, pp. 137–162.
24. Arnold KE, Owens IPF, Marshall NJ (2002) *Science* **295**, 92.
25. Arnold SEJ, Faruq S, Savolainen V, McOwan PW, Chittka L (2010) *PLoS ONE* **5**, e14287.

26. Arunan E, Desiraju GR, Klein RA, Sadlej J, Scheiner S, Alkorta I, Clary DC, Crabtree RH, Dannenberg JJ, Hobza P, Kjaergaard HG, Legon AC, Mennucci B, Nebsbitt DJ (2011) *Pure Appl Chem* **83**, 1637–1641.
27. Asbeck F (1955) *Naturwissenschaften* **42**, 632.
28. de Azevedo Souza C, Barbazuk B, Ralph S, Bohlmann J, Hamberger B, Douglas C (2008) *New Phytol* **179**, 987–1003.
29. de Azevedo Souza C, Kim SS, Koch S, Kienow L, Schneider K, McKim SM, Haughn GW, Kombrink E, Douglas CJ (2009) *Plant Cell* **21**, 507–525.
30. Baby S, Johnson AJ, Govindan B, Lukose S, Gopakumar B, Koshy KC (2013) *Sci Rep* **3**, 2738.
31. Backhaus W, Menzel R (1987) *Biol Cybern* **55**, 321–331.
32. Bänziger H (1996) *Bot J Linnean Soc* **121**, 59–90.
33. Baptista MS, Cadet J, Di Mascio P, Ghogare AA, Greer A, Hamblin MR, Lorente C, Nunez SC, Ribeiro MS, Thomas AH, Vignoni M, Yoshimura TM (2017) *Photochem Photobiol* **93**, 912–919.
34. Barlow HB (1952) *J Exp Biol* **29**, 667–674.
35. Barrett SCH (2002) *Nat Rev Genet* **3**, 274–284.
36. Barrett SCH (2010) *Philos Trans R Soc Lond B Biol Sci* **365**, 99–109.
37. Bassard JE, Ullmann P, Bernier F, Wreck-Reichhart D (2010) *Phytochemistry* **71**, 1808–1824.
38. Beale RN, Roe EMF (1953) *J Chem Soc* **0**, 2755–2763.
39. Beaulieu JM, Leitch IJ, Patel S, Pendharkar A, Knight CA (2008) *New Phytol* **179**, 975–986.
40. Beekman M, Preece K, Schaerf TM (2016) *Insects Soc* **63**, 117–126.
41. Ben Nasri-Ayachi M, Nabli MA (2009) *Grana* **48**, 109–121.
42. Bennini B, Chulia AJ, Kaouadji M, Thomasson F (1992) *Phytochemistry* **31**, 2483–2486.
43. Berger F (1934) *Beitr Biol Pflanzen* **22**, 1–12.
44. Bernays EA (1998) *Bioscience* **48**, 35–44.
45. Blackmore S, Wortley AH, Skvarla JJ, Gabarayeva NI, Rowley JR (2010) *Plant Syst Evol* **284**, 17–32.
46. Blackmore S, Wortley AH, Skvarla JJ, Rowley JR (2007) *New Phytol* **174**, 483–498.
47. Bidlingmeyer BA (1993) Practical HPLC methodology and applications. Wiley, New York.
48. Birkofer L, Kaiser C, Nouvertné W, Thomas U (1961) *Z Naturforsch B* **16**, 249–251.
49. Birkofer L, Kaiser C, Thoman U (1968) *Z Naturforsch B* **23**, 1051–1058.
50. Bitrián M, Zarza X, Altabella T, Tiburcio AF, Alcázar R (2012) *Metabolites* **2**, 516–528.
51. Bloom JWG, Raju RK, Wheeler SE (2012) *J Chem Theory Comput* **8**, 3167–3174.
52. de Boer JG, Dicke M (2004) *J Chem Ecol* **30**, 255–271.
53. Bokern M, Witte L, Wray V, Nimtz M, Meurer-Grimes B (1995) *Phytochemistry* **39**, 1371–1375.
54. Bokern M, Wray V, Strack D (1987) *Phytochemistry* **26**, 3229–3231.
55. Borg M, Twell D (2011) Pollen: Structure and development. in: eLS. John Wiley & Sons, Chichester.
56. Borst A (2009) *Curr Biol* **19**, R36–R47.
57. Bosch J, González AM, Rodrigo A, Navarro D (2009) *Ecol Lett* **12**, 409–419.
58. Bosch J, Retana J, Cerdá X (1997) *Oecol* **109**, 583–591.
59. Bowmaker JK, Dartnall HJA (1980) *J Physiol* **181**, 501–511.
60. Briscoe AD (2008) *J Exp Biol* **211**, 1805–1813.

61. Briscoe AD, Bernard GD, Szeto AS, Nagy LM, White RH (2003) *J Comp Neurol* **458**, 334–349.
62. Briscoe AD, Chittka L (2001) *Annu Rev Entomol* **46**, 471–510.
63. Britt AB (1996) *Annu Rev Plant Physiol Plant Mol Biol* **47**, 75–100.
64. Brooks J, Shaw G (1968) *Grana* **17**, 91–97.
65. Bubert H, Lambert J, Steuernagel S, Ahlers F, Wiermann R (2002) *Z Naturforsch C* **57**, 1035–1041.
66. Burgos L, Alburquerque N, Egea J (2004) *Span J Agric Res* **2**, 227–241.
67. Buta JG, Izac RR (1972) *Phytochemistry* **11,** 1188–1189.
68. Cabanne F, Dalebroux MA, Martin-Tanguy J, Martin C (1981) *Physiol Plant* **53**, 399–404.
69. Carr DE, Haber AI, LeCroy KA, Lee DE, Link RI (2015) *AoB Plants* **7**, plv034.
70. Carrizo García C, Nepi M, Pacini E (2017) *Protoplasma* **254**, 57–73.
71. Carroll WC, Zhao C, Smith MD, Pellechia PJ, Shimizu KD (2011) *Org Lett* **13**, 4320–4323.
72. Carthew SM, Goldingay RL (1997) *Trends Ecol Evol* **12**, 104–108.
73. Ceska O, Styles ED (1984) *Phytochemistry* **23**, 1822–1823.
74. Chang HS, Zhang C, Chang YH, Zhu J, Xu XF, Shi ZH, Zhang XL, Xu L, Huang H, Zhang S, Yang ZN (2012) *Plant Physiol* **158**, 264–272.
75. Charpentier R (1985) *Entomol Exp Appl* **38**, 277–285.
76. Cheminat A, Zawatzky R, Becker H, Brouillard R (1988) *Phytochemisitry* **27**, 2787–2794.
77. Chen PJ, Awata H, Matsushita A, Yang EC, Arikawa K (2016) *Front Ecol Evol* **4**, 18.
78. Chen W, Yu XH, Zhang K, Shi J, De Oliveira S, Schreiber L, Shanklin J, Zhang D (2011) *Plant Physiol* **157**, 842–853.
79. Chittka L (1992) *J Comp Physiol A* **170**, 533–543.
80. Chittka L (1996) *Naturwissenschaften* **83**, 136–138.
81. Chittka L (1997) *Isr J Plant Sci* **45**, 115–127.
82. Chittka L, Ings TC, Raine NE (2004) *Popul Ecol* **46**, 243–251.
83. Chittka L, Menzel R (1992) *J Comp Physiol A* **171**, 171–181.
84. Chittka L, Niven J (2009) *Curr Biol* **19**, R995–1008.
85. Chittka L, Shmida A, Troje N, Menzel R (1994) *Vision Res* **34**, 1489–1508.
86. Choi H, Ohyama K, Kim YY, Jin JY, Lee SB, Yamaoka Y, Muranaka T, Suh MC, Fujioka S, Lee Y (2014) *Plant Cell* **26**, 310–324.
87. Clément C, Laporte P, Audran JC (1998) *Sex Plant Reprod* **11**, 94–106.
88. Clément C, Pacini E (2001) *Bot Rev* **67**, 54–73.
89. Clifford HT (1962) *Nature* **193**, 196.
90. Comba L, Corbet SA, Hunt L, Warren B (1999) *Ann Bot* **83**, 369–383.
91. Couvillon MJ (2012) *Insect Soc* **59**, 297–306.
92. Cox PA (1988) *Ann Rev Ecol Syst* **19**, 261–280.
93. Cox PA, Tomlinson PB (1988) *Am J Bot* **75**, 958–965.
94. Cox PA, Tomlinson PB, Nieznanski K (1992) *Plant Syst Evol* **180**, 65–75.
95. Cronk Q, Ojeda I (2008) *J Exp Bot* **59**, 715–727.
96. Cruden RW (1972) *Science* **176**, 1439–1440.

97. Cruden RW (2000) *Plant Syst Evol* **222**, 143–165.
98. Dafni A, Kevan PG (1996) *Bot J Linnean Soc* **120**, 371–377.
99. Dafni A, Lehrer M, Kevan PG (1997) *Biol Rev* **72**, 239–282.
100. Di Paola-Naranjo RD, Sánchez-Sánchez J, González-Paramás AM, Rivas-Gonzalo JC (2004) *J Chromatogr A* **29**, 205–210.
101. Dickinson BC, Chang CJ (2011) *Nat Chem Biol* **18**, 504–511.
102. Dickinson HG, Elleman CJ (1985) *Micron Microsc Acta* **16**, 255–270.
103. Dickinson HG, Elleman CJ, Doughty J (2000) *Sex Plant Reprod* **12**, 302–309.
104. Dickinson HG, Lewis D (1973) *Proc R Soc Lond B* **184**, 149–165.
105. Dixon RA, Paiva NL (1995) *Plant Cell* **7**, 1085–1097.
106. Dobritsa AA, Coerper D (2012) *Plant Cell* **24**, 4452–4464.
107. Dobritsa AA, Geanconteri A, Shrestha J, Carlson A, Kooyers N, Coerper D, Urbanczyk-Wochniak E, Bench BJ, Sumner LW, Swanson R, Preuss D (2011) *Plant Physiol* **157**, 947–970.
108. Dobritsa AA, Kirkpatrick AB, Reeder SH, Li P, Owen HA (2018) *Plant Physiol* **176**, 326–339.
109. Dobritsa AA, Lei Z, Nishikawa S, Urbanczyk-Wochniak E, Huhman DV, Preuss D, Sumner LW (2010) *Plant Physiol* **153**, 937–955.
110. Dobritsa AA, Reeder SH (2017) Plant Signal Behav **12**, e1393136.
111. Dobritsa AA, Shrestha J, Morant M, Pinot F, Matsuno M, Swanson R, Møller BL, Preuss D (2009) *Plant Physiol* **151**, 574–589.
112. Dobson CH, Hills HG (1966) *Am Orchid Soc Bull* **35**, 720–725.
113. Dobson HEM (1987) *Oecol* **72**, 618–623.
114. Dobson HEM (1988) *Am J Bot* **75**, 170–182.
115. Dobson HEM, Bergström G (2000) *Plant Syst Evol* **222**, 63–87.
116. Dobson HEM, Danielson EM, Van Wesep ID (1999) *Plant Species Biol* **14**, 153–166.
117. Dobson HEM, Groth I, Bergström G (1996) *Am J Bot* **83**, 877–885.
118. Domínguez E, Mercado JA, Quesada MA, Heredia A (1999) *Sex Plant Reprod* **12**, 171–178.
119. Dötterl S, Vereecken N (2010) *Can J Zool* **88**, 668–697.
120. Du ZY, Wang QF (2014) *PLoS ONE* **9**, e115653.
121. Dunning Jr. TH (1989) *J Chem Phys* **90**, 1007–1023.
122. Dyer AG (1996) *Aust J Bot* **44**, 473–488.
123. Dyer AG, Boyd-Gerny S, McLoughlin S, Rosa MGP, Simonov V, Wong BBM (2012) *Proc R Soc B* **279**, 3606–3615.
124. Dyer AG, Boyd-Gerny S, Shrestha M, Lunau K, Garcia JE, Koethe S, Wong BBM (2016) *J Comp Physiol A* **202**, 603–613.
125. Dyer AG, Neumeyer C (2005) *J Comp Physiol A* **191**, 547–557.
126. Dyer AG, Paulk AC, Reser DH (2011) *Proc R Soc B* **278**, 952–959.
127. Eady C, Lindsey K, Twell D (1995) *Plant Cell* **7**, 65–74.
128. Eberhard SH, Hrassnigg N, Crailsheim K, Krenn HW (2007) *J Insect Physiol* **53**, 126–131.
129. Edlund AF, Swanson R, Preuss D (2004) *Plant Cell* **16**, 84–97.

130. El-Ghazaly G, Jensen WA (1987) *Am J Bot* **74**, 1396–1418.
131. Elejalde-Palmett C, de Bernonville TD, Glevarec G, Pichon O, Papon N, Courdavault V, St-Pierre B, Giglioli-Guivarc'h N, Lanoue A, Basseau S (2015) *J Exp Bot* **66**, 7271–7285.
132. Elleman CJ, Dickinson H (1986) *J Cell Sci* **80**, 141–157.
133. Elleman CJ, Dickinson H (1990) *New Phytol* **114**, 511–518.
134. Eltz T, Roubik DW, Lunau K (2005) *Behav Ecol Sociobiol* **59**, 149–156.
135. Erdtman G (1952) Pollen Morphology and Plant Taxonomy: Angiosperms (An Introduction to Palynology. I). Almqvist & Wiksell, Stockholm.
136. Ernst OP, Lodowski DT, Elstner M, Hegemann P, Brown LS, Kandori H (2014) *Chem Rev* **114**, 126–163.
137. Ernst-Schwarzenbach M (1944) *Ber Schweiz Bot Ges* **55**, 33–69.
138. Fægri K, van der Pijl L (1979) The Principles of Pollination Ecology. Pergamon Press, Oxford.
139. Facchini PJ, Hagel J, Zulak KG (2002) *Can J Bot* **80**, 577–589.
140. Fahn A (1967) Plant Anatomy. Pergamon Press, Oxford.
141. Fang Q, Chen YZ, Huang SQ (2012) *Ann Bot* **109**, 379–384.
142. Farrar Jr. RR, Kennedy GG, Roe RM (1992) *Entomol Exp Appl* **62**, 191–200.
143. Fellenberg C, Vogt T (2015) *Trends Plant Sci* **20**, 212–218.
144. Feng H, An L, Tan L, Hou Z, Wang X (2000) *Environ Exp Bot* **43**, 45–53.
145. Ferreres F, Tomás-Barberán FA, Tomás-Lorente F, Nieto JL, Rumbero A, Olías JM (1989) *Phytochemistry* **28**, 1901–1903.
146. Feuda R, Marlétaz F, Bentley MA, Holland PWH (2016) *Genome Biol Evol* **8**, 579–587.
147. Fiebig A, Mayfield JA, Miley NL, Chau S, Fischer RL, Preuss D (2000) *Plant Cell* **12**, 2001–2008.
148. Firon N, Nepi M, Pacini E (2012) *Ann Bot* **109**, 1201–1213.
149. Fischer HOL, Dangschat G (1932) *Ber Dtsch Chem Ges* **65**, 1037–1040.
150. Fleming TH, Geiselman C, Kress WJ (2009) *Ann Bot* **104**, 1017–1043.
151. Fleming TH, Muchhala N (2008) *J Biogeogr* **35**, 764–780.
152. Fraser CM, Chapple C (2011) *Arabidopsis Book* **9**, e0152.
153. Franchi GG, Piotto B, Nepi M, Baskin CC, Baskin JM, Pacini E (2011) *J Exp Bot* **62**, 5267–5281.
154. Frankel R, Galun E (1977) Pollination Mechanisms, Reproduction, and Plant Breeding. Springer, Heidelberg.
155. Frederick JE (1993) *Photochem Photobiol* **57**, 175–178.
156. Friedman J, Barrett SCH (2009) *Ann Bot* **103**, 1515–1527.
157. von Frisch K (1946) *Österr Zool Z* **1**, 1–48.
158. von Frisch K (1967) The Dance Language and Orientation of Bees. Harvard University Press, Cambridge.
159. Fu XP, Wu T, Abdurahim M, Su Z, Hou X, Aisa HA, Wu H (2008) *Phytochem Lett* **1**, 59–62.
160. Fujii S, Kubo K, Takayama S (2016) *Nat Plants* **2**, 16130.
161. Fukui H, Hirai N, Mori S, Goto K, Toyoda J, Tsukioka J (2017) Floral Fluorescence Database. http://labo.kyoto-phu.ac.jp/mpgkpu/ffd.html (Accessed 20 Jun 2018).
162. Furness CA (2007) *Bot J Linnean Soc* **155**, 29–48.
163. Furness CA (2008) *Int J Plant Sci* **169**, 207–223.
164. Furness CA, Rudall PJ (1999) *Int J Plant Sci* **160**, 395–414.

165. Furness CA, Rudall PJ (2001) *Int J Plant Sci* **162**, 375–392.
166. Furness CA, Rudall PJ (2004) *Trends Plant Sci* **9**, 154–158.
167. Furness CA, Rudall PJ, Sampson FB (2002) *Int J Plant Sci* **163**, 235–260.
168. Gabarayeva N, Grigorjeva V (2016) *Plant Syst Evol* **302**, 1135–1156.
169. Gabarayeva N, Grigorjeva V, Kosenko Y (2013a) *Plant Syst Evol* **299**, 1013–1035.
170. Gabarayeva N, Grigorjeva V, Kosenko Y (2013b) *Plant Syst Evol* **299**, 1037–1055.
171. Gabarayeva N, Grigorjeva V, Polevova S (2011) *Plant Sys Evol* **296**, 101–120.
172. Gabarayeva N, Grigorjeva V, Polevova S (2014) *Rev Palaeobot Palynol* **206**, 23–44.
173. Gabarayeva N, Grigorjeva V, Polevova S, Hemsley AR (2016b) *Grana* **56**, 81–111.
174. Gabarayeva N, Grigorjeva V, Rowley JR, Hemsley AR (2009a) *Rev Palaeobot Palynol* **156**, 211–232.
175. Gabarayeva N, Grigorjeva V, Rowley JR, Hemsley AR (2009b) *Rev Palaeobot Palynol* **156**, 233–247.
176. Gabarayeva N, Hemsley AR (2006) *Rev Palaeobot Palynol* **138**, 121–139.
177. Gabarayeva NI (2000) Principles and Recurrent Themes in Sporoderm Development. in: Harley M, Morton CM, Blackmore S (Eds) Pollen and Spores: Morphology and Biology. Royal Botanic Gardens, Kew, London, pp. 1–17.
178. Gabarayeva NI, El-Ghazaly G (1997) *Plant Syst Evol* **204**, 1–19.
179. Gabarayeva NI, Grigorjeva VV (2002) *Rev Palaeobot Palynol* **122**, 185–218.
180. Gabarayeva NI, Grigorjeva VV (2004) *Rev Palaeobot Palynol* **132**, 175–193.
181. Gabarayeva NI, Grigorjeva VV (2010) *Grana* **49**, 91–114.
182. Gabarayeva NI, Grigorjeva VV (2011) *Grana* **50**, 81–101.
183. Gabarayeva NI, Grigorjeva VV (2013) *Grana* **52**, 241–257.
184. Gabarayeva NI, Grigorjeva VV (2017) *Planta* **246**, 471–493.
185. Gabarayeva NI, Grigorjeva VV (2018) *Protoplasma* **255**, 109–128.
186. Gabarayeva NI, Grigorjeva VV, Blackmore S (2016a) *Int J Plant Sci* **177**, 347–370.
187. Gabarayeva NI, Grigorjeva VV, Rowley JR (2003) *Rev Palaeobot Palynol* **127**, 147–73.
188. Gabarayeva NI, Grigorjeva VV, Rowley JR (2010) *Protoplasma* **247**, 65–81.
189. Gabarayeva NI, Polevova SV, Grigorjeva VV, Blackmore S (2018) *Planta* **248**, 323–346.
190. Gallai N, Salles JM, Settele J, Vaissière BE (2009) *Ecol Econ* **68**, 810–821.
191. Gandía-Herrero F, Escribano J, García-Carmona F (2005a) *Planta* **222**, 586–593.
192. Gandía-Herrero F, García-Carmona F, Escribano J (2005b) *Nature* **437**, 334.
193. García-Plazaola JI, Fernández-Marín B, Duke SO, Hernández A, López-Arbeloa F, Becerrila JM (2015) *Plant Sci* **236**, 136–145.
194. Garibaldi LA, Steffan-Dewenter I, Winfree R, Aizen MA, Bommarco R, Cunningham SA, Kremen C, Carvalheiro LG, Harder LD, Afik O, Bartomeus I, Benjamin F, Boreux V, Cariveau D, Chacoff NP, Dudenhöffer JH, Freitas BM, Ghazoul J, Greenleaf S, Hipólito J, Holzschuh A, Howlett B, Isaacs R, Javorek SK, Kennedy CM, Krewenka KM, Krishnan S, Mandelik Y, Mayfield MM, Motzke I, Munyuli T, Nault BA, Otieno M, Petersen J, Pisanty G, Potts SG, Rader R, Ricketts TH, Rundlöf M, Seymour CL, Schüepp C, Szentgyörgyi H, Taki H, Tscharntke T, Vergara CH, Viana BF, Wanger TC, Westphal C, Williams N, Klein AM (2013) *Science* **339**, 1608–1611.

195. Gautier-Hion A, Maisels F (1994) *Behav Ecol Sociobiol* **34**, 203–210.
196. Ghazoul J (2005) *Trends Ecol Evol* **20**, 367–373.
197. Girotti AW (2001) *J Photochem Photobiol B Biol* **63**, 103–113.
198. Giurfa M, Nunez J, Chittka L, Menzel R (1995) *J Comp Physiol A* **177**, 247–259.
199. Giurfa M, Vorobyev M, Kevan P, Menzel R (1996) *J Comp Physiol A* **178**, 699–709.
200. Goldberg RB, Beals TP, Sanders PM (1993) *Plant Cell* **5**, 1217–1229.
201. Goldblatt P, Bernhardt P, Manning JC (2009) *Plant Syst Evol* **278**, 53–65.
202. Goldsmith TH, Collins JS, Perlman DL (1981) *J Comp Physiol A* **143**, 103–110.
203. Gómez JF, Talle B, Wilson ZA (2015) *J Integr Plant Biol* **57**, 876–891.
204. Gong F, Wu X, Wang W (2015) *Front Plant Sci* **6**, 199.
205. Goodale E, Kim E, Nabors A, Henrichon S, Nieh JC (2014) *Naturwissenschaften* **101**, 523–526.
206. Gould KS, Lister C (2006) Flavonoid Functions in Plants. in: Andersen ØM, Markham KR (Eds) Flavonoids: Chemistry, Biochemistry and Applications. CRC Press, Boca Raton, pp. 397–441.
207. Goulson D, Nicholls E, Botías C, Rotheray EL (2015) *Science* **347**, 1255957.
208. Grant BR (1996) *Ecology* **77**, 489–499.
209. Grienenberger E, Besseau S, Geoffroy P, Debayle D, Heintz D, Lapierre C, Pollet B, Heitz T, Legrand M (2009) *Plant J* **58**, 246–259.
210. Grienenberger E, Kim SS, Lallemand B, Geoffroy P, Heintz D, de Azevedo Souza C, Heitz T, Douglas CJ, Legrand M (2010) *Plant Cell* **22**, 4067–4083.
211. Grigorjeva V, Gabarayeva N (2015) *Rev Palaeobot Palynol* **219**, 1–27.
212. Grigorjeva VV, Gabarayeva N (2018) *Protoplasma* **255**, 109–128.
213. Gronquist M, Bezzerides A, Attygalle A, Meinwald J, Eisner M, Eisner T (2001) *Proc Natl Acad Sci USA* **98**, 13745–13750.
214. Gruber B, Eckel K, Everaars J, Dormann CF (2011) *Apidologie* **42**, 564–576.
215. Gu T, Mazzurco M, Sulaman W, Matias DD, Goring DR (1998) *Proc Natl Acad Sci USA* **95**, 382–387.
216. Guan YF, Huan XY, Zhu J, Gao JF, Zhang HX, Yang ZN (2008) *Plant Physiol* **147**, 852–863.
217. Gullan PJ, Cranston PS (2010) The Insects: an Outline of Entomology, 4th Edition. John Wiley & Sons, Chichester.
218. Guilford WJ, Schneider DM, Labovitz J, Opella SJ (1988) *Plant Physiol* **86**, 134–136.
219. Gumbert A (2000) *Behav Ecol Sociobiol* **48**, 36–43.
220. Guo Y-H, Sperry R, Cook CDK, Cox PA (1990) *Aquat Bot* **38**, 341–356.
221. Gutierrez DV, Oh E, Herlitze S (2011) Vertebrate and Invertebrate Rhodopsins: Light Control of G-protein Signaling. in: Chambers JJ, Kramer RH (Eds) Photosensitive Molecules for Controlling Biological Function, Humana Press, New York, pp. 133–146.
222. Haddock SHD, Dunn CW (2015) *Biol Open* **4**, 1094–1104.
223. Halbritter H (2015) Arabidopsis thaliana. in: PalDat - a palynological database. https://www.paldat.org/pub/Arabidopsis_thaliana/300148 (Accessed 20 Jun 2018).
224. Hall JA, Walter GH (2011) *Biol J Linnean Soc* **104**, 75–92.
225. van der Ham RWJM (1991) *Blumea* **36**, 127–159.

226. Hamdorf K (1979) The physiology of invertebrate visual pigments. in: Autrum H (Ed) Comparative Physiology and Evolution of Vision in Invertebrates. Springer, Heidelberg, pp. 145–224.
227. Hamerski L, Bomm MD, Silva DHS, Young MCM, Furlan M, Eberlin MN, Castro-Gamboa I, Cavalheiro AJ, Bolzani VS (2005) *Phytochemistry* **66**, 1927–1932.
228. Hanwell MD, Curtis DE, Lonie DC, Vandermeersch T, Zurek E, Hutchison GR (2012) *J Cheminform* **4**, 17.
229. Harborne JB, Williams CA (2000) *Phytochemistry* **55**, 481–504.
230. Harder LD (1988) *Biol J Linnean Soc* **64**, 513–525.
231. Hart NS (2001) *Prog Retin Eye Res* **20**, 675–703.
232. Hart NS (2002) *J Exp Biol* **205**, 3925–3935.
233. Hart NS, Partridge JC, Cuthill IC (1998) *J Exp Biol* **201**, 1433–1446.
234. Hartley RD, Jones EC (1975) *J Chromatogr* **107**, 213–218.
235. Hausmann F, Arnold KE, Marshall NJ, Owens IPF (2003) *Proc R Soc B* **270**, 61–67.
236. Hayashi K, Shimazu K, Yaegaki H, Yamaguchi M, Iketani H, Yamamoto T (2008) *Breeding Sci* **58**, 401–410.
237. Haydak MH (1970) *Annu Rev Entomol* **15**, 143–156.
238. Hedberg C, Hesse M, Werner C (1996) *Plant Sci* **113**, 149–156.
239. Heizmann P, Luu DT, Dumas C (2000) *Ann Bot* **85**, 23–27.
240. Hegedűs A, Lénárt J, Halász J (2012) *Biol Plant* **56**, 201–209.
241. Helversen O (1972) *J Comp Physiol* **80**, 439–472.
242. Hempel de Ibarra N, Langridge KV, Vorobyev M (2015) *Curr Opin Insect Sci* **12**, 64–70.
243. Hemsley AR, Gabarayeva NI (2007) *Plant Syst Evol* **263**, 25–49.
244. Hemsley AR, Griffiths PC, Mathias R, Moore SEM (2003) *Grana* **42**, 38–42.
245. Henning JA, Peng Y, Montague MA, Teuber LR (1992) *J Econ Entomol* **85**, 233–239.
246. Henze MJ, Oakley TH (2015) *Integr Comp Biol* **55**, 830–842.
247. Herrera CM (1996) Floral Traits and Plant Adaptation to Insect Pollinators: A Devil's Advocate Approach. in: Lloyd DG, Barrett SCH (Eds) Floral Biology. Studies of Floral Evolution in Animal Pollinated Plants. Chapman & Hall, New York, pp 65–87.
248. Heslop-Harrison J (1968a) *Science* **161**, 230–237.
249. Heslop-Harrison J (1968b) *Can J Bot* **46**, 1185–1192.
250. Heslop-Harrison J (1975) *Proc R Soc Lond B* **190**, 275–299.
251. Heslop-Harrison Y, Heslop-Harrison J (1982) *Ann Bot* **50**, 831–842.
252. Hesse M (1981) *Grana* **20**, 145–152.
253. Hesse M (1993) *Plant Syst Evol* **7** (Suppl), 39–52.
254. Hesse M (2000) *Plant Syst Evol* **222**, 1–17.
255. Hesse M (2010) Bonding Single Pollen Grains Together: How and Why? in: von Byern J, Grunwald I (Eds) Biological Adhesive Systems. Springer, Wien, pp. 3–13.
256. Hesse M, Halbritter H, Zetter R, Weber M, Buchner R, Frosch-Radivo A, Ulrich S (2009) Pollen Terminology: An Illustrated Handbook. Springer, Wien.
257. Heymann EW (2011) *Ecotropica* **17**, 41–52.
258. Hiscock SJ (2000) *Genome Biol* **3**, 1004.

259. Hixson JL, Hayasaka Y, Curtin CD, Sefton MA, Taylor DK (2016) *J Agric Food Chem* **64**, 9401–9411.
260. Hollósy F (2002) *Micron* **33**, 179–197.
261. Hopkins R, Rausher MD (2012) *Science* **335**, 1090–1092.
262. Hoque E, Remus G (1999) *Photochem Photobiol* **69**, 177–192.
263. Hou JH, Gao ZH, Zhang Z, Chen SM, Ando T, Zhang JY, Wang XW (2011) *Plant Mol Biol Rep* **29**, 473–480.
264. Hsieh K, Huang AHC (2004) *Plant Physiol* **136**, 3427–3434.
265. Hsieh K, Huang AHC (2005) *Plant J* **43**, 889–899.
266. Hsieh K, Huang AHC (2007) *Plant Cell* **19**, 582–596.
267. Hsieh K, Wu SSH, Ratnayake C, Huang AHC (2003) Tapetosomes and elaioplasts in *Brassica* and *Arabidopsis* floral tapetum. in: Murata N, Yamada, M, Nishida I, Okuyama H, Sekiya J, Hajime W (Eds) Advanced Research on Plant Lipids. Springer, Dordrecht, pp. 215–218.
268. Hu J, Wang Z, Zhang L, Sun M (2014) *New Phytol* **203**, 140–154.
269. Hu W, Werner C, Hesse M (1998*) Helv Chim Acta* **81**, 342–352.
270. Huang MD, Wei FJ, Wu CC, Hsing YIC, Huang AHC (2009) *Plant Physiol* **149**, 694–707.
271. Huang MD, Chen TLL, Huang AHC (2013) *Plant Physiol* **163**, 1218–1229.
272. Hung CY, Tsai YC, Li KY (2012) *Molecules* **17**, 10724–10737.
273. Hung ZH, Luo WH, Huang SX, Huang SQ (2018) *J Syst Evol* **56**, 243–249.
274. Hülskamp M, Kopczak SD, Horejsi TF, Kihl BK, Pruitt RE (1995) *Plant J* **8**, 703–714.
275. Huysmans S, El-Ghazaly G, Smets E (1998) *Bot Rev* **64**, 240–272.
276. Igric B, Lande R, Kohn JR (2008) *Int J Plant Sci* **169**, 93–104.
277. Iriel A, Lagorio MG (2010a) *Photochem Photobiol Sci* **9**, 342–348.
278. Iriel A, Lagorio MG (2010b) *Naturwissenschaften* **97**, 915–924.
279. Israelachvili JN, Mitchell DJ, Barry W. Ninham BW (1976) *J Chem Soc Faraday Trans 2* **72**, 1525–1568.
280. Jablonski A (1935) *Z Phys* **94**, 38–46.
281. Jansen MAK, Gaba V, Greenberg BM (1998) *Trends Plant Sci* **3**, 131–135.
282. Jayanth KP, Mohandas S, Asokan R, Visalakshy PNG (1993) *Bull Entomol Res* **83**, 595–598.
283. Jepson Flora Project (Eds) (2018) Jepson eFlora. http://ucjeps.berkeley.edu/eflora/ (Accessed 6 Aug 2018).
284. Jha S, Burkle L, Kreman C (2013) Vulnerability of Pollination Ecosystem Services. in: Climate Vulnerability: Understanding and Addressing Threats to Essential Resources. Elsevier Academic Press, New York, pp 117–128.
285. Jiang J, Zhang Z, Cao J (2012) *Plant Biol* **15**, 249–263.
286. Jiang JS, Lü L, Yang YJ, Zhang JL, Zhang PC (2008) *J Asian Nat Prod Res* **10**, 447–451.
287. Johansen DA (1940) Plant microtechnique. McGraw-Hill Publications, New York.
288. Johnson BR (2010) *Behav Ecol Sociobiol* **64**, 305–316.
289. Johnson CE, Bovey FA (1958) *J Chem Phys* **29**, 1012–1014.
290. Johnson MA, Preuss D (2002) *Dev Cell* **2**, 273–281.
291. Johnson SD, Burgoyne PM, Harder LD, Dötterl S (2011) *Proc R Soc B* **278**, 2303–2310.
292. Johnson SD, Steiner KE (2000) *Trends Ecol Evol* **15**, 140–143.
293. Jones CE, Buchmann SL (1974) *Anim Behav* **22**, 481–485.

294. de Jong TJ, Waser NM, Klinkhamer PGL (1993) *Trends Ecol Evol* **8**, 321–325.
295. Jun W, Yu-Xin M, Da-Lian C, Ri-Xin W, Yan-Yong L, Jing Q (2011) *Chin J Appl Ecol* **48**, 764–768.
296. Kachroo A, Schopfer CR, Nasrallah ME, Nasrallah JB (2001) *Science* **293**, 1824–1826.
297. Kahnt G (1967) *Phytochemistry* **6**, 755–758.
298. Kanato K, Yoshida M, Kurihara A, Sato T, Harada R, Kyotani H (1980) *Bull Fruit Tree Res Sta A* **7**, 1–6.
299. Kandasamy MK, Nasrallah JB, Nasrallah ME (1994) *Development* **120**, 3405–3418.
300. Kaur D, Kaur R (2015) *J Chem Sci* **127**, 1299–1313.
301. Kaur H, Heinzel N, Schöttner M, Baldwin IT, Gális I (2010) *Plant Physiol* **152**, 1731–1747.
302. Kelber A, Vorobyev M, Osorio D (2003) *Biol Rev* **78**, 81–118.
303. Kennedy GG, Farrar RR, Kashyap R K (1991) 2-Tridecanone - glandular trichome-mediated insect resistance in tomato. in: Hedin PA (Ed) Naturally occurring pest bioregulators. ACS Symp Ser 449, Amer Chem Soc, Washington DC, pp 150–165.
304. Kesseler R, Harley M (2006) Pollen: The Hidden Sexuality of Flowers. Papadakis Publisher, London.
305. Kevan PG (1976) *Science* **194**, 341–342.
306. Kevan PG, Baker HG (1983) *Ann Rev Entomol* **28**, 407–453.
307. Kevan PG, Lane MA (1985) *Proc Natl Acad Sci USA* **82**, 4750–4752.
308. Kim HU, Hsieh K, Ratnayake C, Huang AHC (2002) *J Biol Chem* **277**, 22677–22684.
309. Kim S, Cassidy JJ, Yang B, Carthew RW, Hilgenfeldt S (2016) *Biophys J* **111**, 2735–2746.
310. Kim SS, Grienenberger E, Lallemand B, Colpitts CC, Kim SY, de Azevedo Souza C, Geoffroy P, Heintz D, Krahn D, Kaiser M, Kombrink E, Heitz T, Suh DY, Legrand M, Douglas CJ (2010) *Plant Cell* **22**, 4045–4066.
311. Kirk WDJ (1984) *J Zool Lond* **204**, 107–117.
312. Kirkpatrick AB, Owen HA (2013) *Microsc Microanal* **19**, 134–135.
313. Kiselev A, Subramaniam S (1994) *Science* **266**, 1369–1373.
314. Kitamoto J, Ozaki K, Arikawa K (2000) *J Exp Biol* **203**, 2887–2894.
315. Kitamoto J, Sakamoto K, Ozaki K, Mishina Y, Arikawa K (1998) *J Exp Biol* **201**, 1255–1261.
316. Klein AM, Vaissière BE, Cane JH, Steffan-Dewenter I, Cunningham SA, Kremen C, Tscharntke T (2007) *Proc R Soc B* **274**, 303–313.
317. Knight CA, Clancy RB, Götzenberger L, Dann L, Beaulieu JM (2010) *J Bot* **2010**, 612017.
318. Knudsen JT, Eriksson R, Gershenzon J, Ståhl B (2006) *Bot Rev* **72**, 1–120.
319. Knudsen JT, Tollsten L (1995) *Bot J Linnean Soc* **119**, 45–57.
320. Knudsen JT, Tollsten L, Bergström LG (1993) *Phytochemistry* **33**, 253–280.
321. Koeppe DE, Rohrbaugh LM, Rice EL, Wender SH (1970) *Physiol Plant* **23**, 258–266.
322. Kondo T, Otani T, Lee SL, Tani N (2016) *J Trop For Sci* **28**, 318–323.
323. Konuma A, Okubo S (2015) *Jpn J Ecol* **65**, 217–226.
324. Konzmann S, Lunau K (2014) *PLoS ONE* **9**, e91900.
325. van der Kooi CJ, Elzenga JTM, Staal M, Stavenga DG (2016) *Proc R Soc B* **283**, 20160429.
326. Koshitaka H, Kinoshita M, Vorobyev M, Arikawa K (2008) *Proc R Soc B* **275**, 947–954.
327. Kreman C, Williams NM, Aizen MA, Gemmill-Herren B, LeBuhn G, Minckley R, Packer L, Potts SG, Roulston T, Steffan-Dewenter I, Vázquez DP, Winfree R, Adams L, Crone EE, Greenleaf SS, Keitt TH, Klein

AM, Regetz J, Ricketts TH (2007) *Ecol Lett* **10**, 299–314.

328. Kreunen SS, Osborn JM (1999) *Am J Bot* **86**, 1662–1676.
329. Kroon GH, van Praagh JP, Velthuis HHW (1974) *J Api Res* **13**, 177–188.
330. Kumar A, McClure B (2010) *J Exp Bot* **61**, 2001–2013.
331. Kuprianova LA (1967) *Rev Palaeobot Palynol* **3**, 73–80.
332. Kuromori T, Ito T, Sugimoto E, Shinozaki K (2011) *J Plant Physiol* **168**, 2001–2005.
333. Kurup R, Johnson AJ, Sankar S, Hussain AA, Kumar CS, Sabulal B (2013) *Plant Biol* **15**, 611–615.
334. Kweon MH, Hwang HJ, Sung HC (2001) *J Agric Food Chem* **49**, 4646–4655.
335. Lagorio MG, Cordon GB, Iriel A (2015) *Photochem Photobiol Sci* **14**, 1538–1559.
336. Lakowicz JR (2006) Principles of Fluorescence Spectroscopy, 3rd Edition. Springer, Heidelberg.
337. Lallemand B, Erhardt M, Heitz T, Legrand M (2013) *Plant Physiol* **162**, 616–625.
338. Land MF (1997) *Annu Rev Entomol* **42**, 147–177.
339. Land MF, Chittka L (2013) Vision. in: Simpson SJ, Douglas AE (Eds) The Insects: Structure and Function, 5th Edition, Cambridge University Press, Cambridge, pp. 708–737.
340. Larson RA (1988) *Phytochemistry* **27**, 969–978.
341. Lautenbach S, Seppelt R, Liebscher J, Dormann CF (2012) *PLoS ONE* **7**, e35954.
342. Leach AG, Houk KN (2002) *Chem Commun* **12**, 1243–1255.
343. Lepage M, Boch R (1968) *Lipids* **3**, 530–534.
344. Levin RA, McDade LA, Raguso RA (2003) *Syst Biol* **52**, 334–351.
345. Lewis FD, Elbert JE, Upthagrove AL, Hale PD (1991) *J Org Chem* **56**, 553–561.
346. Li DD, Xue JS, Zhu J, Yang ZN (2017a) *Front Plant Sci* **8**, 1559.
347. Li N, Xu C, Li-Beisson Y, Philippar K (2015) *Trends Plant Sci* **21**, 145–158.
348. Li P, Ben-Menni Schuler S, Reeder SH, Wang R, Suárez Santiago VN, Dobritsa AA (2018) *J Exp Bot* **69**, 983–996.
349. Li WC, Wang XY, Lin PC, Hu N, Zhang QL, Suo YR, Ding CX (2013) *J Chromatogr B* **938**, 75–79.
350. Li WL, Liu Y, Douglas CJ (2017b) *Plant Physiol* **173**, 167–182.
351. Lim MLM, Land MF, Li D (2007) *Science* **315**, 481.
352. Lin H, Gomez I, Meredith JC (2013) *Langmuir* **29**, 3012–3023.
353. Linskens HF (1964) *Annu Rev Plant Physiol* **15**, 255–270.
354. Liu T, Li H, Huang MB, Duan Y, Wang ZX (2008) *J Phys Chem A* **112**, 5436–5447.
355. Lord EM (1981) *Bot Rev* **47**, 421–449.
356. Lu P, Chai M, Yang J, Ning G, Wang G, Ma H (2014) *Plant Physiol* **164**, 1893–1904.
357. Lu Y, Jin B, Wang L, Wang Y, Wang D, Jiang XX, Chen P (2011) *Can J Plant Sci* **91**, 897–906.
358. Lunau K (1988) *Zool Jahrb Physiol* **92**, 487–499.
359. Lunau K (1991) *Ethol* **88**, 203–214.
360. Lunau K (1992) *Can J Zool* **70**, 2139–2144.
361. Lunau K (1995) *Plant Syst Evol* **198**, 235–252.
362. Lunau K (2000) *Plant Syst Evol* **222**, 89–111.
363. Lunau K, Maier EJ (1995) *J Comp Physiol A* **177**, 1–19.

364. Lunau K, Papiorek S, Eltz T, Sazima M (2011) *J Exp Biol* **214**, 1607–1612.
365. Lunau K, Wacht S (1994) *J Comp Physiol A* **174**, 575–579.
366. Luo J, Fuell C, Parr A, Hill L, Bailey P, Elliott K, Fairhurst SA, Martin C, Michael AJ (2009) *Plant Cell* **21**, 318–333.
367. Ma CM, Nakamura N, Hattori M (2001) *Chem Pharm Bull* **49**, 915–917.
368. Mackenzie G, Boa AN, Diego-Taboada A, Atkin SL, Sathyapalan T (2015) *Front Mater* **2**, 66.
369. Maia R, Eliason CM, Bitton PP, Doucet SM, Shawkey MD (2013) *Methods Ecol Evol* **4**, 906–913.
370. Maluf WR, Barbosa LV, Costa Santa-Cecilia LV (1997) *Euphytica* **93**, 189–194.
371. Mallinger RE, Gaines-Day HR, Gratton C (2017) *PLoS ONE* **12**, e0189268.
372. Mamun EA, Alfred S, Cantrill LC, Overall RL, Sutton BG (2006) *Cell Biol Intl* **30**, 583–591.
373. Mamun EA, Cantrill LC, Overall RL, Sutton BG (2010) *Cell Biol Intl* **34**, 469–476.
374. Manten AA (1967) *Earth-Sci Rev* **2**, 277–316.
375. Marr KL, Tang CS (1992) *Biochem Syst Ecol* **21**, 209–217.
376. Marshall J, Johnsen S (2017) *Phil Trans R Soc B* **372**, 20160335.
377. Martin JH, Kunstmann MP, Barbatschi F, Hertz M, Ellestad GA, Dann M, Redin GS, Dornbush AC, Kuck NA (1978) *J Antibiot* **31**, 398–404.
378. Martin-Tanguy J (2001) *Plant Growth Regul* **34**, 135–148.
379. Martin-Tanguy J, Cabanne F, Perdrizet E, Martin C (1978) *Phytochemistry* **17**, 1927–1928.
380. Martinez CR, Iverson BL (2012) *Chem Sci* **3**, 2191–2201.
381. Matsuno M, Compagnon V, Schoch GA, Schmitt M, Debayle D, Bassard J, Pollet B, Hehn A, Heintz D, Ullmann P, Lapierre C, Bernier F, Ehlting J, Werck-Reichhart D (2009) *Science* **325**, 1688-1692.
382. Mayama S, Tani T, Matsuura Y, Ueno T, Fukami H (1981) *Physiol Plant Pathol* **19**, 217–226.
383. Mayer C, Adler L, Armbruster WS, Dafni A, Eardley C, Huang S, Kevan PG, Ollerton J, Packer L, Ssymank A, Stout JC, Potts SG (2011) *J Pollination Ecol* **3**, 8–23.
384. Mayfield JA, Fiebig A, Johnstone SE, Preuss D (2001) *Science* **292**, 2482–2485.
385. Mazel CH, Cronin TW, Caldwell RL, Marshall NJ (2004) *Science* **303**, 51.
386. Mbadiwe AI (1973) *Phytochem Rep* **12**, 2546.
387. McCormick S (1993) *Plant Cell* **5**, 1265–1275.
388. Meester MAM, Schenk H (1971) *Rec Trav Chim Pays Bas* **90**, 508–512.
389. de Meillon B, Wirth WW (1989) *Revue Francaise d'Entomologie* **11**, 85–89.
390. Menzel R (1967) *Z Vergl Physiol* **56**, 22–62.
391. Menzel R, Blakers M (1976) *J Comp Physiol* **108**, 11–33.
392. Meurer B, Wiermann R, Strack D (1988a) *Phytochemistry* **27**, 823–828.
393. Meurer B, Wray V, Wiermann R, Strack D (1988b) *Phytochemistry* **27**, 839–843.
394. Millennium Ecosystem Assessment (2003) Ecosystems and Human Well-being: A framework for assessment. Island Press, Washington DC.
395. Millennium Ecosystem Assessment (2005) Ecosystems and Human Well-being: Synthesis. Island Press, Washington DC.
396. Minckley RL, Roulston TH (2006) Incidental Mutualisms and Pollen Specialization among Bees, in: Waser

NM, Ollerton J (Eds) Plant-Pollinator Interactions from Specialization to Generalization. University of Chicago Press, Chicago, pp 69–98.

397. Ministry of Agriculture, Forestry and Fisheries (2018) Statistical Yearbook of Ministry of Agriculture, Forestry and Fisheries. http://www.maff.go.jp/e/data/stat/nenji_index.htm (Accessed 8 Aug 2018).
398. Miosic S, Knop K, Hölscher D, Greiner J, Gosch C, Thill J, Kai M, Shrestha BK, Schneider B, Crecelius AC, Schubert US, Svatoš A, Stich K, Halbwirth H (2013) *PLoS ONE* **8**, e61766.
399. Moan J (2001) Visible light and UV radiation. in: Brune D, Hellborg R, Persson BRR, Pääkkönen R (Eds) Radiation at Home, Outdoors and in the Workplace. Scandinavian Science Publisher, Oslo, pp 69–85.
400. Møller C, Plesset MS (1934) *Phys Rev* **46**, 618.
401. Morant M, Jørgensen K, Schaller H, Pinot F, Møller BL, Werck-Reichhart D, Bak S (2007a) *Plant Cell* **19**, 1473–1487.
402. Morant M, Schoch GA, Ullmann P, Ertunç T, Little D, Olsen CE, Petersen M, Negrel J, Werck-Reichhart D (2007b) *Plant Mol Biol* **63**, 1–19.
403. Moschou PN, Wu J, Cona A, Tavladoraki R, Angelini R, Roubelakis-Angelakis A (2012) *J Exp Bot* **63**, 5003–5015.
404. da Mota MOS, Nogueira-Couto RH (2002) *Braz J Vet Res Anim Sci* **39**, 124–128.
405. Moyroud E, Wenzel T, Middleton R, Rudall PJ, Banks H, Reed A, Mellers G, Killoran P, Westwood MM, Steiner U, Vignolini S, Glover BJ (2017) *Nature* **550**, 469–474.
406. Muller J (1979) *Ann Mo Bot Gard* **66**, 593–632.
407. Murase K, Shiba H, Iwano M, Che FS, Watanabe M, Isogai A, Takayama S (2004) Science 303, 1516–1519.
408. Murphy DJ (2006) *Protoplasma* **228**, 31–39.
409. Nagy PI (2014) *Int J Mol Sci* **15**, 19562–19633.
410. Naka KI, Rushton WAH (1966) *J Physiol* **185**, 536–555.
411. Nakanishi T (1982) *Sci Hortic* **18**, 57–63.
412. Nakanishi T, Ichii T (1978) *Sci Rep Fac Agric Kobe Univ* **13**, 75–80 (in Japanese with English summary).
413. Nation JL (2016) Insect Physiology and Biochemistry, 3rd Edition. CRC Press, Boca Raton.
414. Nicholls E, Hempel de Ibarra N (2014) *J Exp Biol* **217**, 2783–2788.
415. Nicolson SW, Thornburg RW (2007) Nectar Chemistry. in: Nicolson SW, Nepi M, Pacini E (Eds) Nectaries and Nectar. Springer, Dordrecht, pp. 216–264.
416. Nishimura H, Sasaki H, Inagaki N, Chin M, Mitsuhashi H (1991) *Phytochemistry* **30**, 965–969.
417. Nishio M (2011) *Phys Chem Phys Chem* **13**, 13873–13900.
418. Nishio M, Hirota M (1989) *Tetrahedron* **45**, 7201–7245.
419. Niu BX, He FR, He M, Ren D, Chen LT, Liu YG (2013) *J Integr Plant Biol* **55**, 710–720.
420. Oda S, Kaneko F, Yano K, Fujioka T, Masuko H, Park JI, Kikuchi S, Hamada K, Endo M, Nagano K, Nagamura Y, Kawagishi-Kobayashi M, Suwabe K, Suzuki G, Watanabe M (2010) *Genes Genet Syst* **85**, 107–120.
421. Ödeen A, Håstad O (2010) *J Comp Physiol A* **196**, 91–96.
422. Ohmiya A (2011) *JARQ* **45**, 163–171.
423. Oki M, Mutai K (1965) *Bull Chem Soc Jpn* **38**, 387–392.

424. Olesen JM, Valido A (2003) *Trends Ecol Evol* **18**, 177–181.
425. Ollerton J (2017) *Annu Rev Ecol Evol Syst* **48**, 353–376.
426. Ollerton J, Killick A, Lamborn E, Watts S, Whiston M (2007) *Taxon* **56**, 717–728.
427. Ollerton J, Winfree R, Tarrant S (2011) *Oikos* **120**, 321–326.
428. Ortega-Olivencia A, Rodríguez-Riaño T, Pérez-Bote JL, López J, Mayo C, Valtueña FJ, Navarro-Pérez M (2012) *Ann Bot* **109**, 153–167.
429. Osaka M, Matsuda T, Sakazono S, Masuko-Suzuki H, Maeda S, Sewaki M, Sone M, Takahashi H, Nakazono M, Iwano M, Takayama S, Shimizu KK, Yano K, Lim YP, Suzuki G, Suwabe K, Watanabe M (2013) *Plant Cell Physiol* **54**, 1894–1906.
430. Osorio D, Vorobyev M (2005) *Proc R Soc B* **272**, 1745–1752.
431. Osorio D, Vorobyev M (2008) *Vision Res* **48**, 2042–2051.
432. Owens JN, Takaso T, Runions CJ (1998) *Trends Plant Sci* **3**, 479–485.
433. Pacini E (1996) *Sex Plant Reprod* **9**, 362–366.
434. Pacini E (1997) *Can J Bot* **75**, 1448–1459.
435. Pacini E (2000) *Plant Syst Evol* **222**, 19–43.
436. Pacini E (2010) *Int J Plant Sci* **171**, 1–11.
437. Pacini E, Franchi GG (1992) Diversification and evolution of the tapetum. in: Blackmore S, Barnes S (Eds) Pollen and Spores: Patterns of Diversifications. Oxford University Press, Oxford, pp. 301–316.
438. Pacini E, Franchi GG (1993) *Plant Syst Evol* **7** (Suppl), 1–11.
439. Pacini E, Franchi GG, Hesse M (1985) *Plant Syst Evol* **149**, 155–185.
440. Pacini E, Franchi GG, Ripaccioli M (1999) *Plant Sysy Evol* **217**, 81–99.
441. Pacini E, Hesse M (2005) *Flora* **200**, 399–415.
442. Pacini E, Jacquard C, Clément C (2011) *Planta* **234**, 217–227.
443. Parish RW, Li SF (2010) *Plant Sci* **178**, 73–89.
444. Park KH, Park M, Choi SE, Jeong MS, Kwon JH, Oh MH, Choi HK, Seo SJ, Lee MW (2009) *Biol Pharm Bull* **32**, 2029–2033.
445. Park SB, Song K, Kim YS (2017) *Planta Med Int Open* **4**, e43–e51.
446. Parker CA, Rees WT (1962) *Analyst* **87**, 83–111.
447. Parkinson BM, Pacini E (1995) *Plant Syst Evol* **198**, 55–88.
448. Parks GS, Huffman HM, Thomas SB (1930) *J Am Chem Soc* **52**, 1032–1041.
449. Pavé R, Peker SM, Raño M, Orjuela CR, Zunino GE, Kowalewski MM (2009) *Neotrop Primates* **16**, 61–64.
450. Paxson-Sowders DM, Dodrill CH, Owen HA, Makaroff CA (2001) *Plant Physiol* **127**, 1739–1749.
451. Paxson-Sowders DM, Owen HA, Makaroff CA (1997) *Protoplasma* **198**, 53–65.
452. Pearce S, Ferguson A, King J, Wilson ZA (2015) *Plant Physiol* **167**, 1717–1730.
453. Pearn SM, Bennett ATD, Cuthill IC (2001) *Proc R Soc B* **268**, 2273–2279.
454. Peitsch D, Fietz A, Hertel H, de Souza J, Ventura DF, Menzel, R (1992) *J Comp Physiol A* **170**, 23–40.
455. Pellmyr O, Tang W, Groth I, Bergström G, Thien LB (1991) *Biochem Syst Evol* **19**, 623–627.
456. Peñalver E, Labandeira CC, Barrón E, Delclòs X, Nel P, Nel A, Tafforeau P, Soriano C (2012) *Proc Natl Acad Sci USA* **109**, 8623–8628.

457. Peng YS, Nasr ME, Marston JM (1986) *Ann Entomol Soc Amer* **79**, 804–807.
458. Peng YS, Nasr ME, Marston JM, Yuenzhen F (1985) *Physiol Entomol* **10**, 75–82.
459. Penny JHJ (1983) *New Phytol* **95**, 707–721.
460. Percival MS (1955) *New Phytol* **54**, 353–368.
461. Perkin AG (1909) *J Chem Soc* **95**, 2181–2193.
462. Pernal SF, Currie RW (2002) *Animal Behav* **63**, 369–390.
463. Persson S, Paredez A, Carroll A, Palsdottir H, Doblin M, Poindexter P, Khitrov N, Auer M, Somerville CR (2007) *Proc Natl Acad Sci USA* **104**, 15566–15571.
464. Pettitt JM, Jermy AC (1975) *Micron* **5**, 377–405.
465. Pichersky E, Gershenzon J (2002) *Curr Opin Plant Biol* **5**, 237–243.
466. Piffanelli P, Murphy DJ (1998) *Trends Plant Sci* **3**, 250–252.
467. Piffanelli P, Ross JHE, Murphy DJ (1997) *Plant J* **11**, 549–556.
468. Piffanelli P, Ross JHE, Murphy DJ (1998) *Sex Plant Reprod* **11**, 65–80.
469. Polevova SV (2011) *Microsc Microanal* **17**, 166–167.
470. Polevova SV (2014) *Paleontol J* **48**, 1324–1329.
471. Potts SG, Biesmeijer JC, Kreman C, Neumann P, Schweiger O, Kunin WE (2010) *Trends Ecol Evol* **25**, 345–353.
472. Potts SG, Imperatriz-Fonseca V, Ngo HT, Aizen MA, Biesmeijer JC, Breeze TD, Dicks LV, Garibaldi LA, Hill R, Settele J, Vanbergen AJ (2016) *Nature* **540**, 220–229.
473. Preuss D, Lemieux B, Yen G, Davis RW (1993) *Genes Dev* **7**, 974–985.
474. Prötzel D, Heß M, Scherz MD, Schwager M, van't Padje A, Glaw F (2018) *Sci Rep* **8**, 698.
475. Punt W, Hoen PP, Blackmore S, Nilsson S, Le Thomas A (2007) *Rev Palaeobot Palynol* **143**, 1–81.
476. Qin P, Tu B, Wang Y, Deng L, Quilichini TD, Li T, Wang H, Ma B, Li S (2013) *Plant Cell Physiol* **54**, 138–154.
477. Quilichini TD, Douglas CJ, Samuels AL (2014a) *Ann Bot* **114**, 1189–1201.
478. Quilichini TD, Friedmann MC, Samuels AL, Douglas CJ (2010) *Plant Physiol* **154**, 678–690.
479. Quilichini TD, Grienenberger E, Douglas CJ (2015) *Phytochemistry* **113**, 170–182.
480. Quilichini TD, Samuels AL, Douglas CJ (2014b) *Plant Cell* **26**, 4483–4498.
481. R Core Team (2016) R: A Language and Environment for Statistical Computing. R Foundation for Statistical Computing, Vienna, Austria. https://www.R-project.org/.
482. Rader R, Bartomeus I, Garibaldi LA, Garratt MPD, Howlett BG, Winfree R, Cunningham SA, Mayfield MM, Arthur AD, Andersson GKS, Bommarco R, Brittain C, Carvalheiro LG, Chacoff NP, Entling MH, Foully B, Freitas BM, Gemmill-Herren B, Ghazoul J, Griffin SR, Gross CL, Herbertsson L, Herzog F, Hipólito J, Jaggar S, Jauker F, Klein A-M, Kleijn D, Krishnan S, Lemos CQ, Lindström SAM, Mandelik Y, Monteiro VM, Nelson W, Nilsson L, Pattemore DE, Pereira N de O, Pisanty G, Potts SG, Reemer M, Rundlöf M, Sheffield CS, Scheper J, Schüepp C, Smith HG, Stanley DA, Stout JC, Szentgyörgyi H, Taki H, Vergara CH, Viana BF, Woyciechowski M (2015) *Proc Natl Acad Sci USA* **113**, 146–151.
483. Radmacher S, Strohm E (2010) *Apidologie* **41**, 169–177.
484. Raguso RA (2001) Floral scent, olfaction, and scent driven foraging behavior. in: Chittka L, Thomson JD (Eds)

Cognitive ecology of pollination: Animal behavior and floral evolution. Cambridge University Press, Cambridge, pp. 83–105.

485. Raguso RA (2004) Floral scent, olfaction, and sccent-driven foraging behavior. Chittka L, Thompson JD (Eds) Cognitive Ecology of Pollination: Animal Behaviour and Floral Evolution. Cambridge University Press, Cambridge, pp.
486. Raguso RA (2008) *Annu Rev Ecol Evol Syst* **39**, 549–569.
487. Raine NE, Chittka L (2005) *Uludag Bee J* **5**, 145–150.
488. Raine NE, Ings TC, Dornhaus A, Saleh N, Chittka L (2006) *Adv Study Behav* **36**, 305–354.
489. Ratto F, Simmons BI, Spake R, Zamora-Gutierrez V, MacDonald MA, Merriman JC, Tremlett CJ, Poppy GM, Peh KSH, Dicks LV (2018) *Front Ecol Environ* **16**, 82–90.
490. Reeder SH, Lee BH, Fox R, Dobritsa AA (2016) *PLoS Genet* **12**, e1006060.
491. Reiter R (1947) *Ohio J Sci* **47**, 137–152.
492. Regan EC, Santini L, Ingwall-King L, Hoffmann M, Rondinini C, Symes A, Taylor J, Butchart SHM (2015) *Conserv Lett* **8**, 397–403.
493. Rejón JD, Delalande F, Schaeffer-Reiss C, Alché JD, Rodríguez-García MI, van Dorsselaer A, Castro AJ (2016) *Proteomes* **4**, 5.
494. Rejón JD, Delalande F, Schaeffer-Reiss C, Carapito C, Zienkiewicz K, de Dios Alché J, Rodríguez-García MI, Van Dorsselaer A, Castro AJ (2014) *Plant Signal Behav* **9**, e28274.
495. von Röpenack E, Parr A, Schulze-Lefert P (1998) *J Biol Chem* **273**, 9013–9022.
496. Roschina VV (2003) *J Fluoresc* **13**, 403–420.
497. Roschina VV (2012) *Int J Spectrosc* **2012**, 124672.
498. Roshchina VV, Melnikova EV (1999) Microspectrofluorimetry of Intact Secreting Cells with Application to the Study of Allelopathy. in: Inderjit, Dakshini KMM, Foy CL (Eds) Principles and Practices in Plant Ecology: Allelochemical Interactions. CRC Press, Boca Raton, pp 99–126.
499. Ross MD (1973) *Heredity* **30**, 169–176.
500. Roulston TH, Cane JH (2000) *Plant Syst Evol* **222**, 187–209.
501. Rourke J, Wiens D (1977) *Ann Mo Bot Gard* **64**, 1–17.
502. Rowley JR (1973) *Grana* **13**, 129–138.
503. Rowley JR, Dahl AO, Rowley JS (1981) *Rev Palaeobot Palynol* **35**, 1–38.
504. Rowley JR, Skvarla JJ (2007) *Grana* **46**, 130–139.
505. Rowley JR, Skvarla JJ, Gabarayeva NI (1999) *Taiwania* **44**, 212–229.
506. Rowley JR, Southworth D (1967) *Nature* **213**, 703–704.
507. Rozema J, Broekmana RA, Blokkerb P, Meijkampa BB, de Bakkera N, van de Staaij J, van Beem A, Ariese F, Kars SM (2001) *J Photochem Photobiol B Biol* **62**, 108–117.
508. Rubinelli P, Hu Y, Ma H (1998) *Plant Mol Biol* **37**, 607–619.
509. Rueden CT, Schindelin J, Hiner MC, DeZonia BE, Walter AE, Arena ET, Eliceiri KW (2017) *BMC Bioinfomatics* **18**, 529.
510. Ruhland W, Wetzel K (1924) *Ber Dtsch Bot Ges* **42**, 3–14.
511. Russo L (2016) *Insects* **7**, 69.

512. Sakuma M, Fukami H (1985) *Appl Ent Zool* **20**, 387–402.
513. Sanders PM, Bui AQ, Weterings K, McIntire KN, Hsu YC, Lee PY, Truong MT, Beals TP, Goldberg RB (1999) *Sex Plant Reprod* **11**, 297–322.
514. Sannier J, Baker WJ, Anstett MC, Nadot S (2009) *BMC Res Notes* **2**, 145
515. Santos RP, Mariath JEA, Hesse M (2003) *Plant Syst Evol* **237**, 185–198.
516. Satina S, Blakeslee AF, Avery AG (1940) *Am J Bot* **27**, 895–905.
517. Saunders ME (2018) *Insect Conserv Diver* **11**, 13–31.
518. Scarpati ML, Guiso M (1964) *Tetrahedron Lett* **5**, 2851–2853.
519. Schilmiller AL, Stout J, Weng JK, Humphreys J, Ruegger MO, Chapple C (2009) Plant J 60, 771–782.
520. Schindelin J, Arganda-Carreras I, Frise E, Kaynig V, Longair M, Pietzsch T, Preibisch S, Rueden C, Saalfeld S, Schmid B, Tinevez JY, White DJ, Hartenstein V, Eliceiri K, Tomancak P, Cardona A (2012) *Nat Methods* **9**, 676–682.
521. Schlangen K, Miosic S, Castro A, Freudmann K, Luczkiewicz M, Vitzthum F, Schwab W, Gamsjäger S, Musso M, Halbwirth H (2009) *Phytochemistry* **70**, 889–898.
522. Schopfer CR, Nasrallah ME, Nasrallah JB (1999) *Science* **266**, 1697–1700.
523. Scogin R, Zakar K (1976) *Biochem Syst Ecol* **4**, 165–167.
524. Scott RJ (1994) Pollen exine: the sporopollenin enigma and the physics of pattern. in: Scott RJ, Stead MA (Eds) Molecular and Cellular Aspects of Plant Reproduction. Cambridge University Press, New York, pp. 49–81.
525. Scott RJ, Spielman M, Dickinson HG (2004) *Plant Cell* **16**, S46–60.
526. Seeley TD (1995) The Wisdom of the Hive: The Social Physiology of Honey Bee Colonies. Harvard University Press, Cambridge.
527. Sekercioglu CH (2006) *Trends Ecol Evol* **21**, 464–471.
528. Shao Y, Molnar LF, Jung Y, Kussmann J, Ochsenfeld C, Brown ST, Gilbert ATB, Slipchenko LV, Levchenko SV, O'Neill DP, DiStasio RA Jr., Lochan RC, Wang T, Beran GJO, Besley NA, Herbert JM, Lin CY, Van Voorhis T, Chien SH, Sodt A, Steele RP, Rassolov VA, Maslen PE, Korambath PP, Adamson RD, Austin B, Baker J, Byrd EFC, Dachsel H, Doerksen RJ, Dreuw A, Dunietz BD, Dutoi AD, Furlani TR, Gwaltney SR, Heyden A, Hirata S, Hsu CP, Kedziora G, Khalliulin RZ, Klunzinger P, Lee AM, Lee MS, Liang WZ, Lotan I, Nair N, Peters B, Proynov EI, Pieniazek PA, Rhee YM, Ritchie J, Rosta E, Sherrill CD, Simmonett AC, Subotnik JE, Woodcock III HL, Zhang W, Bell AT, Chakraborty AK, Chipman DM, Keil FJ, Warshel A, Hehre WJ, Schaefer HF, Kong J, Krylov AI, Gill PMW, Head-Gordon M (2006) *Phys Chem Chem Phys* **8**, 3172–3191.
529. Sharma N, Koul P, Koul AK (1993) *Bot J Linn Soc* **111**, 129–138.
530. Sharma KD, Nayyar H (2016) *Front Plant Sci* **7**, 402.
531. Shi J, Cui M, Yang L, Kim YJ, Zhang D (2015) *Trend Plant Sci* **20**, 741–753.
532. Shimosato H, Yokota N, Shiba H, Iwano M, Entani T, Che FS, Watanabe M, Isogai A, Takayama S (2007) *Plant Cell* **19**, 107–117.
533. Shrestha M, Dyer AG, Boyd-Gerny S, Wong BBM, Burd M (2013) *New Phytol* **198**, 301–310.
534. Silberglied RE (1979) *Ann Rev Ecol Syst* **10**, 373–398.

535. Silva NF, Goring DR (2001) *Cell Mol Life Sci* **58**, 1988–2007.
536. Simpson MG (1989) *Ann Bot* **64**, 257–269.
537. Singh VP (2006) Gymnosperm (Naked Seeds Plant) Structure and Development, 1st Edition. Sarup & Sons, New Delhi.
538. Sinha RP, Häder DP (2002) *Photochem Photobiol Sci* **1**, 225–236.
539. Skrzipek KH, Skrzipek H (1974) *Z Zellforsch Mikrosk Anat* **147**, 589–593.
540. Sloggett JJ (2018) *Curr Zool* **64**, 319–320.
541. Sobolev VS, Sy AA, Gloer JB (2008) *J Agric Food Chem* **56**, 2960–2969.
542. Song JH, Moon H-K, Hong S-P (2016) *Plant Syst Evol* **302**, 853–869.
543. Song JH, Oak M-K, Roh H-S, Hong S-P (2017) *Grana* **56**, 351–367.
544. Southworth D, Jernstedt JA (1995) *Protoplasma* **187**, 79–87.
545. Srinivasan MV (2010) *Annu Rev Entomol* **55**, 267–284.
546. Stanley DA, Garratt MPD, Wickens JB, Wickens VJ, Potts SG, Raine NE (2015) *Nature* **528**, 548–550.
547. Stanley RG, Linskens HF (1974) Pollen: Biology Biochemistry Managemant. Springer, Heidelberg.
548. Stavenga DG (2010) *J Comp Physiol A* **196**, 869–878.
549. Stockman A, Sharpe LT (2000) *Vision Res* **40**, 1711–1737.
550. Stokes GG (1852) *Philos Trans R Soc Lond* **142**, 463–562.
551. Stone SL, Arnoldo M, Goring DR (1999) *Science* **286**, 1729–1731.
552. Strack D, Eilert U, Wray V, Wolff J, Jaggy H (1990) *Phytochemistry* **29**, 2893–2896.
553. Stroo A (2000) *Plant Syst Evol* **222**, 225–242.
554. Suárez-Cervera M, Asturias JA, Vega-Maray A, Castells T, López-Iglesias C, Ibarolla I, Arilla MC, Gabarayeva NI, Seone-Camba JA (2005) *Sex Plant Reprod* **18**, 101–112.
555. Suárez-Cervera M, Marquez J, Seoane-Camba J (1995) *Rev Palaeobot Palynol* **85**, 63–84.
556. Suen DF, Huang AH (2007) *J Biol Chem* **282**, 625–636.
557. Suen DF, Wu SS, Chang HC, Dhugga KS, Huang AH (2003) *J Biol Chem* **278**, 43672–43681.
558. Sugahara M, Izutsu K, Nishimura Y, Sakamoto F (2013) *Zool Sci* **30**, 99–104.
559. Sun H, Shi T, Song J, Xu Y, Gao Z, Song X, Ni Z, Cai B (2016) *Acta Physiol Plant* **38**, 114.
560. Suzuki I, Tsuboi M, Shimanouchi T, Mizushima S (1959) *J Chem Phys* **31**, 1437–1438.
561. Taboada C, Brunettic AE, Pedron FN, Neto FC, Estrin DA, Bari SE, Chemes LB, Lopes NP, Lagorio MG, Faivovich J (2017) *Proc Natl Acad Sci USA* **114**, 3672–3677.
562. Takasaki T, Hatakeyama K, Suzuki G, Watanabe M, Isogai A, Hinata K (2000) Nature 403, 913–916.
563. Takayama S, Isogai A (2005) *Ann Rev Plant Biol* **56**, 467–489.
564. Takayama S, Shiba H, Iwano M, Shimosato H, Che FS, Kai N, Watanabe M, Suzuki G, Hinata K, Isogai A (2000) *Proc Natl Acad Sci USA* **97**, 1920–1925.
565. Takayama S. Shimosato H, Shiba H, Funato M, Che FK, Watanabe M, Iwano M, Isogai A (2001) *Nature* **413**, 534–538.
566. Tang LK, Chu H, Yip WK, Yeung EC, Lo C (2009) *New Phytol* **181**, 576–587.
567. Tao R, Habu T, Namba A, Yamane H, Fuyuhiro F, Iwamoto K, Sugihara S (2002) *Theor Appl Genet* **105**, 222–228.

568. Tautz J (2008) The Buzz about Bees: Biology of a Superorganism. Springer, Heidelberg.
569. Taylor LP, Hepler PK (1997) *Ann Rev Plant Physiol Plant Mol Biol* **48**, 461–491.
570. Tchuenguem Fohouo FN, Pauly A, Messi J, Brückner D, Ngamo Tinkeu L, Basga E (2004) *Ann Soc Entomol Fr* **40**, 131–143.
571. Terakita A (2005) *Genome Biol* **6**, 213.
572. Thompson WR, Meinwald J, Aneshanslet D, Eisner T (1972) *Science* **177**, 528–530.
573. Thorp RW, Briggs DL, Estes JR, Erickson EH (1975) *Science* **189**, 476–478.
574. Thorp RW, Briggs DL, Estes JR, Erickson EH (1976) *Science* **194**, 342.
575. Tomás-Lorente F, Garcia-Grau MM, Nieto JL, Tomás-Barberán FA (1992) *Phytochemistry* **31**, 2027–2029.
576. Torabinejad J, Caldwell MM, Flint SD, Durham S (1998) *Am J Bot* **85**, 360–369.
577. Triantaphylidès C, Havaux M (2009) *Trends Plant Sci* **14**, 219–228.
578. Tsou CH, Fu YL (2002) *Am J Bot* **89**, 734–747.
579. van Tussenbroek BI, Villamil N, Márquez-Guzmán J, Wong R, Monroy-Velázquez LV, Solis-Weiss V (2016) *Nat Commun* **7**, 12980.
580. Tsuzuki S, Fujii A (2008) *Phys Chem Chem Phys* **10**, 2584–2594.
581. Tsuzuki S, Honda K, Uchimaru T, Mikami M, Fujii A (2006) *J Phys Chem A* **110**, 10163–10168.
582. Tsuzuki S, Honda K, Uchimaru T, Mikami M, Tanabe K (2000a) *J Am Chem Soc* **122**, 11450–11458.
583. Tsuzuki S, Honda K, Uchimaru T, Mikami M, Tanabe K (2000b) *J Am Chem Soc* **122**, 3746–3753.
584. Tsuzuki S, Honda K, Uchimaru T, Mikami M, Tanabe K (2002) *J Am Chem Soc* **124**, 104–112.
585. Vanbergen AJ, The Insect Pollination Initiative (2013) *Front Ecol Environ* **11**, 251–259.
586. Varbanova MP, Atanassov AI, Atanassov II (2003) *Plant Sci* **164**, 525–530.
587. Vázquez-Lobo A (2009) Sexual reproduction in gymnosperms: An overview. in: Gamboa-deBuen A, Orozco-Segovia A, Cruz-Garcia F (Eds) Functional Diversity of Plant Reproduction. Research Signpost, Kerala, pp. 1–16.
588. Vizcay-Barrena G, Wilson ZA (2006) *J Exp Bot* **57**, 2709–2717.
589. Vogt K, Kirschfeld K (1983) *Biophys Struct Mech* **9**, 319–328.
590. Vogt T (2010) *Mol Plant* **3**, 2–20.
591. Vorobyev M, Hempel de Ibarra N (2012) Honey Bee Vision in Relation to Flower Patterns. in: Galizia CG, Eisenhardt D, Giurfa M (Eds) Honeybee Neurobiology and Behavior: A Tribute to Randolf Menzel. Springer, Heidelberg.
592. Wakakuwa M, Stavenga DG, Arikawa K (2007) *Photochem Photobiol* **83**, 27–34.
593. Wakakuwa M, Stavenga DG, Kurasawa M, Arikawa K (2004) *J Exp Biol* **207**, 2803–2810.
594. Wald B, Wray V, Galensa R, Herrmann K (1989) *Phytochemistry* **28**, 663–664.
595. Wallace S, Fleming A, Wellman CH, Beerling DJ (2011) *AoB Plants*, plr027.
596. Walters D, Meurer-Grimes B, Rovira I (2001) *FEMS Microbiol Lett* **201**, 255–258.
597. Walters DR (2003) *Phytochemistry* **64**, 97–107.
598. Warrant EJ (2017) *Phil Trans R Soc B* **372**, 20160063.
599. Waser NM, Price MV (1983) *Nature* **302**, 422–424.
600. Waser NM, Price MV (1985) *Oecol* **67**, 121–126.

601. Watanabe M, Shiozawa H, Isogai A, Suzuki A, Takeuchi T, Hinata K (1991) *Plant Cell Physiol* **32**, 1039–1047.
602. Watanabe M, Suwabe K, Suzuki G (2012) *Proc Jpn Acad Ser B* **88**, 519–534.
603. Webby R, Bloor S (2000) *Z Naturforsch* **55**, 503–505.
604. Weber M (1996) *Int J Plant Sci* **157**, 195–202.
605. Werner C, Hu W, Lorenzi-Riatsch A, Hesse M (1995) *Phytochemistry* **40**, 461–465.
606. White GM, Boshier DH, Powell W (2002) *Proc Natl Acad Sci USA* **99**, 2038–2042.
607. Whitaker AH (1987) *NZ J Bot* **25**, 315–328.
608. Whitehead DR (1968) *Evolution* **23**, 28–35.
609. Wiebes JT (1979) *Ann Rev Ecol Syst* **10**, 1–12.
610. Wiermann R (1981) *Z Naturforsch* **36**, 204–206.
611. Wiermann R, Gubatz S (1992) *Int Rev Cytol* **140**, 35–72.
612. Wiermann R, Vieth K (1983) *Protoplasma* **118**, 230–233.
613. Wilson ZA, Song J, Taylor B, Yang C (2011) *J Exp Bot* **62**, 1633–1649.
614. Wilson ZA, Zhang DB (2009) *J Exp Bot* **60**, 1479–1492.
615. Williams JH, Taylor ML, O'Meara BC (2014) *Am J Bot* **101**, 559–571.
616. Williamson CG, Zepp RG, Lucas RM, Madronich S, Austin AT, Ballaré CL, Norval M, Sulzberger B, Bais AF, McKenzie RL, Robinson SA, Häder DP, Paul ND, Bornman JF (2014) *Nat Clim Change* **4**, 434–441.
617. Willmer P (2011) Pollination and Floral Ecology. Princeton University Press, New Jersey.
618. Wimalasekera R, Tebartz F, Scherer GFE (2011) *Plant Sci* **181**, 593–603.
619. Winston ML (1987) The Biology of the Honey Bee. Harvard University Press, Cambridge.
620. Woodcock TS, Larson BMH, Kevan PG, Inouye DW, Lunau K (2014) *J Pollinat Ecol* **12**, 63–94.
621. Wortley AH, Wang H, Lu L, Li D, Blackmore S (2015) *Ann Mo Bot Gard* **100**, 177–226.
622. Wright A, Bubb WA, Hawkins CL, Davies MJ (2002) *Photochem Photobiol* **76**, 35–46.
623. Wu SSH, Moreau RA, Whitaker BD, Huang AHC (1999) *Lipids* **34**, 517–523.
624. Wu SSH, Platt KA, Ratnayake C, Wang TW, Ting JTL, Huang AHC (1997) *Proc Natl Acad Sci USA* **94**, 12711–12716.
625. Wu SSH, Suen DF, Chang HC, Huang AHC (2002) *J Biol Chem* **277**, 49055–49064.
626. Xie H, Chen L, Xu F, Guo W, Wang S, Yang Z, Zhang S (2017) *J Plant Biol* **60**, 404–412.
627. Xu D, Shi J, Rautengarten C, Yang L, Qian X, Uzair M, Zhu L, Luo Q, An G, Waßmann F, Schreiber L, Heazlewood JL, Scheller HV, Hu J, Zhang D, and Liang W (2017) *Plant Physiol* **173**, 240–255.
628. Xue Z, Xu X, Zhou Y, Wang X, Zhang Y, Liu D, Zhao B, Duan L, Qi X (2018) *Nat Commun* **9**, 604.
629. Yadav V, Molina I, Ranathunge K, Castillo IQ, Rothstein SJ, Reed JW (2014) Plant Cell 26, 3569–3588.
630. Yaegaki H, Miyake M, Haji T, Yamaguchi M (2003) *HortScience* **38**, 1422–1423.
631. Yang Z, Dong F, Baldermann S, Murata A, Tu Y, Asai T, Watanabe N (2012) *J Sci Food Agric* **92**, 2128–2132.
632. Yoshihara T, Katsuyoshi Y, Takamatsu S, Sakamura S (1981) *Agric Biol Chem* **45**, 2593–2598.
633. Yu J, Meng Z, Liang W, Behera S, Kudla J, Tucker MR, Luo Z, Chen M, Xu D, Zhao G, Wang J, Zhang S, Kim YJ, Zhang D (2016) *Plant Physiol* **172**, 1772–1786.
634. Yuan F, Bernard GD, Le J, Briscoe AD (2010) *Mol Biol Evol* **27**, 2392–2405.

635. Zana R (2005) Introduction to Surfactants and Surfactant Self-Assemblies. in: Zana R (Eds) Dynamics of Surfactant Self-Assemblies: Micelles, Microemulsions, Vesicles, and Lyotropic Phases. CRC Press, Boca Raton, pp. 1–35.
636. Zavada MS (1983) *Bot Rev* **49**, 331–379.
637. Zerback R, Bokel M, Geiger H, Hess D (1989) *Phytochemistry* **28**, 897–899.
638. Zhang C, Yang YP, Duan YW (2014) *Sci Rep* **4**, 4520.
639. Zhao G, Qin GW, Gai Y, Guo LH (2010) *Chem Pharm Bull* **58**, 950–952.
640. Zhao G, Shi J, Liang W, Zhang D (2016) *Plant Signal Behav* **11**, e1136764.
641. Zinkl GM, Zwiebel BI, Grier DG, Preuss D (1999) *Development* **126**, 5431–5440.
642. Zinn KE, Tunc-Ozdemir M, Harper JF (2010) *J Exp Bot* **61**, 1959–1968.

List of Publication

Mori S, Fukui H, Oishi M, Sakuma M, Kawakami M, Tsukioka J, Goto K, Hirai N (2018) Biocommunication between plants and pollinating insects through fluorescence of pollen and anthers. *J Chem Ecol* **44**, 591–600.

Chapters II & III, adapted by permission from Springer Customer Centre GmbH: Springer Nature, Journal of Chemical Ecology, Biocommunication between Plants and Pollinating Insects through Fluorescence of Pollen and Anthers, Mori S, Fukui H, Oishi M, Sakuma M, Kawakami M, Tsukioka J, Goto K, & Hirai N, 2018 (https://doi.org/10.1007/s10886-018-0958-9).